NATIONAL ADVISORY COMMITTEE FOR AERONAUTICS

TECHNICAL NOTE 3413

INVESTIGATION OF THE USE OF A RUBBER ANALOG IN THE STUDY OF STRESS DISTRIBUTION IN RIVETED AND CEMENTED JOINTS

By Louis R. Demarkles

Massachusetts Institute of Technology

Washington

November 1955

NATIONAL ADVISORY COMMITTEE FOR AERONAUTICS

TECHNICAL NOTE 3413

INVESTIGATION OF THE USE OF A RUBBER ANALOG IN THE STUDY OF STRESS DISTRIBUTION IN RIVETED AND CEMENTED JOINTS

By Louis R. Demarkles

SUMMARY

This investigation was undertaken to study the stress distribution within cemented and riveted metal joints by use of an analogous joint constructed of a highly flexible material. By means of displacement measurements obtained from foam-rubber analogs it is shown that the distribution of shear in these joints is not uniform over the length of the joint, but that it is greater near the ends than it is in the middle as long as the stresses are kept within the elastic range in which most fatigue loads occur.

Because of the very low modulus of elasticity of the foam rubber, all displacements occurring in the analogs are greatly exaggerated, some so greatly as to indicate that certain factors hitherto unknown, and others whose existence has been suspected but unproved, may, when properly evaluated, explain the concentrations and redistributions of stress that cause the discrepancies between the results of tests and currently accepted methods of analysis. Displacements on the cemented-joint analogs were great enough to be measured to 0.01 inch on grids drawn on the edges of the specimens. Displacements at 11 points in each of several sections in the riveted rubber analogs were measured with the same precision on X-ray photographs showing indicators - thin metal rods or pieces of thread soaked in lead nitrate - which were inserted into the rubber before the loads were applied.

INTRODUCTION

The distribution of loads within riveted, bolted, and cemented joints has been the subject of many investigations (for example, refs. 1 to 6). From these investigations and from fatigue tests of such joints (refs. 7 to 9), it is evident that there is a lack of complete understanding of the internal stress distribution within joints. Previous studies, in which mechanical or electrical strain gages were used, were

tedious at best and were frequently limited in scope because the structural elements were not extremely simple sections.

Strain-gage data were often affected by preconceived notions on the part of the person who located the gages. Important strains could go unmeasured if the research scientist had no suspicion of their presence, and evidence of their possible existence could be obscured by inaccuracies in the determination of very small deflections. Attempts to correlate strain-gage data from various sources on structural elements of various sizes and shapes have been disappointing and the conclusion has been reached that a different approach was needed to indicate how and where significant strains would occur.

It is impracticable to measure internal strains in metal members and impossible to obtain a metal having a low-enough modulus of elasticity to give displacements visible to the naked eye. The purpose of this report, therefore, is to describe an investigation in which the stress distribution within a cemented or riveted metal joint was studied by means of an analogous joint constructed of a highly flexible material. The aim was to magnify all displacements that could be expected in metal specimens of practicable size so greatly that they would become visible.

Few plastics have linear stress-strain curves and all tend to creep under loads of moderate magnitude when they are imposed for moderate periods. Investigation of several other materials and study of previous work (refs. 10 to 13) indicated that foam rubber would be the most suitable material to use since it had a very low modulus of elasticity, a linear stress-strain relation up to 50 percent elongation, and reasonable creep characteristics. Under the low stress intensities involved, it was found that foam-rubber specimens showed no effects from creep or hysteresis.

Preliminary X-ray tests indicated that specimens 5 inches or more in depth could be penetrated without difficulty. Such specimens gave clear images and, when suitable indicators were used, showed the relative movements of the internal fibers of the specimens in considerable detail.

Subsequent tests were confined to perfecting techniques for measuring surface displacements and internal strains in foam-rubber specimens built to simulate cemented and riveted joints in metal plates.

This work was done at the Massachusetts Institute of Technology under the sponsorship and with the financial assistance of the National Advisory Committee for Aeronautics. Much of this work could not have been carried out had it not been for the able assistance of Mr. G. Falabella, Jr., in fabricating test specimens and offering many valuable suggestions in testing and in the preparation of this report. The assistance of Mr. J. E. Gieck of the Firestone Industrial Company in

obtaining the necessary sizes and quantities of Foamex rubber greatly aided this work. Appreciation is also extended to the U. S. Rubber Company for supplying Koylon rubber and to the Goodyear Tire and Rubber Company for supplying Airfoam rubber.

FOAM-RUBBER PROPERTIES

The tensile and shear properties of available commercial foam rubbers were determined by test. The foam-rubber materials considered included Koylon, Foamex, and Airfoam, products of U. S. Rubber Company, Firestone Industrial Company, and Goodyear Tire and Rubber Company, respectively. Foamex was used for most of the analog specimens.

Tensile tests of these materials were performed on a simple testing machine consisting of a rectangular guillotine-type frame having a fixed base and sliding head, as shown in figure 1. Load was transmitted by a cable and pulley system to the sliding head and thus to any specimen inserted between base and head. The sheet material, as delivered, was 15 inches wide and 45 inches long. A gage distance of 10 inches in the middle of this length was considered beyond the influence of secondary effects from the plates which were cemented to each end of the rubber sheet to distribute the load and permit the specimen to be held in the testing machine by a simple bolted connection. Preliminary tests showed that the tensile properties were independent of width; however, the full 15-inch width was used in view of the size of the proposed models. The strain was computed from caliper measurements between gage lines for a range of loads. The results, plotted in figure 2, include various sheet thicknesses for foam materials available at the time of testing. Strains in the direction of width and thickness of the sheet were also recorded.

Shear properties of Koylon, Foamex, and Airfoam were obtained from torsion tests. Disks 3 inches in diameter, cut from each of the materials, were cemented between two metal plates. One of the plates was rigidly attached to a vertical test rig, leaving the other plate free to rotate. A suitable harness attached to the free plate allowed torque to be applied to it without imposing bending or simple shear on the specimen. Figure 3 shows how targets suspended on horizontal arms were used to find angular displacements or twist of the disks. Vertical displacements of the targets were measured by a motor-driven cathetometer and small angles were computed from their tangents. The modulus of elasticity in shear was obtained from the relation

$$G = \frac{Tt}{\phi I_p}$$

where

T torque, in-lb

t thickness of specimen, in.

ϕ angle of twist, radians

I_p polar moment of inertia, in.^{4}

The thicknesses of materials used are listed in figure 4. No torsion tests were performed on Airfoam since insufficient material was available.

The results of the tensile tests for all three materials are summarized in figure 2. It is evident that the tensile stress-strain relationships are linear up to relatively large loads. Excluding the Airfoam material, linearity continues to an elongation of 40 percent at a stress between $2\frac{1}{2}$ and $4\frac{1}{2}$ psi. The three grades of Airfoam cover quite a large range of Young's modulus compared with the other foam-rubber materials tested, and linearity appears to continue over a greater percent stretch. It is important to note, however, that all materials show a close similarity to the tensile property curves for aluminum within the elastic range.

Young's moduli E were determined from the straight-line portions of the plots. For convenient comparison the values obtained are listed in table I. These values indicate that Koylon is stiffer than Foamex but less stiff than Airfoam (firm). Thickness apparently has an effect on the modulus as shown by the results of 1/4-, 1/2-, and 1-inch sheets of Foamex. The thickest sheet has the lowest modulus. This may be caused by the presence of a "skin" on one side of the sheets and a difference in porosity throughout the sheets. Such skin was thin, and the differences in porosity slight, but the skin thickness for the thinner sheets represents a larger percent of the total, and the porosity, due to gases escaping during cooling of the rubber, is finer in the thinner sheets. The "bubbling" is less violent and the resulting porosity more uniform.

The shear moduli in figure 4 do not include the Airfoam material because the material available was inadequate for preparing specimens. However, it is probable that the Airfoam is linear in shear as well as in tension and that the G-values vary about in proportion to the modulus of elasticity for Airfoam of different grades. Measurement of the straight-line portions of the curves provided the values of moduli of rigidity G given in table I. As would be expected from the tensile tests, Koylon is stiffer in shear than Foamex. It seems reasonable to expect that it would be less stiff than Airfoam (firm) had the latter been tested.

The ratios of moduli of rigidity to elasticity G/E are as follows: For 1/4-inch Koylon, 0.303; for 1/4-inch Foamex, 0.300; for 1/2-inch Foamex, 0.255; and for 1-inch Foamex, 0.290. These results indicate a possible error in the determination of G or E for the 1/2-inch sheet. Since E was found from a 10- by 15-inch test area and G from a 3-inch disk, it is possible that the value of G found for the 1/2-inch Foamex is the quantity in error. Excluding the 1/2-inch sheet, the G/E ratio for foam rubber may be taken as 0.30, whereas for aluminum-alloy sheet of aircraft thickness this ratio varies from 0.38 to 0.40. It is felt that this difference is acceptable for the present investigation, although it is recognized that displacements involving both shear and normal stress may not be correctly represented in the rubber models.

Using the experimental value of 0.30 for the G/E ratio for foam rubber, Poisson's ratio μ computed from the relation for isotropic materials $E = 2G(1 + \mu)$ is 0.67, or twice the value usually accepted for aluminum alloys. However, Poisson's ratio, as found experimentally from measured changes in length, thickness, and width for foam rubber, was about 0.33, as shown in table I; this value approximately equals that for aluminum alloy. The slight variation in Poisson's effect for the thickness and width directions in foam rubber probably indicates the nonisotropic nature of the material, but the approximate formulas developed for cemented lap joints do not include Poisson's ratio so that a determination of its importance need not be made at this time.

After the tensile and shear properties of these materials had been determined, models were constructed to simulate cemented and riveted joints between aluminum sheets. Because of the availability of Foamex, it was selected for use, although either Koylon or Airfoam could have been used with comparable results.

CEMENTED JOINTS

Recent developments in processes for cementing metals have provided another method for the fabrication of aircraft structures. The relative simplicity of cemented joints (fig. 5), their relatively high strengths with both light- and heavy-gage materials, and their potential savings in weight favor their substitution for riveted joints, but a lack of engineering data and reliable design criteria is retarding their use at present.

The analysis of a cemented joint is not the simple matter that the continuous nature of the bond would indicate. Although load is continuously transmitted along the length of a cemented lap joint, as contrasted with a riveted joint, the ends of the cemented area may carry the greater part of that load and the inner portion may be lightly

stressed. This tendency to concentrate stress at the ends of the lap results from the differential straining of the joined members and indicates that the common assumption that the load carried by a joint of constant width varies directly as its length is, in general, untenable. Theory indicates the assumption to be reasonable when the shear properties of the cement and the material joined are essentially equal and when the members are scarfed or tapered in thickness to equalize strains. A completely rational analysis for even a simple lap joint is still to be achieved, but the present explorative investigation making use of Foamex rubber and metal joints shows promising possibilities for an approximate procedure which includes a number of simplifying assumptions.

Test Procedure

Several cemented lap joints constructed of Foamex were investigated under various tensile loads. Three sheet thicknesses, 1/4, 1/2, and 1 inch, were used in the construction of the first lap joints. The length of overlap varied, but the over-all length and width of the specimens, 20 by $6\frac{7}{8}$ inches, were the same for all. The overlap used for the 1/4-inch and 1/2-inch materials was 2 inches and for the 1-inch-thick material, 3 inches. A type of latex cement which, when dry, possesses properties similar to the foam rubber was used for bonding the sheets.

Black shellac (a suspension of fine lamp black in shellac) proved very satisfactory for marking a 1/4-inch grid on the rubber in the regions of the joint at which displacements were to be measured. The shellac, with its fast-drying quality, minimized broadening of the lines due to seepage into the rubber and the lamp black provided an indicator sufficiently opaque to be clearly recorded when photographed on contrast film. Figures 6(a) and 6(b) are tracings of this grid as made from the photographs.

The marking device used was a grid of wire, chosen to give the desired spacing and thickness of line, mounted in a wooden frame. After a thin layer of black shellac had been brushed onto the wires, the prepared grid was pressed against the rubber and the shellac transferred to it.

Metal clamps were bonded to the free ends of the sheets by special metal-to-rubber cement so that the load would be distributed uniformly across the specimens when they were mounted in the apparatus used for the modulus-of-elasticity tests of the sheet materials (fig. 1).

Certain precautions were found necessary in the actual testing and photographing of these specimens. Each specimen was mounted to have

freedom in bending and vertical translation but to be restricted in torsion and horizontal translation. This allowed the desired movements of the model under load and stabilized the rather flexible material. Since the lines of action of the forces on the lap joint and the center lines of each sheet were not coincident, care was taken to offset the points of application of the loads to obtain colinearity of the applied forces.

Photographic methods for recording the displacements of the grid required developing a technique having an accuracy that would allow duplication of results. Care was found to be necessary both in taking the photographs and in processing the film. For each loading, the camera was positioned and leveled so that the plane of the film was parallel to the plane of the grid and the center of the lens was at the same height from the floor as the center of the grid. This minimized optical distortion. Since the cut film used was $2\frac{1}{2}$ inches by $3\frac{1}{2}$ inches, enlarging was necessary to indicate full-scale displacements of the grid, and, in order to record and follow the angular and linear displacements from model to enlargement, it was found necessary to place targets ruled with 1-inch squares on each side of the model so that portions of each target were included in each negative. These targets did not move when the models were loaded and, hence, all displacement of the grid due to translation or rotation of the joint area under load could be referenced to lines on the fixed targets. The displacement data for the rubber-analog joints included and analyzed in the body of this report are for the 3-inch-lap, 1-inch-sheet model at a 16-pound tensile load.

Four cemented magnesium specimens were also tested under tensile loads. Two single lap specimens (fig. 7(a)) having a 1-inch overlap were made from 1/4- by 1- by 6-inch pieces of magnesium. Two double lap specimens (fig. 7(b)) having a 2-inch overlap were made from 1/4- by 15/16- by 6-inch pieces with 1/8- by 1- by 2-inch cover plates. Photogrids with 0.01-inch spacing were placed on each edge of the laps as shown in figures 7(a) and 7(b) in an effort to get strain distribution along the lap. The ends of the single lap specimens held by testing machine grips were adjusted to have the plane of the cement coincide with the plane of loading to reduce bending or tearing forces on the joint.

Results and Discussion

The results of the tensile test on the 3-inch-length lap, 1-inch sheet simple Foamex cemented joint under the 16-pound load are presented in figures 8 to 14. These curves represent the first

attempt to obtain normal and shear stress distributions throughout a lap joint by the rubber-analog method. (The method of computing the normal and shear stresses is given in appendix A.) A qualitative summary of these distributions is shown in figures 12 and 13, where regions of essentially equal stress are connected by continuous contour lines.

The normal stress distribution across the lap is plotted for each row of the grid in figures 8(a) to 8(f). The curves indicate uniform stresses across each sheet thickness for regions at the extremities of the joint and rapidly changing stresses near the faying surface. They show a gradual change in distribution until, at a section about halfway along the length of lap, the normal stress distribution becomes nearly uniform across the thickness of the lap. Maximum normal stress occurs at the loaded ends of the lap and is about equal to the average normal stress for the single sheet. Maximum shear stress occurs on the faying surface near each end of the joint.

The experimental data used for figures 8(a) to 8(f) are cross-plotted in figures 9(a) to 9(d). Proceeding from the free edge, the normal stress distribution from free end to loaded end varies quite linearly at first and then changes gradually until the distribution is nearly uniform along the faying surface. The uniform normal stress distribution along the faying surface and across the lap halfway along its length accounts for the crosslike distribution pictured in figure 12.

The distribution of shear stress across the lap is presented for each row of grid in figures 10(a) to 10(f). The values of shear stress rise nearly linearly from low values near the free edges to maximum at or near the faying surface. The experimental curve of figure 14 is a cross plot of the shear values at the faying surface. Although a closer spacing of the grid might yield more consistent data, values from these faired curves are used in this investigation. The maximum shear stress along the faying surface occurs at the ends of the lap and the minimum, halfway between the ends; and the experimental plot of stress closely agrees with the theoretical curves of figure 14 in distribution and magnitude. The experimental curve indicates a maximum shear stress about 30 percent greater than the average (load/cemented area) and about 70 percent greater than the minimum. As would be expected from this agreement, the theoretical curve indicates similar differences among the maximum, minimum, and average stresses.

Cross-plotting the experimental data of figures 10(a) to 10(f) yields a distribution of shear stress along the lap (figs. 11(a) and 11(d)). Columns C, D, E, and F, in the vicinity of the faying surface, have maximum and minimum values located at positions similar to those along the faying surface. In columns A, B, G, and H the reverse is true. This change in location of maximum stresses accounts for the difference in character of the lines of equal stress drawn in figure 13.

An investigation of the strength of glued joints made by De Bruyne (ref. 14) indicates the existence and importance of the stress concentrations at the ends of the lap joint and emphasizes the nonlinear variation of failing load with changes in lap length. The concentration of stress probably involves large shear stresses plus sizeable transverse "tearing" stresses across the cement. Goland and Reissner (ref. 15) as well as Jenkins (ref. 16) agree with this idea. Experimental verification of the types and magnitudes of the stresses is desired, and ultimately required, but not yet available. Evidence of shear stress concentration near the ends of the lap in the rubber analog can be seen in figure 13, but sufficient data are not available to show quantitatively or qualitatively the relative ratios of the tearing and the shearing stresses.

The loads at failure in the tests of the cemented magnesium lap joint are shown in figures 7(a) and 7(b), but no data are included to show the strains indicated by the photogrid. The grid was photographed with and without load and the results were enlarged. Displacements were so small, however, that, when the scale of enlargement was sufficient to show them, the lines of the grid were so greatly magnified that accurate measurements could not be made from them. Failure of the bond did not occur until the yield point of the metal was passed. The magnesium used in these tests met Army-Navy specification AN-M-29 type A and had a yield of about 22,000 psi. Shear stress near the end of the bond at maximum load was about 3,900 psi for the double lap specimens. Cemented joints formed with thin-gage materials often do not fail until the yield point of the metal has been reached, but it was not anticipated that the cement would transmit so large a load in the case of heavy-gage material.

If a material having a higher yield point than magnesium had been used, the joints might not have failed until that metal yielded, but insufficient data are available to establish this as fact; hence, it cannot be determined whether the factor producing failure in the adhesive is a critical rate of change in strain or a critical total strain. The Redux cement used in these tests appeared to be a rather brittle material but one having high tensile and shear properties. The thickness of the cement was between 0.005 inch and 0.008 inch and average shear stresses between 2,000 and 4,000 psi were developed across the thin layers.

The cemented joint failed immediately when the magnesium reached its yield point, with separation occurring at the end of the joint away from the free end of each metal piece. In the single lap specimens, the additional stresses due to small bending or tearing forces introduced because the plane of the faying surface did not coincide with the lines of action of the loads apparently caused failure at a lower load and stress than was the case in the double lap specimens. No warning

of impending failure was given, but a slight cracking sound could be heard the instant before the bond failed. The cement used had a high creep rate and it was found that a constant low rate of load application had to be maintained to hold the specimen at a definite load.

Since the transfer of load between two metal pieces cemented together occurs primarily by shearing forces in the plane of the cement, the shearing stress distribution along the faying surface appears to be of first importance in the development of a theory to be used as the basis of a design procedure. The simplified mathematical analysis included in this report, appendix B, was developed with this in mind, and the results from the tests of the metal specimens, when compared with the theoretical formulas, are in good agreement. The correlation between theory and experiment appears sufficiently close to warrant additional experimentation on metal models of different lap lengths and loading conditions for several different cements and metals.

It is believed that data back-figured from specimens having joint lengths great enough to fail at essentially constant loads may be used for the prediction of the failing loads to be expected on shorter lap lengths. The data available show that a reasonable approximation may be expected, but they are not adequate to indicate the probable error involved when stresses on the longer joints exceed the proportional limit of the metal while those on the shorter joints remain within the elastic range. It is probable that the parameter k back-figured from tests involving plastic deformation of the metal will, when used in the theoretical formulas, yield unsafe values for predicted failing loads on joints stressed below the proportional limit. The extent to which this is true has not yet been determined.

In appendix C, consideration is given the increases in stress in the cement when bending occurs in one of the sheets in a single lap joint. The analysis is approximate and applicable only to joints having sheets of equal thickness.

RIVETED JOINTS

It has long been accepted practice in the design of riveted joints to assume that a load having a line of action passing through the centroid of the rivet group is distributed uniformly among the rivets. This assumption is tenable for static ultimate loads on joints in ductile materials. It is not acceptable for the analysis of joints loaded in the elastic range, nor for the less-ductile, high-strength aluminum alloys. Rosenfeld (ref. 17) found analytically and experimentally that the load on a riveted joint is not equally distributed among the rivets but that the end rivets carry a greater portion of

the load than the inner rivets. Hill and Holt (ref. 18), Jenkins (ref. 16), and Moisseiff, Hartman, and Moore (ref. 19) obtained experimental results confirming this nonuniform load distribution among rivets in a multirivet joint and pointed out that, as the ultimate load is approached for a riveted structure, the load is redistributed equally among the rivets. Since most repeated or dynamic loads associated with fatigue in aircraft produce stresses below the elastic limit of the materials in the joint, it is imperative that a more accurate procedure be established for distributing load among rivets which are used in groups.

Spot-welded or bolted connections are analogous to, but not identical with, riveted joints in that the load acting on a group is not distributed uniformly to all elements in the group. Local stress concentrations associated with welding and with the play in bolts differ from those occurring with rivets, but it is believed that a practicable design procedure which indicates a safe and satisfactory distribution in a riveted connection can be modified without excessive difficulty to apply to spot welds or bolts.

Because of their discontinuous nature, such joints present a more difficult problem than does one made with cement, and solutions based on the calculus of finite differences may be required in place of those found by infinitesimal calculus. It seems probable, however, that the end rivets in a line will be loaded more heavily than those near the center, just as a cemented joint transmits a heavier shear stress near its ends. For a first approximation to the determination of the distribution, it therefore seems reasonable to consider methods of modifying the cemented-joint formulas to indicate the loads carried by individual rivets, bolts, or spot welds when the stresses produced by static loads are within the elastic range.

If such methods can be found, they should be useful in the approximate analysis of joints subjected to repeated- or dynamic-force systems. If adequate for such purposes and simple enough to be practicable in routine design, they should be helpful in the analysis of joints subjected to fatigue conditions until further study can be given the effects of each of the variables involved in this very complex problem. Available fatigue data, for the most part, lack dimensions or other information required in an analysis based on modifications of the cemented-joint formulas, but the results from a very limited number of specimens indicate that such an analysis is feasible.

The results of the investigation reported herein indicate that much can be learned as to local bending, local stress concentrations, and similar factors by the use of a foam-rubber analog subjected to static loadings. All deformations are greatly exaggerated in such an analog and effects that might pass entirely unnoticed in a metal specimen show up as factors to be considered when seen in rubber.

Since Foamex and similar rubbers can be procured with an essentially straight line relation between tensile stress and strain over a reasonable working range, and since they may be worked and X-rayed without great difficulty, they should be very useful in future studies of tensile load distribution. Because of their porous texture, foam rubbers do not behave like isotropic solids under compressive loadings; hence, they may not make perfect analogs where compression or shear or both are significant. Where stresses are predominantly tensile, as with the riveted joints investigated herein, it is believed that the relative deformations of the sheets between rivets are correctly indicated. To attempt strain measurements to five significant figures would, of course, not be justifiable, but to be able to measure them with a foot rule, or a scale divided into hundredths of an inch, is a feature not to be passed over lightly.

Test Procedure

Two experimental rubber models were constructed for preliminary tests, a single- and a triple-rivet double lap joint. The deformations of rivets and sheets under various tensile loads were indicated by markers and recorded by X-ray photography.

The single-rivet lap joint of figure 15(a) was made from sheets of Foamex 5 inches wide and 16 inches long. The joint consists of a 1-inch Foamex inner sheet with two outer sheets of 1/2-inch thickness. The triple-rivet model was similarly constructed except that the sheets were twice as long. Rivet holes $1\frac{1}{4}$ inches in diameter with edge distances twice the hole diameter were cut by a specially designed tool. Shanks, $1\frac{3}{8}$ inches in diameter and $1\frac{7}{8}$ inches long, were cemented to round heads $2\frac{1}{4}$ inches in diameter to form Foamex rivets. The above combination of dimensions gave somewhat the effect of a driven aluminum rivet and helped to stabilize the model. These riveted models were mounted in the tensile test apparatus of figure 1 in the same manner as were the cemented models.

Cotton threads soaked in lead nitrate and then dried were placed along the center line of the model parallel to the rivet shanks and along the center line of the 1-inch sheet perpendicular to the shanks. Insertion of these threads was made possible by first passing a small hollow needle through the model at desired locations and threading the cotton line through the needle before withdrawal of the needle. Because of their flexible nature these threads offered little bending restraint but did restrict longitudinal displacement of the rubber. When X-rayed, these threads, the sheets, and the rivets were all visible on the

negative when the proper X-ray voltage and exposure time were used. Figures 15(a) and 15(b) are tracings from an X-ray negative of the single-rivet joint under a 5-pound tensile load.

Based on the results of these preliminary tests, a third model was constructed. This was designed for two rivets but was proportioned so that it could be converted into a three-rivet model. Any major discrepancy between test results of the two- and three-rivet specimens arising from slight variations found in rubber sheets from the same manufacturing process were eliminated by this means, but minor effects resulting from variations in rivet properties were not. The deformations of rivets and sheets under various loads were indicated by an improved marking system and recorded by X-ray photography as before.

The model was made from sheets of Foamex 5 inches wide and 26 inches long. The joint lap consisted of a $1\frac{1}{16}$-inch-thick sheet with two outer sheets of 1/2-inch thickness. Rivet holes $1\frac{1}{4}$ inches in diameter with edge distances twice the hole diameter were cut with a special hole saw. Shanks, $1\frac{3}{8}$ inches in diameter and $1\frac{3}{4}$ inches long, were cemented to round heads $2\frac{1}{4}$ inches in diameter to form Foamex rivets. The length of the rivet shank was chosen to develop some tension in the rivet and to produce a clamping action on the rubber sheets; the diameter was chosen so that the rivet shank would "fill" the hole. A plain round-head rivet was used since other shapes did not provide enough stiffness to produce satisfactory clamping action. This combination of dimensions gave somewhat the effect of a "tight" aluminum rivet and helped to stabilize the model.

The markers used to indicate deformations in these models consisted of both fine cotton threads soaked in lead nitrate as before and 1/64-inch-diameter steel drill rods. Both thread and steel rod were inserted by the hollow-steel-needle method. The location of these markers across the width of the 1-inch and 1/2-inch sheets is shown in figure 16. In order to identify the individual threads, and also the steel rods, a system of knots was employed. Starting at one edge of the rubber sheet, the first thread contained no knots, the second had one, and so forth, with the fifth thread containing four knots. The steel rods were inserted halfway between each pair of threads and halfway between the outer threads and the edge of the rubber. The combination of leaded threads and steel rods offered no restraint against local bending deformation or longitudinal displacement of the rubber. Threads, rods, sheets, and rivets were all visible on the X-ray negatives when proper exposures were made.

The rivet model was placed in the testing machine of figure 1 with one end held fixed. Weights were applied to the other end and were free to find their equilibrium position so that pure tensile loading was applied to the specimen. A 1/32-inch-diameter steel marker was inserted in the 1-inch rubber sheet a short distance from the other markers and this was used as the reference point for alining the X-ray beam. The X-ray machine used emitted rays from a point source, and by setting the head on a horizontal line with the reference marker, the rays passing through all other markers were inclined. The relative displacements of adjacent markers in the joint area were amplified by the parallax of the inclined rays so that each thread and rod could be readily identified on the X-ray film.

The plane of the rubber model was oriented so that the reference marker and the thread having no knots were near the edge closest to the X-ray head. The thread having four knots and the X-ray film container were near the edge farthest from the head. The film container was as close to the edge of the specimen as was possible without interfering with the displacement of the model under load.

Since the images of the markers were projected onto the film by inclined rays, corrections had to be made to the displacements measured on the film in order to obtain the true "elongations" between the markers in the model. These displacements were measured with a scale graduated into hundredths of an inch and corrected by the procedure outlined in appendix D. The resulting strains were converted to stresses and the loads on the sheets between rivets were then obtained by summing the stresses over the width and thickness of each sheet. The differences in loads carried by sections above and below each rivet were taken as the load on the rivet.

Type-M Eastman Kodak X-ray film was found to give satisfactory results. The steel markers and cotton threads showed up well with an exposure time of 135 seconds on a 17- by 13-inch negative. A Picker 150-kilovolt portable X-ray unit with a Machlet Thermax Tube was used in these tests. The voltage used was 40-kilovolt at 8 milliamperes. The size of joint and the loads that can be employed are directly dependent on the size of film available.

Results and Discussion

The preliminary, exploratory tests were used to evaluate the X-ray technique for studying the behavior of riveted joints. No measurements were made on these models, but general observations were recorded.

From a consideration of the single-riveted lap joint (figs. 15(a) and 15(b)), the following observations are significant:

(1) The cross-sectional area of the rivet shank changes from circular to elliptical under the influence of the bending and shearing forces exerted by the sheets. Likewise, the rivet holes in the inner and outer sheets are distorted. These shape changes undoubtedly indicate large local stress concentrations and gradients.

(2) The 1/2-inch sheets separate from the 1-inch sheet at their free ends causing bending across the rivet hole. This is believed to explain fatigue failures through the holes near the "unloaded" ends of riveted joints.

(3) Rivet heads are compressed where they bear into the outer sheets on the side of the hole away from the free ends of the sheets. This action may account for rivet-head failures under repeated loads.

(4) There is evidence of compression between the inner sheet and outer sheets in the region near the free end of the inner sheet. Some of the load is transmitted by friction on the faying surfaces so that the stresses producing concentrations around the edges of the hole are not constant over the thickness of the sheet.

(5) The tendency of the rivet heads to pull through the outer sheets indicates the presence of large bending effects in the rivet and compressive stresses in the sheet under part of the rivet head.

The triple-riveted lap joint discloses the following additional information:

(6) Large distortion of the end rivets indicates that they are carrying a larger part of the load than the inner rivet.

Further tests were carried out on improved rivet models to obtain stress and load data on the sheets and rivets. In a two-rivet joint, each rivet carries half the load and the load is distributed in the sheets between the rivets as shown in figure 17(a). In a three-rivet joint the load is not uniformly distributed among the rivets, the usual design method, but the outer rivets carry the greater portion, with the inner rivet lightly loaded. The result for one load condition on a three-rivet model is shown in figure 17(b).

The outer rivets carry between 35 and 40 percent of the load; the inner, about 25 percent. Results of several tests indicate that each outer rivet in a three-rivet joint carries 36 percent of the load and the inner, 28 percent. These figures are in very close agreement with those found experimentally by Francis (ref. 7) on a three-rivet aluminum-alloy joint whose outer rivets each carried 37.5 percent of the load and the inner, 25 percent. The nonuniform load-carrying capacity of rivets of a multirivet joint was further demonstrated experimentally by Francis

in a 12-rivet aluminum-alloy joint. In the elastic range the outer two rivets each carried 15.5 percent, while the inner rivets each took 3.75 percent of the load.

The significance of this nonuniform load distribution in a multi-rivet joint is not so evident in terms of percentages as it is when these figures are converted to a multiple of the load that each rivet should carry if loaded uniformly. For the three-rivet joint under a load P, each rivet is assumed to carry 0.333P by the usual design procedure; however, from the rubber analog the outer rivets carry 0.375P and the inner rivet, 0.25P. Each outer rivet therefore takes about 12.5 percent more than the average and the inner, about 25 percent less or, on another basis, the outer rivets carry $1\frac{1}{2}$ times the load on the inner rivet. The 12-rivet metal joint shows that the outer rivets carry four times the load carried on those near the center of the joint. Under repetitive loads or reversals of stress, a riveted joint of this nature will be subject to fatigue failure in the outer rivets because of the much larger loads at these locations. Hill and Holt (ref. 18) suggest that, under such conditions, the unusual load distributions among rivets must be taken into account for a rational design. The absurdity of correlating static or fatigue strengths on the basis of "average" loads is apparent.

The loads on the rivets in the rubber specimens were determined by measuring strains in the 1- and 1/2-inch sheets at the locations between rivets shown in figure 16. Data of one run for the two- and three-rivet model are given in table IV. Large gage lengths were used for measuring strains because of the low modulus of the rubber and method of measurement employed. The loading on the entire model was checked by determining strains in the 1-inch sheet at a location free from stress concentrations induced by the grips or the joint itself. In each case the load on the model as calculated from these strains checked the actual load within 1 or 2 percent and indicated that the method of strain measurement was satisfactory. By repeating this operation several times for different loads and checking each time, the effects of hysteresis were found to be negligible. From the loads on the sheets computed from strains measured at sections between the rivets and the known load on the model, the load carried by each rivet was determined. The load on each sheet was computed independently from the displacements of the markers at three cross sections, each located where the local strain effects of the rivet and rivet hole were small. The stresses for each indicator were multiplied by the area associated with it; then, the product was totaled across the section as shown in appendix D to give the computed load. This should equal the load applied to the specimen. The results checked fairly well for the two-rivet model but not so well for the three. The missing load can be accounted for partly by friction between the sheets and partly by the accuracy of the method of measurement. The

gage length and elongation between any two corresponding markers in different rows could be read to the second decimal place, but accuracy to the third decimal place is desirable because small differences between essentially equal numbers are involved. The diameters of the markers defeated any attempt to make readings to the third decimal place.

The tensile stress distributions across the width of the sheets between the rivets in the two- and three-rivet joints under load are shown in figures 18 and 19. The stresses computed from the strains for the three gage-length locations are plotted for the 1- and 1/2-inch sheets for the two- and three-rivet models. The average stress for each plotted cross section is also shown with these curves. For both models, the stresses across the sheets reach a maximum near the edges and a minimum near the center.

In the two-rivet models, the average stress for the three gage lengths of the 1/2-inch sheet 1 are greater than those for the 1/2-inch sheet 2 as shown in figure 18. The load on 1/2-inch sheet 1 is apparently greater than that on the 1/2-inch sheet 2. Small misalinements of the holes between the 1/2-inch sheet 1 and 1/2-inch sheet 2 and the 1-inch sheet and differences in rivet tension are believed to cause this nonuniform elongation of the 1/2-inch sheets. The X-ray tracing in figure 20(a) shows this condition. Since differences are to be expected in driven metal rivets, the rubber analog indicates visually some of the possible effects.

The maximum stress which occurs near the edges for all sheets is about $1\frac{1}{2}$ times the average, while the minimum stress near the center line is about half the average. The effect of the rivet holes and rivets on the sheets between the rivets seems to be the same on the 1/2- and 1-inch sheets when under load. If the combination of rivet hole and rivet under load causes the stress at the center of the sheets to be one-third of that near the edge, as it appears to be in these rubber models, the resulting stress concentrations may explain, in part, the poor fatigue strengths of riveted connections.

In the three-rivet model the tensile stresses across the width of the sheets, together with the average stresses, are shown in figure 19. The load on the 1/2-inch sheet 1 is again greater than on the 1/2-inch sheet 2 as shown by the average stresses. The stresses for the 1-inch sheet between the upper rivets are considerably larger than for the 1-inch sheet between the lower rivets. The reverse is true for the 1/2-inch sheets where the larger stresses occur between the lower rivets. The X-ray tracing in figure 20(b) shows this condition. The smaller loads on the 1/2-inch sheets occur near sections MN, NO, and OP (fig. 17(b)) while the larger loads occur near sections FG, GH, and HI. On the 1-inch sheet, the smaller loads are at sections FG, GH, and HI

and the larger, at sections MN, NO, and OP. The combination of rivet hole and rivet again produces the same stress-concentration effect under load as it does in the two-rivet model. The minimum stress near the center of the sheet is about one-third the maximum stress near each edge.

The threads in the experimental models apparently carried a portion of the load; when they were removed the bending action in both sheets and rivets (observations made at beginning of this section) was more pronounced.

Failures in fatigue through a row of rivet holes near a free edge (fig. 21) in the outer plates of a lap joint may be explained by observation (2). Under repeated loading the free ends continually bend apart and straighten so that the net section through the rivet hole, with its several possible stress concentrations, quickly becomes a victim of fatigue. With local shear and bending displacements along the length of the rivet (fig. 15(a)), it is improbable that the stress distribution is constant throughout the thickness of the sheet. It seems more probable that stress concentrations around the circumference of each rivet hole exceed, in some parts of each sheet, the values obtained from theory or from photoelastic studies based on uniform distribution throughout the thickness of the sheet or on uniform bearing along the length of the rivet. This bending apart of the cover plates in aluminum-alloy joints has been reported by Francis (ref. 7), but such effects as nonuniform bearing between rivet and sheet are not apparent in metal test specimens, nor can they be measured when their presence is suspected. Because of the behavior of foam rubber in compression (bearing) these effects are not determinable quantitively in rubber-analog specimens, but their existence is indicated qualitatively by the X-ray images of the distorted sheets and rivets.

The distortion of the cross-sectional area of the rivet shank (observation (1)) and the distortion of the rivet head (observation (3)) under load indicate the severe conditions that a rivet undergoes. Failures in rivet heads and rivet shanks in fatigue can be traced to such strains. It is not only a question of the load applied to the rivet but of the interaction of the plates and rivets on one another.

Local failure of sheet material around rivet heads, where the rivet heads pull through the cover plates under loading, may be explained by observations (4) and (5).

Observation (6) was checked experimentally as previously explained. The visual indication of the bent rivets with their very pronounced differences in amount of bending leaves no doubt that the load distribution is anything but uniform in a multirivet joint loaded to produce stresses in the elastic range.

The fact that designers desire methods that relate the fatigue strengths of riveted joints to their static strengths has led engineers to try to correlate repeated-load test data with the results of single-application loads which were increased until the joint failed. Such attempts at correlation have been unsatisfactory, and there are at least three reasons for this. In the first place, most repeated loads cause stresses in the elastic range and result in different distributions of load among a group of rivets than the distributions found when parts of the joint are stressed in the plastic range so that overstressed areas undergo displacements which tend to equalize the loads acting on the rivets. Efforts to correlate data from two joints, one having two rivets and the other three, are obviously fruitless if each rivet in the two-rivet assembly is assumed to carry one-half the load while each one in the three-rivet joint takes one-third. The most stressed in the latter group will probably carry about three-eighths of the load and that will not be transmitted to the sheet in any simple manner.

Efforts to obtain correlation by including stress concentration factors computed on the assumption of a uniform distribution of stress throughout the thickness of a riveted sheet would also appear to be fruitless if the bearing between sheet and rivet is concentrated near the faying surface as is indicated by the rubber analog or if stresses of appreciable magnitude are produced in the sheet near the rivet holes by the bending of the "free" ends of the sheet. Such factors have not been considered in the past nor are there sufficient data in hand from the tests on the rubber specimens to permit quantitative evaluation of them at present. Evidence of their existence has, however, been obtained and further study will undoubtedly lead to methods for evaluating their effects. Until rational procedures have been developed to take such effects into account, little success can be expected from correlations of test data obtained from joints having different arrangements of "identical" rivets. The neglected variables in the problem are, apparently, not negligible. There are probably others not brought out by these tests.

It is almost certain, though no tests have been made to show it, that the heads of countersunk rivets would have different clamping effects from those of the round heads used in these tests and, hence, that the bending of the rivet shank and the distribution of bearing stress along it would differ from those of the rivets tested. It is equally probable that rivets which are driven hot, which shrink when they cool and clamp the faying surfaces tightly enough to transmit part of the load by friction between sheets, will also produce differences in the primary factors affecting load distribution and in the secondary effects which produce local stress concentrations. There are many factors yet to be determined quantitatively that affect the static strengths and endurance limits of riveted, bolted, or spot-welded joints, but it is believed that the rubber analog, with its greatly exaggerated deformations, can be very helpful in indicating which of the possible variables are significant and which are unimportant.

The load distribution among the rivets was the simplest action of the joint that could be determined quantitatively by direct measurement of local displacements on the rubber specimens. Attempts to measure other actions were complicated by locating markers so that they could be readily identified on the X-ray negatives or by the need to overcome problems associated with the three-dimensional nature of the stress concentration factors. Despite this, the ability to see what happens within the parts of a riveted joint under load permits qualitative evaluation of effects which must be considered if design methods are to be revised. Careful use of X-ray photography will produce negatives from which the complex interactions of sheets and rivets represented in the rubber analog can be clearly seen and studied, and, if the test apparatus is constructed so that the model can be X-rayed in both plan and edge view, a fairly complete indication of the joint behavior under load may be obtained.

No attempt was made to vary the geometry of the joint by changing rivet size, rivet spacing, stagger, sheet thickness, sheet length, and so forth. The round-head rivet was the only type used because of the low stiffness of this foam rubber. Stiffer rubbers can be obtained, but no studies were made with them. The two- and three-rivet double lap joints were selected because they represented a type of joint in general use that would yield information representative of multirivet joints without the stress concentrations due to bending which would be expected in a single lap joint. This same type, with four or more rivets, was considered for tests, but the limitations of the X-ray equipment available prevented the use of the longer specimens. Only one rivet was used in each row since results from actual metal joints indicate that the load distribution in a riveted joint having several lines of several rivets each is essentially identical in each line. The marking system and interpretation of data were obviously simplified by this means.

The use of a rubber analog in the study of riveted joints is subject to certain limitations. The tensile modulus of the rubber is of the order of one-millionth of that of aluminum alloys and the shear modulus, of the order of one two-millionth. Tensile stresses in the rubber are about one five-thousandth of those in an aluminum-alloy joint. Poisson's ratio is close to the value for aluminum alloys but is directional so that some effects are distorted. The low moduli cause all effects in a rubber model to be exaggerated, whereas the low stresses tend to reduce displacements. The more significant effects are magnified in the rubber so that they are about 500 times those in the metal. Foam rubber is best used in tension models since its ability to resist buckling under compressive loading is very low and its modulus of elasticity in compression is not the same as it is in tension. The load on a rubber model must be kept small to insure that the stress does not exceed the elastic limit, yet enough load must be

used to overcome any slack in the test section. It was found from tests that the model did not behave properly if the load was too low and it was found necessary to use load enough to insure that all slack would be taken up.

Conclusions

Exploratory tests using the rubber analog have provided another means of studying the action of riveted joints. The models allowed a closer study of the interactions of parts of the joint because of their greatly exaggerated displacements and because the X-ray method showed what happened inside the sheets and rivets. The following conclusions have been reached from the results of these tests:

(1) In a multirivet joint, a load in the elastic range is not distributed uniformly among the rivets in a line. The outer rivets carry a large part of that load and the inner rivets are lightly loaded.

(2) The maximum stresses across the sheets on a cross section of a joint between rivets occur near the edges and are about $1\frac{1}{2}$ times the average stress on that section.

(3) There is a tendency for the cover sheets to bend apart at their free ends under load. This condition, coupled with the stress concentrations occurring in the end rivet holes, probably explains the common fatigue failure of these cover sheets on cross sections which pass through the end rivet holes.

(4) The problem of stress distribution around the rivet hole and rivet shank is three-dimensional and not amenable to elementary mathematical analysis. The present experimental method gives a visual indication of the actions involved and can probably be developed to yield information useful in a more elaborate mathematical analysis.

(5) Complete static tests, including the determination of material properties and the dimensions of each sheet and rivet in each specimen, should be made on each type of joint for which fatigue tests are to be conducted so that static strength data may be available for eventual correlation with results of the fatigue tests.

(6) A single-row lap joint is not recommended for use under fatigue conditions because its low bending stiffness and eccentric loading produce local stresses which result in a poor fatigue resistance.

(7) If several rivets lying on an axis parallel to the line of action of the load are defined as a "line" and several lying on a

perpendicular axis, as a "row," it is better for both static and fatigue conditions to design a joint to have several lines of few rows rather than to have several rows in few lines. There will then be fewer "inactive" rivets near the center of each line, so that a more efficient distribution of load will be obtained.

Massachusetts Institute of Technology,
Cambridge, Mass., April 14, 1952.

APPENDIX A

METHOD OF COMPUTING NORMAL AND SHEAR STRESSES

The tearing stresses were not measured since their effect on the normal and shearing stresses is assumed small and since they would require a calculation for each square involving Poisson's ratio which in the case of foam rubber is directional (table I).

The normal stress was taken as the difference between the lengths of the side of a square in the direction of pull for the load and no-load conditions. The stress was then obtained from the relation $f_t = E\epsilon_t$ where E is the modulus of elasticity of the rubber determined from figure 2 and ϵ_t is the strain in the direction of load.

Assuming that all angular distortion is attributable to shear and that the square deforms symmetrically, the shear strain γ_{xy} can be found from measurement of the diagonals and sides of the square. This distortion is shown in the following sketch:

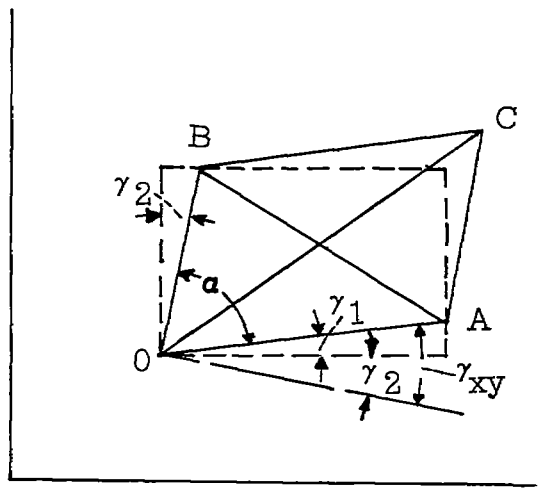

Application of the law of cosines to the above sketch results in the expressions

$$\overline{BA^2} = \overline{OA^2} + \overline{OB^2} - \overline{2OA}\ \overline{OB} \cos \alpha$$

$$\overline{OC^2} = \overline{OA^2} + \overline{OB^2} + \overline{2OA}\ \overline{OB} \cos \alpha$$

Combining and assuming small angular displacements,

$$\frac{\overline{OC^2} - \overline{BA^2}}{4(\overline{OA})(\overline{OB})} = \cos \alpha = \cos\left(90^\circ - \gamma_{xy}\right) = \sin \gamma_{xy} = \gamma_{xy}$$

The stress was then obtained from the relation $f_s = G\gamma_{xy}$, where G is the modulus of rupture of the rubber determined from figure 4 and γ_{xy} is the strain calculated as above.

In practice, average lengths were used in the determination of normal and shear stresses where symmetry was lacking. In addition, all curved lengths were approximated by their chords. The degree of approximation inherent in these assumptions would have been reduced if the size of rectangle used in the grip had been smaller.

APPENDIX B

CEMENTED-JOINT ANALYSIS

The transmission of load by cemented joints is a continuous though not constant function, whereas that by a mechanical joint having bolts or rivets is discontinuous; hence, the former should be the more amenable to mathematical analysis. Exact procedures, however, are cumbersome and often involve impracticable computational labor. The method which follows is based in part on exact relations and in part on simplifying assumptions.

Consider two sheets to be cemented along the surface AB as shown in figure 22(a). Since the lines of action of the forces P are not coincident so long as one sheet lies above the other, the sheets will bend until the forces come into line. Moments M_1 and M_2 will be developed as indicated. These will be divided between the sheets in some way dependent upon the relative stiffnesses, coefficients α and β, of the two sheets as shown in figures 22(b) and 22(c). The axial forces will also be distributed in accord with the sheet thicknesses or areas, as represented by the coefficients γ and Δ. The combined effects will be those produced by adding the force and moment systems of figure 22(b) to those of figure 22(c).

Study of these systems shows that the axial forces in figure 22(b) produce shear along the faying surfaces while the moment system in figure 22(c) tends to peel one sheet from the other causing both tension and shear in the cement. The moment system in figure 22(b) tends to bend the sheets to produce shear between elements adjacent to surface AB, and the axial forces in figure 22(c) cause some shear if $\Delta_1 \neq \Delta_2$ since the two sheets will not undergo identical axial strains. Each of these effects is present, and all should be taken into account in an exact analysis. The effects of the bending are ignored because the faying surface of the joint in figure 6(b) shows practically no bending displacement and the analysis is based on the relative motions of the flat sheets shown in the simple lap joint of figure 23 or the double lap joint of figure 24.

If cross sections which are planar under zero load remained planes under load P, the section abcd, at the origin in figure 23, would be displaced to abc'd' because of the strain in the adhesive under the shear stresses f_s. However, these shear stresses do cause strains within the sheets so plane ab is curved to ab" and plane c'd', to c"d'. The shear stress f_s in the cement is somewhat reduced by this warping of planar sections in the sheets. The displacement U_O is the projection of ad' on the plane of the cement, and the stress f_s depends upon the shear strain represented by angle b"c"c.

The loads P are transmitted between the sheets so that the force carried by the upper sheet at a section x-units from the origin is $P_1 = \int_0^x f_s w \, dx$ where w is the joint width. The force remaining in the lower sheet is then $P_2 = P - P_1 = P - \int_0^x f_s w \, dx$.

Then plane mnop in the unloaded joint is displaced to become m'n'o'p' when abcd is displaced to abc'd'. Plane m'n' in the upper sheet moves to m"n" because of the tension due to P_1, then to m"s because of the shear stress in sheet 1. At the same time, o'p' is displaced to o"p" by the axial force P_2 and to p"v by the shear in sheet 2. The complement of the angle nsv is a measure of the shear strain in the cement and its tangent is U/t_c where $U = U_0 + U_1 - (U_2 + U_3 + U_4)$. The displacements $U_0, \ldots U_4$ are shown in figure 23 to represent these various displacement components. Since the shear stress f_s in the cement may be found from $f_s = G_c U/t_c$, where G_c and t_c are the shear modulus of elasticity and thickness of the cement, respectively, it is necessary to obtain expressions for each displacement component.

The initial movement of the lower sheet with respect to the upper is represented by U_0, the displacement of the origin of coordinates in the lower sheet with respect to that in the upper. This displacement U_0 does not vary with x.

The longitudinal movement of plane mn due to the elongation of sheet 1 between 0 and x under the axial load $P_1 = \int f_s w \, dx$ is represented by U_1. Under the tensile stress f_t an element of length dx such as that shown in figure 25 would elongate $dU_1 = f_t \, dx/E$. Over the distance x this elongation would be $U_1 = \int_0^x (f_t/E) dx$ or,

since $f_t = P_1/A = \int_0^x (f_s w/wt_1) dx = \int_0^x (f_s/t_1) dx$,

$$U_1 = \int_0^x \int_0^x (f_s/t_1 E) dx \, dx \qquad (1)$$

Equilibrium in the element of figure 25 requires that shear stress f_s' on longitudinal plane qr be $f_s' = f_s - (df_t yw)/w\,dx$. It also requires that $-f_t wt_1 - f_s w\,dx + (f_t + df_t)wt_1 = 0$ and, hence, that $df_t/dx = f_s/t_1$. This leads to $f_s' = f_s(1 - y/t_1)$ so that the displacement n"s = U_2 at the faying surfaces becomes

$$U_2 = \int_0^{t_1} f_s'\,dy/G = f_s t_1/2G \tag{2}$$

Similar manipulation of the displacements for the lower sheet yields

$$\left.\begin{aligned} U_3 &= \int_0^x \left[\frac{P}{wt_2E} - \int_0^x (f_s/t_2E)dx\right]dx \\ U_4 &= f_s t_2/2G \end{aligned}\right\} \tag{3}$$

The expression for displacement U is then

$$U = U_0 + \int_0^x \int_0^x \frac{f_s}{t_1 E}\,dx\,dx - \frac{f_s t_1}{2G} - \int_0^x \left(\frac{P}{wt_2E} - \int_0^x \frac{f_s}{t_2E}\,dx\right)dx - \frac{f_s t_2}{2G} \tag{4}$$

Differentiating this expression twice with respect to x yields

$$\frac{d^2U}{dx^2} = \frac{f_s}{E}\left(\frac{1}{t_1} + \frac{1}{t_2}\right) - \frac{d^2 f_s}{dx^2}\left(\frac{t_1 + t_2}{2G}\right)$$

Since the shear stress in the cement is $f_s = G_c U/t_c$, it is apparent that $d^2U/dx^2 = (t_c/G_c)(d^2 f_s/dx^2)$; so equation (4) may be written

$$\frac{d^2 f_s}{dx^2} - k^2 f_s = 0 \tag{5}$$

if k^2 represents

$$k^2 = \frac{2GG_c(t_1 + t_2)}{Et_1t_2\left[2Gt_c + G_c(t_1 + t_2)\right]} \tag{6}$$

The solution for equation (5) is

$$f_s = a_0 \cosh kx + \frac{a_1}{k} \sinh kx \tag{7}$$

and the displacement U becomes

$$U = \frac{t_c}{G_c}\left(a_0 \cosh kx + \frac{a_1}{k} \sinh kx\right) = a_2 \cosh kx + \frac{a_3}{k} \sinh kx \qquad (8)$$

To establish the constants of integration, let $dU/dx = -P\beta/A_2E$ at $x = 0$ and $P\beta/A_1E$ at $x = L$, β being equal to $2Gt_c/\left[2Gt_c + G_c(t_1 + t_2)\right]$. Simple substitution gives $a_3 = -P\beta/A_2E$ and $a_2 = (P\beta/kE \sinh kL)(1/A_1 + \cosh kL/A_2)$. Since $a_0 = G_c a_2/t_c$ and $a_1 = G_c a_3/t_c$, these are readily obtained. Then, from equation (7),

$$f_s = \frac{G_c P\beta}{t_c kE}\left[\frac{\cosh kx}{\sinh kL}\left(\frac{A_2 + A_1 \cosh kL}{A_1 A_2}\right) - \frac{\sinh kx}{A_2}\right] \qquad (9)$$

This may be simplified to

$$f_s = f_{s_{av}} \frac{kL}{\sinh kL}\left[\frac{t_2 \cosh kx + t_1 \cosh (kL - kx)}{t_1 + t_2}\right] \qquad (10)$$

when it is observed that $f_{s_{av}} = P/wL$ and that $A_1 = wt_1$ and $A_2 = wt_2$. With $t_2 = nt_1$, and $f_s = f_{s_{max}}$ at $x = 0$ or $x = L$, equation (10) becomes

$$f_{s_{max}} = f_{s_{av}} \frac{kL}{\sinh kL}\left(\frac{n + \cosh kL}{1 + n}\right) \qquad (x = 0) \qquad (11a)$$

$$f_{s_{max}} = f_{s_{av}} \frac{kL}{\sinh kL}\left(\frac{n \cosh kL + 1}{1 + n}\right) \qquad (x = L) \qquad (11b)$$

A glance at a table of hyperbolic functions shows that sinh kL is very nearly equal to cosh kL for $kL > 6$ and that both are very large compared with n or 1, so that the ratio $f_{s_{max}}/f_{s_{av}}$ for $kL > 6$ is very nearly

$$f_{s_{max}}/f_{s_{av}} = \frac{kL}{1 + n} \qquad (x = 0) \qquad (12a)$$

$$f_{s_{max}}/f_{s_{av}} = n\left(\frac{kL}{1 + n}\right) \qquad (x = L) \qquad (12b)$$

The end of the joint at which the thicker sheet is discontinued therefore carries the greater shear stress.

The rate of shear flow across the joint is not uniform, but the force transmitted between sections x_1 and x_2 is $F = \int_{x_1}^{x_2} f_s w \, dx$, or

$$F = \frac{PG_c\beta}{t_c kE}\left\{\frac{t_2(\sinh kx_2 - \sinh kx_1) + t_1\left[\sinh (kL - kx_1) - \sinh (kL - kx_2)\right]}{t_1 t_2 \sinh kL}\right\} \tag{13a}$$

which may be abbreviated to

$$F = PN \tag{13b}$$

where

$$N = \frac{t_2(\sinh kx_2 - \sinh kx_1) + t_1\left[\sinh (kL - kx_1) - \sinh (kL - kx_2)\right]}{(t_1 + t_2) \sinh kL}$$

Values of N are given in table II.

If the end of the joint at which the thicker of the two sheets is discontinued is taken as the origin of x and if the ultimate shear strength of the cement $f_{s_{max}}$ is known, the load P to start failure at the most stressed point in the joint $x = 0$ is

$$P = \frac{f_{s_{max}} wL}{kL}\left[\frac{(1 + n) \sinh kL}{n + \cosh kL}\right] \tag{14}$$

The maximum shear stress at $x = 0$ will be

$$f_{s_{max}} = kLf_{s_{av}}\left[\frac{n + \cosh kL}{(1 + n) \sinh kL}\right] \tag{15}$$

Table III presents values of $(1 + n) \sinh kL/kL (n + \cosh kL)$ for use in equations (14) and (15) which are shown in graph form in figure 26. With the values kL and n known, the ratio of $f_{s_{av}}/f_{s_{max}}$ can be obtained directly. It should be noted that $\sinh kL/(n + \cosh kL)$ has a value very close to unity when kL is equal to or greater than 6. A value of k suitable for use with joints of various lap lengths may

therefore be obtained from equation (15) if test data are available to give failing loads P for specimens of sufficient length for this load to reach an essentially constant value. The equation is

$$k = \frac{(1 + n)f_{s_{max}}}{Lf_{s_{av}}} \tag{16}$$

To determine $f_{s_{max}}$ for a new cement, test a series of specimens having lap lengths ranging from 1/8 or 1/4 inch to 2 or 3 inches. Divide the loads at failure by the joint areas to obtain the average shear stresses $f_{s_{av}} = P/wL$. Plot $f_{s_{av}}$ versus joint length L, draw a curve through the plotted points, and extrapolate it to intersect the f_s-axis at $L = 0$. The value of $f_{s_{av}}$ at $L = 0$ may be taken to be $f_{s_{max}}$. The procedure will be illustrated subsequently.

When the properties and dimensions of the cement and the sheets in a given joint are all known, k may be determined without recourse to a series of tests. Equation (6) is the analytical expression for k^2.

At the present time, values of the shearing modulus of elasticity G_c for the commonly used adhesives are not well established. Few data are available as to the values of t_c or $f_{s_{max}}$ which may be expected in practice, though t_c ordinarily runs between 0.005 and 0.010 inch. It is possible to obtain values of G_c from test data by use of the following equation:

$$G_c = \frac{t_c k^2 E n t_1}{(1 + n)\left(1 - \frac{k^2 E n t_1^2}{2G}\right)} \tag{17}$$

when all values except G_c are known.

To illustrate the use of the preceding equations, consider the set of test data on the simple lap joints reported by De Bruyne (ref. 1). For the 0.0425- by 1.00-inch Duralumin specimens the following values are given for the loads producing failure on joints of various lengths:

L	$P_{observed}$	$f_{s_{av}}$
0.125	712	5,700
.250	1,225	4,900
.375	1,550	4,130
.500	1,800	3,600
.625	2,075	3,320
.750	2,109	2,810
.875	2,070	2,390
1.000	2,050	2,050
2.000	2,057	1,030
3.500	2,050	585

By plotting $f_{s_{av}}$ against L and extending the curve drawn through the plotted points, $f_{s_{av}}$ at L = 0 is 6,700 psi. Assume this to correspond with the maximum shear stress in any joint in this set when the cement is at the point of rupture. Then, since n = 1 for specimens having sheets of equal thickness, equation (16) may be used to obtain k from the data on the longer specimens in the group if written

$$k = 2(6,700)/Lf_{s_{av}} = 13,400w/P_{observed}$$

Since the width w was 1 inch for these joints, $k = 13,400/P_{observed}$.

For the last four specimens, k is found to be 6.46, 6.54, 6.52, and 6.54, giving an average value of 6.515. The value of G_c, obtained from equation (17) for $E = 10.4 \times 10^6$, $G = 3.95 \times 10^6$, $t_c = 6 \times 10^{-3}$, n = 1.0, k = 6.515, and $t_1 = 425 \times 10^{-4}$ is $G_c = 62,600$ psi. This is somewhat lower than other values obtained from other tests on Redux cement. That may be due to an erroneous assumption for t_c since De Bruyne did not state the cement thickness for these specimens.

Recent tests in which t_c was known indicate G_c to lie between 100,000 and 125,000 psi. They also indicate $f_{s_{max}}$ for Redux to be between 7,000 and 10,000 psi.

In order to indicate the applicability of equation (14) to the prediction of the loads required to produce failure, the equation was applied to the shorter specimens in De Bruyne's set on the assumption that k = 6.515 and $f_{s_{max}} = 6,700$ psi. The results are tabulated as follows:

L	kL	$\frac{2 \sinh kL}{1 + \cosh kL}$	$P_{predicted}$	$P_{predicted}/P_{observed}$
0.125	0.8144	0.768	790	1.11
.250	1.629	1.356	1,395	1.14
.375	2.443	1.680	1,730	1.12
.500	3.258	1.846	1,900	1.06
.625	4.072	1.928	1,980	.955
.750	4.886	1.968	2,025	.960
.875	5.701	1.986	2,040	.985
1.000	6.515	1.993	2,050	1.00

The last column shows that the predicted loads exceed the test values for the shorter specimens and that the unconservative error of 14 percent is greater than could be desired. This error may result from the fact that k is based on data from specimens stressed beyond the proportional limit of the metal and used with specimens stressed in the elastic range. The agreement is far better over the entire range than it would have been had any of the values of $f_{s_{av}}$ computed from the tests been taken as an "allowable" stress to be multiplied by the area of the cement in order to obtain the load at failure.

The preceding equations can be used to some extent on the present test data from the cemented magnesium lap joints. Since a series of specimens of varying lap lengths was not available, equations (11b) and (6) were plotted on a common k-scale for several assumed values of $f_{s_{max}}$ and G_c. The point of intersection of the resulting curves gave the desired values of $f_{s_{max}}$ and G_c. With the following data for single lap specimen 1, $w = 0.92$ inch, $L = 1$ inch, $f_{s_{av}} = 2{,}100$ psi, $k = 2.855$, $f_{s_{max}} = 3{,}370$ psi, $n = 1$, and $G_c = 102{,}000$ psi, equation (14) gives

$$P = \frac{(3{,}370)(0.92)(1)}{(2.855)(1)}\left[\frac{(1 + 1)\sinh(2.855)(1)}{1 + \cosh(2.855)(1)}\right]$$

$$= 1{,}934 \text{ lb}$$

The actual failing load for this specimen was 1,936 pounds.

In the case of the double lap specimen 1, using the preceding method for determining $f_{s_{max}}$, k, and G_c, the data are as follows:

$w = 0.99$ inch, $L = 1$ inch, $f_{s_{av}} = 3{,}910$ psi, $k = 4.40$, $f_{s_{max}} = 9{,}110$ psi, $n = 0.093$, and $G_c = 99{,}100$ psi. Equation (14) yields

$$P = \frac{(9{,}110)(0.99)(1)}{(4.40)(1)}\left[\frac{(1 + 0.93)\sinh(4.40)}{0.93 + \cosh(4.40)}\right]$$

$$= 3{,}852 \text{ lb}$$

The actual failing load for this specimen was 3,910 pounds. Slight variations in the thickness of the plates and the cover plates and slight variations in the dimensions of the cemented area probably account for the small difference between the actual and the calculated failing loads.

The following data for a thin gage 2024-T alclad sheet cemented single lap joint were analyzed by the above method: $t_1 = t_2 = 0.0392$ inch, $n = 1$, $w = 0.984$ inch, $L = 0.511$ inch, $t_c = 0.0055$ inch, $f_{s_{av}} = 4{,}427$ psi, $f_{s_{max}} = 10{,}110$ psi, $k = 8.735$, and $G_c = 101{,}000$ psi. Thus,

$$P = \frac{(10{,}110)(0.984)(0.511)}{(8.735)(0.511)}\left[\frac{(1 + 1)\sinh(8.735)}{1 + \cosh(8.735)}\right]$$

$$= 2{,}276 \text{ lb}$$

The actual failing load for this specimen was 2,226 pounds.

The formulas derived here for studying the behavior of cemented joints must be used with caution. In this analysis $f_{s_{max}}$ and k were determined from a single specimen, not a family of specimens as described previously. Therefore, these values were correct only for that one specimen and should not be applied to others of different lap lengths or cement thicknesses. The value of $f_{s_{max}}$ for a cement should be a constant and should not be appreciably affected by thickness of cement or sheet. However, $f_{s_{max}}$ varies widely for these three specimens although all are Redux bonded. The variation was felt to be too great to attribute solely to approximations in the determination of its value. An explorative analysis of the effects of bending action in these joints (made in appendix C) shows bending to be of major importance in the single lap specimens, which explains, in part, the discrepancies between $f_{s_{max}}$ for single and double lap joints.

Equation (13b) indicates that the force F transmitted across the cement between x_1 and x_2 is directly proportional to the coefficient N, and the values of N for $kL = 1.0$ in table II show that N

increases about 0.10 for each 0.1L increment in x/L. The conclusion may be drawn that the stress distribution over the length of the cemented joint is essentially uniform when $kL = 1.0$ or less. This is possible in joints between wooden members of practicable length but not between metal members.

Consider two members of aircraft spruce, each 1 inch thick, so that $t_1 = t_2 = 1$ and $n = 1$. Take $E = 1{,}300{,}000$ psi, $G = 100{,}000$ psi, $G_c = 100{,}000$ psi, and $t_c = 0.006$ inch. Reference 22 gives $E = 1{,}950{,}000$ and G between 72,000 and 104,000 for aircraft spruce at 12-percent moisture, but the value for E in most specifications and lists of properties is 1,300,000. The assumed values are, in any case, reasonable.

When $G_c = G$, and $t_1 = t_2 = n = 1$, equation (6) for k^2 may be written

$$k^2 = 2G/E\left[t_1^2(t_c + t_1)\right] = 2G/E(t_c + 1)$$

Since t_c is very small as compared with 1, k^2 may be taken equal to $2G/E$. For the joint under consideration, $k^2 = 200{,}000/1{,}300{,}000$ or $k = 0.392$. Hence, for $L = 2.5$ inches or less, $kL = 1.0$ or less, and the shear stress along the joint would be essentially uniformly distributed. The error resulting from an assumption of uniform stress distribution for joints between wood members somewhat longer than this would not be great, and it would be reduced as the thickness of the members increased.

Next consider a joint between two sheets of 2024-T4 aluminum alloy having $E = 10{,}500{,}000$ psi, $G = 4{,}000{,}000$ psi, $t_1 = t_2 = 0.040$ inch, and $n = 1$. Assume $G_c = 100{,}000$ psi and $t_c = 0.006$ inch. Then, k^2 as computed from equation (6) becomes 68.03, and k, about 8.25. To obtain $kL = 1.0$ for an approximately uniform shear stress in the cement, the lap length would be less than 1/8 inch which is possible but not practicable for structural purposes.

It is seen, then, that the assumption of uniform distribution is tenable for materials having values of G approximately equal to those of G_c but not for those having large values of G as compared with G_c. Other factors enter the problem, but the ratio G/G_c is the important one for members of normal proportions in the various materials used in aircraft structures.

The tensile or tearing stress transmitted across the cement between sheets may be approximated (for more exact equations see ref. 15) by the method often used to obtain shear flows. An element y-units from the origin in the section shown in figure 27 carries the shear stress f_s

which, from the development of equation (2), is $f_s' = f_s(t_1 - y)/t_1$. The shear force S on plane m'n' is then

$$S = \int_0^{t_1} f_s' w \, dy = f_s w t_1/2 \tag{18}$$

The tearing stress f_{te} between points x_1 and x_2 on the cemented surface will be $(S_2 - S_1)/(x_2 - x_1)w$; whence, with f_s from equation (10) and $t_2 = nt_1$,

$$f_{te} = \frac{f_{s_{av}} t_1 kL\left\{n(\cosh kx_2 - \cosh kx_1) + \left[\cosh(kL - kx_2) - \cosh(kL - kx_1)\right]\right\}}{2(x_2 - x_1)(1 + n)\sinh kL} \tag{19}$$

This stress will be greatest where the shear stress is greatest, at the end of the joint where the thicker sheet is discontinued.

A symmetrical, double lap joint such as that shown in figure 24 may be considered to be separated along the plane of symmetry so that each half may be analyzed by the above equations, or the equations may be readily modified to apply to that type of connection.

APPENDIX C

A CONSIDERATION OF PROBLEMS INTRODUCED BY BENDING AT ENDS OF SINGLE LAP JOINTS

Consider the single lap cemented joint shown in figure 28(a). When it is put into a testing machine and subjected to an axial tensile load P, it bends so that the lines of action of the forces P pass through the specimen approximately as indicated in figure 28(b). The actual curves of deflection of the centroidal axes of the three segments, AB, CDE, and FG, will be such as to produce a minimum change in the strain energy of the system. For sheets of unequal thickness a minimum energy analysis would be required for the evaluation of moments M_1 and M_2 at the ends of the specimen, and this analysis would require a knowledge of the characteristics of the jaws of the testing machine since they will affect both the slopes and moments at A and G.

To avoid the need for such data, assume the sheets in the joint to be of equal thickness but thin enough that the tangents to the elastic curve at A and G will coincide with the line of action of the loads when P is relatively large. Point D in such a specimen will lie on the line of action of loads P, and points B and F will lie near it. Assume the deflection of B to be $(1 - \alpha)t/2$ and that of C to be $\alpha t/2$, where α has a value close to unity. Since the centroidal axes of segments AB and CDE are offset, the moment on the cross section of the single sheet at B is not equal to that on the two-sheet segment at C. The moment of inertia of the two-sheet "beam" is eight times that for the single-sheet, so the radii of curvature of the two segments differ. The displacements occurring in the cement at the end of the top sheet are shown in figure 29.

Plane abcd before loading becomes ab'c'''d" under load. The shear stress f_s on the faying surface of the upper sheet warps plane ab to ab'. The axial tensile stress in the lower sheet causes cd to move axially to c'd' and the bending rotates it to c"d". Then the shear stress f_s on the faying surface of the lower sheet warps c"d" to c'''d". The original plane bc at the end of the cement is displaced to b'c'''. Since arc cc'c''' has a smaller radius of curvature than bb', the thickness of the layer of cement tends to increase with increasing distance to the left of bc. Tensile stresses normal to the faying surfaces are therefore developed in the cement in addition to the shear stresses. The combination produces a concentration of stress at the end of the lap which tends to start failure in the joint.

Similar effects are to be expected in riveted joints, effects which tend to separate the sheets beyond the outer rivets and, hence, to apply forces tending to bend rivet shanks, to pry off rivet heads, and to produce nonuniform bearing between the shank and the edge of the hole so that the actual concentration of stress in a sheet adjacent to a rivet hole becomes a highly indeterminate problem. It would appear that the simplifying assumptions customarily made in the analysis of riveted joints, and the use of stress concentration factors based on two-dimensional stress variations, are misleading and dangerous.

An exact analysis of either a cemented or a riveted joint seems impossible at this time, but it is possible to provide for some of the effects just noted and to do so in a way that will indicate the order of magnitude of the stresses involved, though not their correct values.

To do so, set up equations for the moments on the segments of the specimen shown in figure 28(b). For segment AB

$$M_x = M_1 + (M_2 - M_1)x/S + Py$$

or, since $M_2 = -M_1$,

$$M_x = M_1\left[1 - 2(x/S)\right] + Py \tag{20}$$

At B, $x = (S - L)/2$ and $y = (1 - \alpha)t/2$, so that

$$M_B = M_1(L/S) + (1 - \alpha)Pt/2 \tag{21}$$

and, at C,

$$M_C = M_B + \alpha P(t/2) = M_1(L/S) + (1 - 2\alpha)Pt/2 \tag{22}$$

The moment between C and E is $M_{x'} = M_C + (M_2 - M_1)(x'/S) + Py'$, and, since $M_2 = M_1$, this becomes

$$M_{x'} = M_1\left[(L - 2x')/S\right] + Py' \tag{23}$$

This indicates $M_{x'} = 0$ at $x' = L/2$ (at point D), as it should since the system is antisymmetrical about a plane through D.

If equation (20) is differentiated twice with respect to x,

$$d^2M_x/dx^2 = P\, d^2y/dx^2$$

But $M_x/EI = d^2y/dx^2$ for stresses below the proportional limit, so

$$d^2M_x/dx^2 - PM_x/EI = 0$$

The solution of this equation gives

$$M_x = C_1 \sinh(x/j) + C_2 \cosh(x/j) \tag{24}$$

where $j = \sqrt{EI/P}$. Had the axial load been compressive instead of tensile, the functions would have been circular instead of hyperbolic.

At $x = 0$, $\sinh x/j = 0$, $\cosh x/j = 1$, and $M_x = M_1$ so $C_2 = M_1$. At $x = 0$, the shear $dM_x/dx = -2M_1/S = \frac{C_1}{j}\cosh(x/j) + \frac{C_2}{j}\sinh(x/j)$; hence,

$$M_x = -2M_1(j/S)\sinh(x/j) + M_1 \cosh(x/j) \tag{25}$$

If the same operations are performed on equation (23) and if $j' = \sqrt{EI'/P}$,

$$M_{x'} = C_3 \sinh(x'/j') + C_4 \cosh(x'/j') \tag{26}$$

At $x' = 0$, $M_{x'} = M_C = C_4$, and, at $x' = L/2$, $M_{x'} = 0$; hence,

$$M_{x'} = \frac{-\left[\frac{M_1 L}{S} - (1 - 2\alpha)\frac{Pt}{2}\right]\cosh(L/2j')}{\sinh(L/2j')}\sinh(x'/j') + \left[\frac{M_1 L}{S} - (1 - 2\alpha)\frac{Pt}{2}\right]\cosh(x'/j') \tag{27}$$

Equations (25) and (27) involve the unknowns M_1 and α. By inserting equation (25) into equation (20) and equation (27) into equation (23) and solving for y and y' and then by substituting $x = (S - L)/2$ and $x' = 0$ in these expressions, y_B and y_C' are obtained. Since $y_B + (t/2) = y_C'$, it is then possible to obtain M_1 in terms of α. The result is

$$M_1 = \frac{Pt(1 - \alpha)}{\frac{S - L}{S} - 1 - \frac{2j}{S}\sinh\left(\frac{S - L}{2j}\right) + \cosh\left(\frac{S - L}{2j}\right)} \tag{28}$$

If α is taken as unity, $M_1 = 0$. If α is some value less than unity, as it is presumed to be, substitution of equation (28) into equation (21) gives

$$M_B = -Pt(1 - \alpha)\left[\frac{L/S}{\cosh\left(\frac{S - L}{2j}\right) - \frac{2j}{S}\sinh\left(\frac{S - L}{2j}\right) - \frac{L}{S}} + \frac{1}{2}\right] \tag{29}$$

In order to explore the probable magnitudes of M_B, assume that the ratio of specimen length to lap length S/L is 5, and consider that the material is aluminum alloy having $E = 10.5 \times 10^6$ psi. For one condition, assume $P/A = 8{,}750$ psi; for a second, take $P/A = 35{,}000$ psi. Since

$$j = \sqrt{EI/P} = \sqrt{EAt^2/12P} = \frac{t}{2}\sqrt{EA/3P}$$

$j = \frac{t}{2}\sqrt{\frac{10.5 \times 10^6}{2.625 \times 10^4}} = 10t$ for $P/A = 8{,}750$, and $j = 5t$ for $P/A = 35{,}000$ psi.

The first term in brackets in equation (29) then becomes

$$\frac{1/5}{\cosh\left(\frac{4L}{20t}\right) - \frac{20t}{5L}\sinh\left(\frac{4L}{20t}\right) - \frac{1}{5}}$$

or

$$\frac{1/5}{\cosh\left(\frac{4L}{10t}\right) - \frac{10t}{5L}\sinh\left(\frac{4L}{10t}\right) - \frac{1}{5}}$$

If L/t is taken as 2, 5, and 15 in the first expression, the values for the term are 3.36, 0.473, and 0.0278, respectively. Then $M_B/(1 - \alpha) = -3.86Pt$, $-0.973Pt$, and $-0.5278Pt$, respectively. For greater values of S/L these coefficients would be smaller, and for higher ratios of L/t they would approximate 0.50.

Using the same values for L/t in the second expression, the values 0.801, 0.0945, and 0.0011 are obtained. Then $M_B/(1 - \alpha) = -1.391Pt$, $-0.5945Pt$, and $-0.5011Pt$, respectively.

For a specimen of given width and thickness, these computations indicate that, with very short specimens and very short lap lengths, $S/t = 10$ and $L/t = 2$, the bending moment in the single sheet at the end of the lap does not vary in proportion to the load. Since the values of P have been assumed to vary by four to one, assume that $P = 1{,}000$ pounds in the first case and 4,000 pounds in the second and that M_B increases from $-3{,}860(1 - \alpha)t$ to $-5{,}204(1 - \alpha)t$, or about 35 percent. If this is even approximately correct, it is apparent that the proportions of the specimens used will have appreciable effects on the results obtained in fatigue tests. It seems reasonable to assume that similar effects could be expected on riveted, bolted, or welded specimens.

If S/L and L/t are each great enough that the first term in brackets of equation (29) is very small, M_B becomes $-(1 - \alpha)Pt/2$. The strain in a distance dx for the upper fiber of the lower sheet at section B is $-\epsilon\, dx = (M_B C/EI)dx = -\left\{\left[(1 - \alpha)Pt/2\right](t/2)\Big/(EAt^2/12)\right\}dx = -\left[3P(1 - \alpha)/AE\right]dx$ due to bending. The strain due to the tensile load is $-(P/AE)dx$, so the total strain at B is $-\left[P(4 - 3\alpha)/AE\right]dx$. Under the assumptions, $P = 0$ in the upper sheet at B, and the bending strain is zero because the point lies on the neutral axis of the lap-joint segment. The rate of strain in the cement at the end of the lap is therefore $-P(4 - 3\alpha)/AE$ if the effect of the transverse tensile stresses at that point is ignored. Then $dU/dx = -(4 - 3\alpha)P\beta/AE$ instead of the $-P\beta/AE$ used in going from equation (8) to equation (9). The maximum shear stress at $x = 0$ and $x = L$, since the sheets are of equal thickness, is therefore

$$f_{s_{max}} = (2 - 1.5\alpha)f_{s_{av}} \frac{KL}{\sinh KL}(1 + \cosh KL) \qquad (30)$$

No data are available for the probable magnitudes of α but it would be reasonable to assume values of 0.8 or 0.9 when investigating the changes in maximum shear stress when bending effects are included.

Although this analysis of the effect of bending on the action of a cemented joint contains several simplifying approximations and assumptions, and although it has been limited to lap joints in which the two sheets are of equal thickness, the results are believed to be of the right order of magnitude. If so, they provide a partial explanation for the discrepancies observed when specimens which are dimensionally similar, on the basis of "standard" methods of joint analysis, are tested under fatigue conditions. Further work must be done to determine the magnitudes of the errors in this analysis, or to develop more exact procedures, before satisfactory correlation of fatigue test data on

cemented joints can be expected. Such joints are "continuous" and amenable to mathematical analysis. Riveted, bolted, spot welded, and similar "discontinuous" joints will presumably be subject to nonuniform stress distributions analogous to those in cemented joints, and the resulting stress concentrations will be more serious because they will occur at points instead of in bands extending across the width of the specimen.

APPENDIX D

METHOD OF CORRECTING PARALLAX ON X-RAY NEGATIVE

Since the X-rays were emitted from a point source and were inclined as they passed through the rubber model to the X-ray negative, corrections had to be made to the displacements measured on the film in order to obtain the true elongations of the markers in the model. The displacement of a marker from the reference marker (described in the body of the text) was measured to a hundredth of an inch and corrected to obtain the true displacement by the following procedure:

Ray 1 from the X-ray source causes point A (fig. 30), a distance x_1 from the reference, in the rubber model to appear at point C on the X-ray negative, a distance x_1' from the reference. Under load, point A moves to A' and ray 2 causes A' to appear at C' on the negative, a distance x_2' from reference. The change in displacement in the model is

$$\Delta x = x_2 - x_1 \tag{31}$$

but, referring to the diagram,

$$x_1 = x_1' - h_1 \tag{32}$$

$$x_2 = x_2' - h_2' \tag{33}$$

Substituting equations (32) and (33) for x_1 and x_2 in equation (31) yields

$$\Delta x = (x_2' - h_2') - (x_1' - h_1) \tag{34}$$

From similar triangles ONC and ABC

$$\frac{D}{L} = \frac{h_1}{x_1'} \tag{35}$$

and from ONC' and A'B'C'

$$\frac{D}{L} = \frac{h_2'}{x_2'} \tag{36}$$

Introducing the expression for h_1 and h_2' from equations (35) and (36) into equation (34) gives

$$\Delta x = (x_2' - x_1')\left(\frac{L - D}{L}\right) \tag{37}$$

The term $x_2' - x_1'$ is the change in displacement between points C and C' on the X-ray negative corresponding to points A and A' in the model and when multiplied by the correction factor $\frac{L - D}{L}$ yields the actual change in displacement of a marker in the model under load.

REFERENCES

1. Vogt, F.: The Distribution of Loads on Rivets Connecting a Plate to a Beam Under Transverse Loads. NACA TM 1134, 1947.

2. Volkersen, Olaf: The Distribution of Forces on the Rivet in Stretched Joints With Constant Strap Cross Section. R.T.P. Translation No. 2373, British Ministry of Aircraft Production. Durand Reprinting Committee, C.I.T.; also, Rivet Load Distribution in Lap Joints of Constant Cross-Section Under Tension. R.T.P. Translation No. 2497, British Ministry of Aircraft Production. Durand Reprinting Committee, C.I.T. (From Luftfahrtforschung, Bd. 15, Lfg. 1/2, Jan. 20, 1938, pp. 41-47.)

3. Vogt, F.: The Load Distribution in Bolted or Riveted Joints in Light-Alloy Structures. NACA TM 1135, 1947.

4. Anon.: Structural Characteristics of Bonded Metal to Metal Lap Joints. Rep. No. MP 2020-2, Chance Vought Aircraft, June 1945.

5. Anon.: Distribution of Shear Stresses in Bonded Joints. Rep. No. 7441, Chance Vought Aircraft, Feb. 1948.

6. Rinker, R. C., and Kline, G. M.: Survey of Adhesives and Adhesion. NACA TN 989, 1945.

7. Russell, H. W., Jackson, L. R., Grover, H. J., and Beaver, W. W.: Fatigue Strength and Related Characteristics of Aircraft Joints. I - Comparison of Spot-Weld and Rivet Patterns in 24S-T Alclad Sheet - Comparison of 24S-T Alclad and 75S-T Alclad. NACA WR W-56, 1944. (Formerly NACA ARR 4F01.)

8. Russell, H. W., Jackson, L. R., Grover, H. J., and Beaver, W. W.: Fatigue Strength and Related Characteristics of Aircraft Joints. II - Fatigue Characteristics of Sheet and Riveted Joints of 0.040-Inch 24S-T, 75S-T, and R303-T275 Aluminum Alloys. NACA TN 1485, 1948.

9. Russell, H. W., Jackson, L. R., Grover, H. J., and Beaver, W. W.: Fatigue Strength and Related Characteristics of Joints in 24S-T Alclad Sheet. NACA WR W-63, 1944. (Formerly NACA ARR 4E30.)

10. Williams, D., Starkey, R. D., Leggett, D. M. A., Grinstead, F., and Jones, R. P. N.: The Use of Rubber Models in Stress Investigations. R. & M. No. 2433, British A.R.C., 1951.

11. Anon.: Rubber in Engineering. Chemical Pub. Co., Inc. (New York), 1946.

12. Burton, W. E.: Engineering With Rubber. McGraw-Hill Book Co., Inc., 1949.

13. Anon.: Handbook of Molded and Extruded Rubber. Goodyear Tire and Rubber Co., Inc. (Akron, Ohio), 1949.

14. De Bruyne, N. A.: The Strength of Glued Joints. Aircraft Eng., vol. XVI, no. 182, Apr. 1944, pp. 115-118.

15. Goland, M., and Reissner, E.: The Stresses in Cemented Joints. Jour. Appl. Mech., vol. 11, no. 1, Mar. 1944, pp. A-17 - A-27.

16. Jenkins, E. S.: Rational Design of Fastenings. SAE Jour., vol. 52, no. 9, Sept. 1944, pp. 421-429.

17. Rosenfeld, Samuel J.: Analytical and Experimental Investigation of Bolted Joints. NACA TN 1458, 1947.

18. Hill, H. N., and Holt, Marshall: Discussion of "Work of Rivets in Riveted Joints" by A. Hrennikoff. Trans. Am. Soc. Civil Eng., vol. 99, Oct. 1934, pp. 464-469.

19. Moisseiff, L. S., Hartmann, E. C., and Moore, R. L.: Riveted and Pin-Connected Joints of Steel and Aluminum Alloys. Reprinted from Trans. Am. Soc. Civil Eng., vol. 109, 1944, pp. 1359-1399.

20. Francis, A. J.: Investigations on Aluminum Alloy Riveted Joints Under Static Loading. Research, Engineering Structures, Butterworths Scientific Publications (London), and Academic Press, Inc. (New York), 1949, pp. 187-216.

21. March, H. W.: Flat Plates of Plywood Under Uniform or Concentrated Loads. Mimeo. No. 1312, Forest Products Lab., U. S. Dept. Agric., Mar. 1942.

TABLE I

CHARACTERISTICS OF MATERIALS TESTED

Material	E, psi	G, psi	Poisson's ratio, μ	
			With respect to width	With respect to thickness
1/4-in. Koylon	11.10	3.36	0.303	0.356
1/4-in. Foamex	9.86	2.96	.331	.321
1/2-in. Foamex	8.68	2.21	.323	.343
1-in. Foamex	7.80	2.26	.333	.318
1/2-in. Airfoam (soft)	4.85			
1/2-in. Airfoam (medium)	7.14			
1/2-in. Airfoam (firm)	15.20			

TABLE II

N-FUNCTIONS FOR CEMENTED JOINTS

$\frac{x}{L}$	N-functions at -				
	$t_1/t_2 = 1/3$	$t_1/t_2 = 1/2$	$t_1 = t_2$	$t_1/t_2 = 2/1$	$t_1/t_2 = 3/1$
			kL = 1.0		
0.1	0.09556	0.09900	0.10588	0.11276	0.11620
.2	.18956	.19565	.20781	.21997	.22605
.3	.28297	.29092	.30681	.32271	.33066
.4	.37670	.38576	.40389	.42201	.43107
.5	.47170	.48114	.50000	.51886	.52830
.6	.56893	.57799	.59611	.61424	.62330
.7	.66934	.67729	.69319	.70908	.71303
.8	.77395	.78003	.79219	.80435	.81044
.9	.88380	.88724	.89412	.90100	.90444
1.0	1.00000	1.00000	1.00000	1.00000	1.00000
			kL = 2.0		
0.1	0.08883	0.09994	0.12215	0.14436	0.15546
.2	.17120	.19050	.22913	.26776	.28707
.3	.25039	.27534	.32524	.37514	.40009
.4	.32960	.35785	.41434	.47083	.49908
.5	.41201	.44134	.50000	.55866	.58799
.6	.50092	.52917	.58566	.64215	.67040
.7	.59991	.62486	.67476	.72466	.74961
.8	.71293	.73224	.77087	.80950	.82880
.9	.84454	.85564	.87785	.90006	.91117
1.0	1.00000	1.00000	1.00000	1.00000	1.00000
			kL = 3.0		
0.1	0.08797	0.10716	0.14555	0.18393	0.20312
.2	.16125	.19382	.25895	.32408	.35665
.3	.22648	.26782	.35050	.43318	.47452
.4	.28958	.33589	.42849	.52110	.56740
.5	.35627	.40418	.50000	.59582	.64373
.6	.43260	.47890	.57151	.66411	.71042
.7	.52548	.56682	.64950	.73218	.77352
.8	.64335	.67592	.74105	.80618	.83875
.9	.79688	.81607	.85445	.89284	.91203
1.0	1.00000	1.00000	1.00000	1.00000	1.00000

TABLE II.- Continued

N-FUNCTIONS FOR CEMENTED JOINTS

$\frac{x}{L}$	N-functions at -				
	$t_1/t_2 = 1/3$	$t_1/t_2 = 1/2$	$t_1 = t_2$	$t_1/t_2 = 2/1$	$t_1/t_2 = 3/1$
			kL = 4.0		
0.1	0.09378	0.12002	0.17250	0.22499	0.25123
.2	.16222	.20545	.29190	.37836	.42159
.3	.21644	.27015	.37756	.48499	.53869
.4	.26520	.32460	.44337	.56215	.62154
.5	.31645	.37763	.50000	.62237	.68355
.6	.37846	.43785	.55663	.67540	.73480
.7	.46131	.51501	.62244	.72985	.78356
.8	.57841	.62164	.70810	.79455	.83778
.9	.74877	.77501	.82750	.87998	.90622
1.0	1.00000	1.00000	1.00000	1.00000	1.00000
			kL = 5.0		
0.1	0.10365	0.13585	0.20027	0.26468	0.29689
.2	.16994	.22130	.32403	.42676	.47813
.3	.21579	.27815	.40288	.52761	.58997
.4	.25291	.32092	.45694	.59295	.66097
.5	.29077	.36050	.50000	.63950	.70923
.6	.33903	.40705	.54309	.67908	.74709
.7	.41003	.47239	.59712	.72185	.78421
.8	.52187	.57324	.67597	.77870	.83006
.9	.70311	.73532	.79973	.86415	.89635
1.0	1.00000	1.00000	1.00000	1.00000	1.00000
			kL = 6.0		
0.1	0.11517	0.15250	0.22718	0.30185	0.33919
.2	.18032	.23793	.35315	.46838	.52599
.3	.21962	.28797	.42466	.56135	.62970
.4	.24766	.32118	.46822	.61527	.68879
.5	.27483	.34989	.50000	.65011	.72517
.6	.31121	.38473	.53178	.67882	.75234
.7	.37030	.43865	.57534	.71203	.78038
.8	.47401	.53162	.64685	.76207	.81968
.9	.66081	.69815	.77282	.84750	.88483
1.0	1.00000	1.00000	1.00000	1.00000	1.00000

TABLE II.- Continued

N-FUNCTIONS FOR CEMENTED JOINTS

$\frac{x}{L}$	N-functions at -				
	$t_1/t_2 = 1/3$	$t_1/t_2 = 1/2$	$t_1 = t_2$	$t_1/t_2 = 2/1$	$t_1/t_2 = 3/1$
			kL = 7.0		
0.1	0.12689	0.16873	0.25240	0.33607	0.37791
.2	.19096	.25345	.37844	.50343	.56592
.3	.22490	.29741	.44244	.58748	.66000
.4	.24601	.32303	.47707	.63112	.70814
.5	.26508	.34339	.50000	.65661	.73492
.6	.29186	.36888	.52293	.67697	.75399
.7	.34000	.41252	.55756	.70259	.77510
.8	.43408	.49657	.62156	.74655	.80904
.9	.62209	.66393	.74760	.83127	.87311
1.0	1.00000	1.00000	1.00000	1.00000	1.00000
			kL = 8.0		
0.1	0.13812	0.18395	0.27563	0.36731	0.41315
.2	.20072	.26710	.39985	.53260	.59898
.3	.23007	.30554	.45648	.60741	.68288
.4	.24597	.32522	.48373	.64223	.72148
.5	.25916	.33944	.50000	.66056	.74084
.6	.27852	.35777	.51627	.67478	.75403
.7	.31712	.39259	.54352	.69446	.76993
.8	.40102	.46740	.60015	.73290	.79928
.9	.58685	.63269	.72437	.81605	.86188
1.0	1.00000	1.00000	1.00000	1.00000	1.00000
			kL = 9.0		
0.1	0.14855	0.19798	0.29684	0.39571	0.44514
.2	.20922	.27872	.41770	.55671	.62621
.3	.23457	.31215	.46731	.62247	.70005
.4	.24655	.32723	.48860	.64996	.73064
.5	.25555	.33708	.50000	.66292	.74445
.6	.26936	.35004	.51140	.67277	.75345
.7	.29995	.37753	.53269	.68785	.76543
.8	.37379	.44329	.58230	.72128	.79078
.9	.55486	.60429	.70316	.80202	.85145
1.0	1.00000	1.00000	1.00000	1.00000	1.00000

TABLE II.- Concluded

N-FUNCTIONS FOR CEMENTED JOINTS

$\frac{x}{L}$	N-functions at -				
	$t_1/t_2 = 1/3$	$t_1/t_2 = 1/2$	$t_1 = t_2$	$t_1/t_2 = 2/1$	$t_1/t_2 = 3/1$
	kL = 10.0				
0.1	0.15811	0.21078	0.31610	0.42145	0.47412
.2	.21641	.28844	.43250	.57655	.64858
.3	.23824	.31734	.47556	.63378	.71289
.4	.24728	.32888	.49208	.65528	.73688
.5	.25337	.33558	.50000	.66442	.74663
.6	.26312	.34472	.50792	.67112	.75272
.7	.28711	.36622	.52444	.68266	.76176
.8	.35142	.42345	.56750	.71156	.78359
.9	.52588	.57855	.68390	.78922	.84189
1.0	1.00000	1.00000	1.00000	1.00000	1.00000

TABLE III

VALUES OF $\frac{(1 + n)\sinh kL}{kL(n + \cosh kL)}$

kL	$\frac{(1 + n)\sinh kL}{kL(n + \cosh kL)}$ for -					
	n = 0	n = 0.20	n = 0.40	n = 0.60	n = 0.80	n = 1.00
0.25	0.9772	0.9828	0.9864	0.9896	0.9920	0.9940
.50	.9242	.9420	.9550	.9652	.9732	.9796
.75	.8455	.8833	.9046	.9250	.9414	.9550
1.00	.7616	.8090	.8466	.8774	.9028	.9242
1.25	.6667	.7240	.7718	.8124	.8474	.8836
1.50	.6034	.6673	.7220	.7692	.8105	.8566
1.75	.5339	.5998	.6579	.7097	.7560	.8023
2.00	.4820	.5492	.6099	.6651	.7154	.7616
2.50	.3946	.4586	.5186	.5751	.6283	.6786
3.00	.3316	.3902	.4465	.5007	.5650	.6033
3.50	.2852	.3381	.3898	.4403	.4897	.5379
4.00	.2498	.2976	.3447	.3911	.4369	.4820
4.50	.2221	.2654	.3082	.3507	.3929	.4346
5.00	.1999	.2393	.2784	.3174	.3561	.3946
6.00	.1666	.1997	.2328	.2658	.2987	.3316
7.00	.1328	.1713	.1998	.2283	.2567	.2851
8.00	.1250	.1499	.1749	.1998	.2248	.2498
9.00	.1111	.1333	.1555	.1777	.1999	.2221
10.00	.1000	.1199	.1399	.1599	.1799	.1999

TABLE IV

DATA TAKEN FROM X-RAY

(a) Two-Rivet Joint

Knots	$\frac{L - D}{L}$	x_1' (No load)	x_2' (6-lb load)	x_1' (No load)	x_2' (6-lb load)	x_1' (No load)	x_2' (6-lb load)
				F station			
	0.933	8.49	9.42	9.09	11.09	8.56	10.35
0	.936	8.46	9.39	9.07	11.05	8.56	10.35
	.943	8.43	9.36	8.99	10.93	8.62	10.40
1	.950	8.35	9.29	8.93	10.83	8.65	10.41
	.957	8.31	9.23	8.82	10.67	8.73	10.44
2	.964	8.23	9.15	8.77	10.60	8.76	10.47
	.971	8.20	9.11	8.73	10.55	8.84	10.55
3	.978	8.12	9.04	8.66	10.53	8.91	10.67
	.984	8.08	8.99	8.63	10.52	8.99	10.79
4	.991	8.00	8.91	8.58	10.48	9.04	10.87
	.998	7.99	8.90	8.54	10.45	9.08	10.92
				G station			
	0.933	7.64	8.51	8.25	10.17	7.77	9.50
0	.936	7.63	8.50	8.25	10.16	7.80	9.52
	.943	7.57	8.44	8.17	10.05	7.84	9.56
1	.950	7.51	8.40	8.11	9.97	7.88	9.58
	.957	7.46	8.35	8.06	9.89	7.97	9.66
2	.964	7.41	8.30	8.01	9.81	7.99	9.67
	.971	7.36	8.23	7.96	9.77	8.05	9.74
3	.978	7.30	8.17	7.88	9.69	8.10	9.82
	.984	7.26	8.11	7.85	9.67	8.18	9.93
4	.991	7.19	8.03	7.79	9.61	8.21	9.97
	.998	7.16	8.00	7.76	9.59	8.28	10.05
				H station			
	0.933	6.86	7.65	7.50	9.35	7.04	8.73
0	.936	6.84	7.64	7.47	9.31	7.04	8.74
	.943	6.79	7.61	7.39	9.21	7.10	8.78
1	.950	6.76	7.60	7.35	9.15	7.15	8.82
	.957	6.71	7.57	7.33	9.11	7.20	8.85
2	.964	6.65	7.51	7.24	9.02	7.21	8.87
	.971	6.61	7.46	7.21	8.97	7.29	8.94
3	.978	6.55	7.37	7.13	8.90	7.32	8.99
	.984	6.49	7.28	7.10	8.87	7.38	9.06
4	.991	6.46	7.22	7.01	8.79	7.40	9.11
	.998	6.40	7.15	7.01	8.79	7.46	9.17
				I station			
	0.933	6.04	6.75	6.66	8.47	6.27	7.92
0	.936	6.00	6.75	6.63	8.41	6.28	7.92
	.943	5.97	6.74	6.57	8.33	6.33	7.96
1	.950	5.94	6.74	6.53	8.27	6.37	7.99
	.957	5.90	6.71	6.51	8.25	6.41	8.02
2	.964	5.86	6.71	6.45	8.17	6.42	8.03
	.971	5.83	6.65	6.41	8.13	6.48	8.07
3	.978	5.77	6.53	6.35	8.07	6.50	8.11
	.984	5.71	6.43	6.33	8.05	6.54	8.17
4	.991	5.67	6.36	6.26	7.97	6.56	8.20
	.998	5.65	6.33	6.25	7.96	6.60	8.25

TABLE IV.- Concluded

DATA TAKEN FROM X-RAY

(b) Three-Rivet Joint

Knots	$\frac{L-D}{L}$	1-inch sheet, lower rivet		1/2-inch sheet 1, lower rivet		1/2-inch sheet 2, lower rivet		1-inch sheet, upper rivet		1/2-inch sheet 1, upper rivet		1/2-inch sheet 2, upper rivet	
		x_1' (No load)	x_2' (8-lb load)	x_1' (No load)	x_2' (8-lb load)	x_1' (No load)	x_2' (8-lb load)	x_1' (No load)	x_2' (8-lb load)	x_1' (No load)	x_2' (8-lb load)	x_1' (No load)	x_2' (8-lb load)
		F station						M station					
0	0.931	11.83	13.13	12.26	14.35	12.24	14.43	6.35	7.22	6.78	8.33	6.80	8.15
	.934	11.83	13.13	12.20	14.28	12.20	14.07	6.33	7.19	6.78	8.32	6.76	8.10
1	.942	11.73	13.03	12.15	14.19	12.11	13.96	6.29	7.15	6.71	8.23	6.71	8.04
	.949	11.62	12.91	12.03	14.07	12.01	13.79	6.25	7.10	6.66	8.14	6.63	7.94
2	.956	11.55	12.83	11.95	13.89	11.90	13.65	6.19	7.03	6.58	8.03	6.56	7.85
	.963	11.44	12.73	11.83	13.75	11.82	13.54	6.14	6.97	6.55	7.97	6.50	7.77
3	.970	11.38	12.65	11.77	13.69	11.75	13.47	6.11	6.94	6.52	7.93	6.47	7.74
	.977	11.27	12.55	11.68	13.65	11.69	13.43	6.04	6.87	6.47	7.90	6.39	7.68
4	.984	11.21	12.47	11.61	13.62	11.60	13.37	6.00	6.83	6.45	7.88	6.31	7.67
	.991	11.11	12.36	11.53	13.53	11.52	13.32	5.95	6.77	6.40	7.85	6.31	7.60
	.998	11.09	12.33	11.49	13.49	11.47	13.26	5.93	6.74	6.37	7.82	6.31	7.60
		G station						N station					
0	0.931	10.99	12.24	11.44	13.43	11.43	13.23	5.56	6.31	5.93	7.43	6.00	7.30
	.934	10.96	12.21	11.41	13.38	11.40	13.17	5.56	6.31	5.93	7.43	5.93	7.23
1	.942	10.87	12.12	11.33	13.28	11.32	13.07	5.46	6.23	5.87	7.33	5.91	7.19
	.949	10.79	12.03	11.23	13.17	11.21	12.93	5.45	6.23	5.85	7.29	5.83	7.11
2	.956	10.70	11.93	11.16	13.05	11.15	12.85	5.40	6.18	5.81	7.21	5.78	7.03
	.963	10.61	11.86	11.06	12.94	11.06	12.73	5.36	6.13	5.76	7.16	5.72	6.96
3	.970	10.55	11.78	11.01	12.87	11.00	12.67	5.31	6.09	5.73	7.11	5.71	6.93
	.977	10.46	11.68	10.94	12.81	10.91	12.57	5.27	6.01	5.67	7.06	5.61	6.86
4	.984	10.39	11.61	10.85	12.76	10.85	12.52	5.23	5.97	5.66	7.05	5.58	6.83
	.991	10.30	11.50	10.81	12.69	10.77	12.45	5.20	5.92	5.61	7.00	5.54	6.79
	.998	10.27	11.47	10.74	12.64	10.71	12.39	5.15	5.87	5.60	6.99	5.51	6.77
		H station						O station					
0	0.931	10.21	11.39	10.61	12.51	10.60	12.27	4.69	5.36	5.18	6.63	5.19	6.43
	.934	10.17	11.38	10.57	12.46	10.57	12.24	4.68	5.36	5.16	6.60	5.13	6.39
1	.942	10.09	11.29	10.51	12.39	10.51	12.17	4.65	5.33	5.10	6.52	5.10	6.33
	.949	10.03	11.24	10.43	12.29	10.40	12.03	4.63	5.33	5.10	6.47	5.04	6.28
2	.956	9.95	11.17	10.37	12.20	10.35	11.96	4.59	5.31	5.07	6.44	5.03	6.24
	.963	9.85	11.09	10.28	12.09	10.29	11.88	4.55	5.29	5.01	6.36	4.96	6.17
3	.970	9.79	11.00	10.21	12.02	10.19	11.78	4.53	5.24	4.99	6.33	4.94	6.15
	.977	9.71	10.90	10.15	11.95	10.13	11.72	4.49	5.17	4.94	6.27	4.89	6.11
4	.984	9.62	10.79	10.08	11.88	10.05	11.65	4.45	5.11	4.91	6.26	4.85	6.07
	.991	9.56	10.72	9.99	11.81	9.95	11.55	4.44	5.07	4.87	6.20	4.79	6.01
	.998	9.49	10.64	9.99	11.78	9.93	11.55	4.40	5.02	4.87	6.20	4.79	6.01
		I station						P station					
0	0.931	9.39	10.51	9.82	11.62	9.83	11.41	3.84	4.46	4.34	5.73	4.33	5.54
	.934	9.33	10.46	9.76	11.55	9.75	11.33	3.84	4.46	4.33	5.72	4.29	5.50
1	.942	9.27	10.41	9.72	11.50	9.67	11.25	3.82	4.42	4.28	5.65	4.28	5.47
	.949	9.21	10.37	9.68	11.40	9.61	11.17	3.82	4.40	4.25	5.59	4.25	5.42
2	.956	9.15	10.34	9.58	11.34	9.55	11.11	3.79	4.39	4.25	5.57	4.22	5.39
	.963	9.07	10.25	9.51	11.26	9.49	11.04	3.78	4.39	4.21	5.51	4.16	5.32
3	.970	9.01	10.19	9.46	11.20	9.40	10.93	3.73	4.39	4.20	5.47	4.15	5.32
	.977	8.93	10.07	9.37	11.10	9.35	18.87	3.71	4.29	4.17	5.44	4.12	5.28
4	.984	8.84	9.95	9.31	11.03	9.26	10.79	3.65	4.21	4.16	5.43	4.07	5.24
	.991	8.79	9.87	9.22	10.95	9.18	10.71	3.64	4.17	4.10	5.38	4.03	5.20
	.998	8.76	9.84	9.21	10.92	9.17	10.69	3.59	4.11	4.10	5.39	4.01	5.19

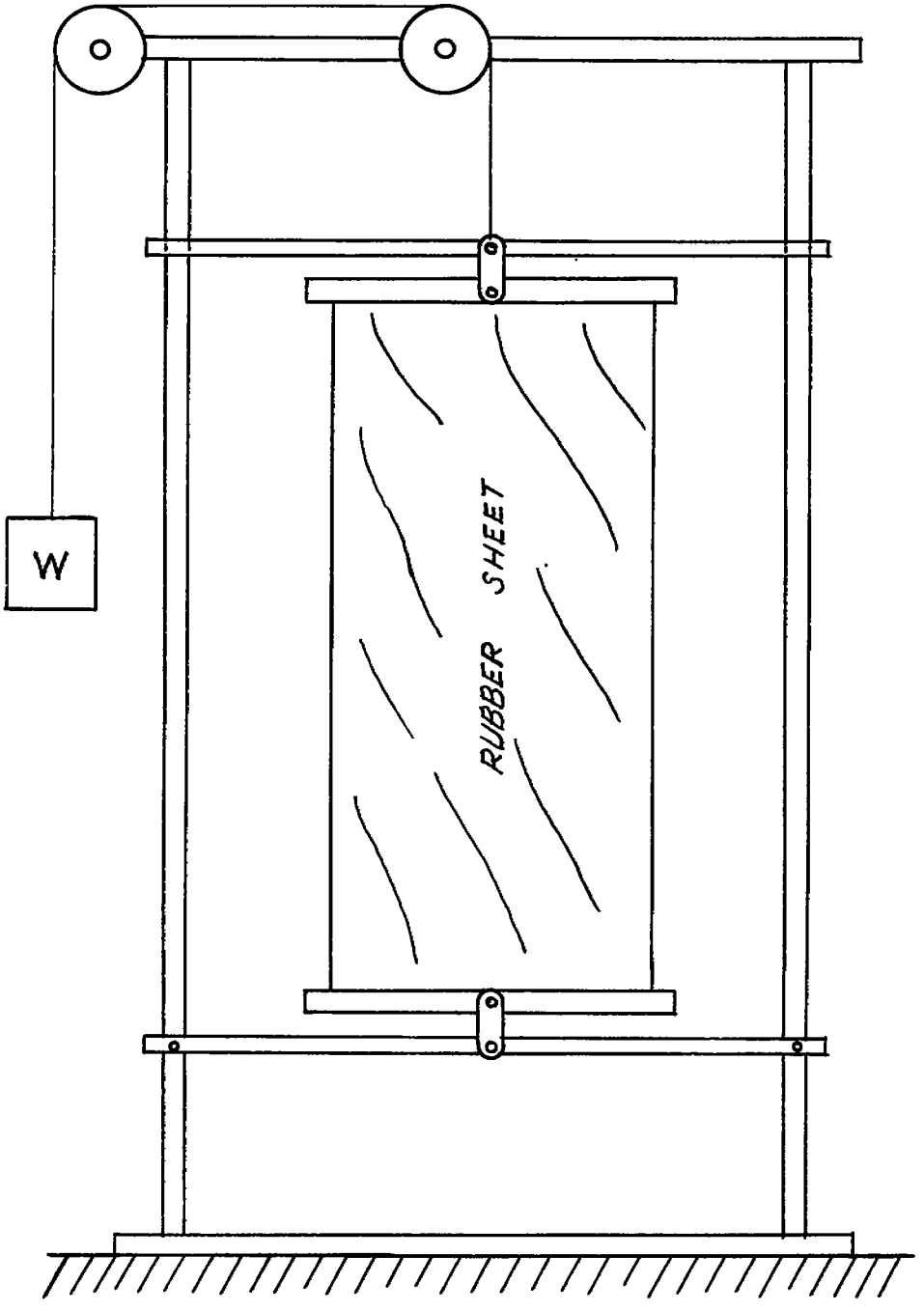

Figure 1.- Tensile test apparatus.

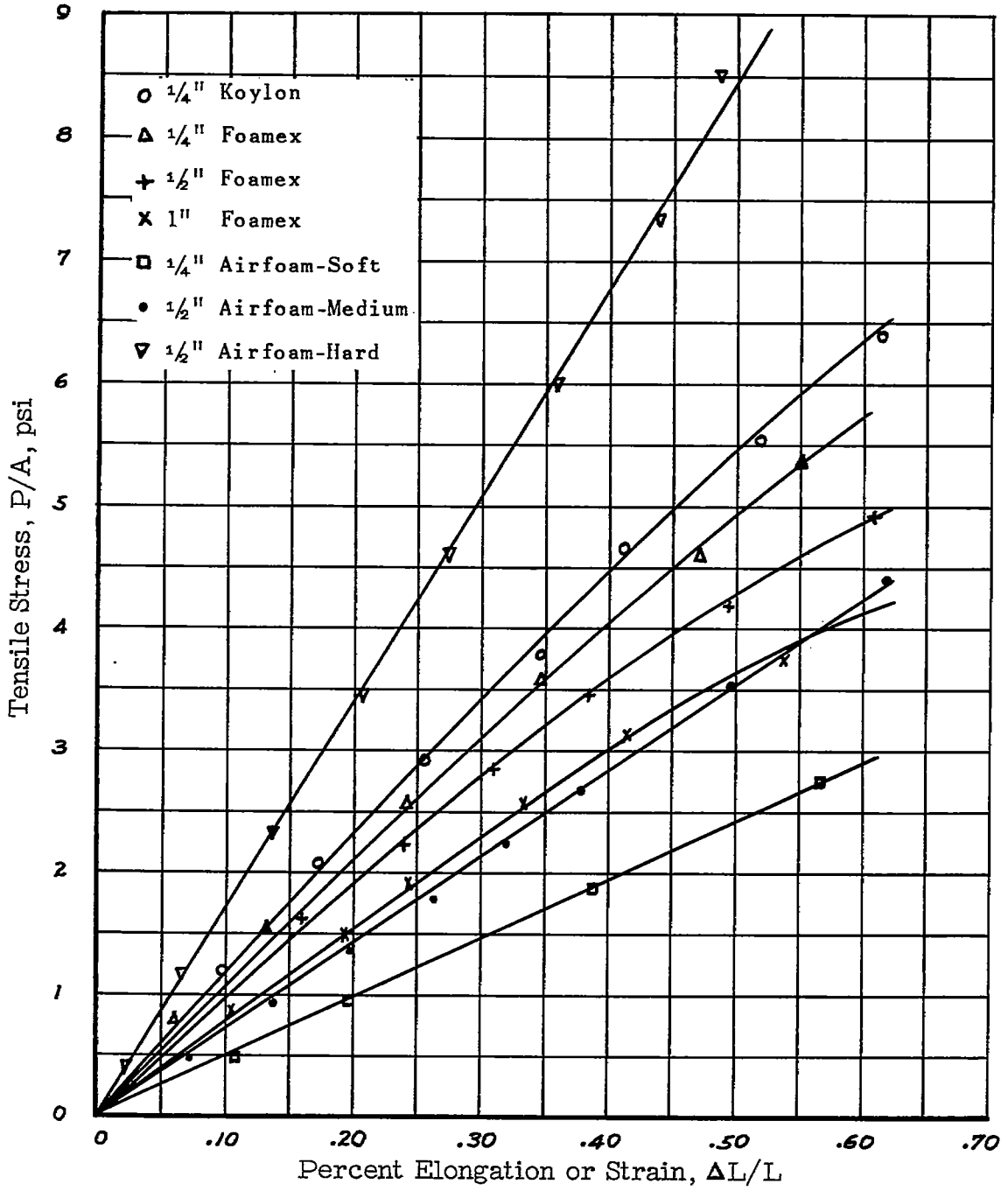

Figure 2.- Stress-strain relations for different foam-rubber samples.

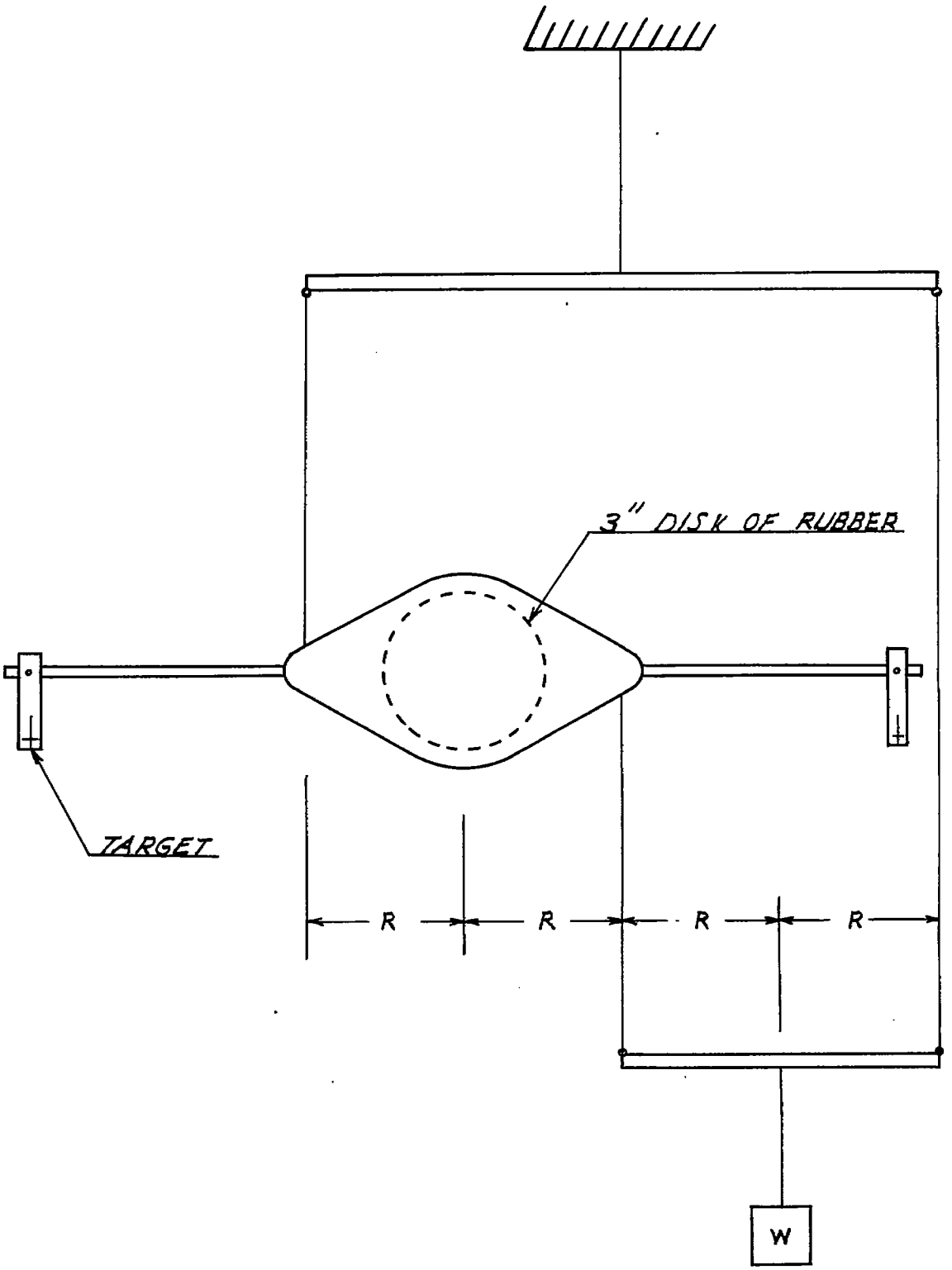

Figure 3.- Torsion test apparatus.

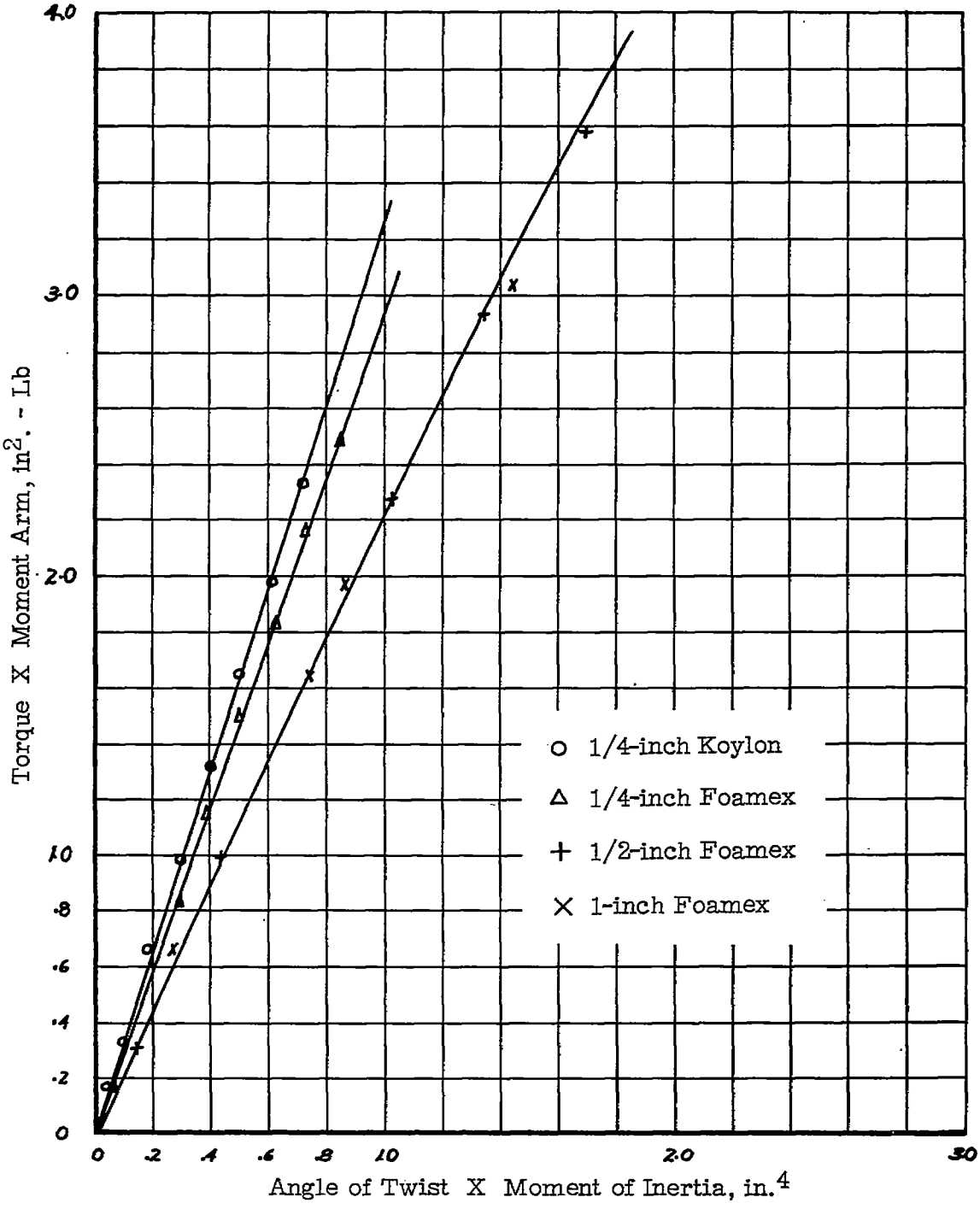

Figure 4.- Modulus of elasticity in shear for different foam-rubber samples.

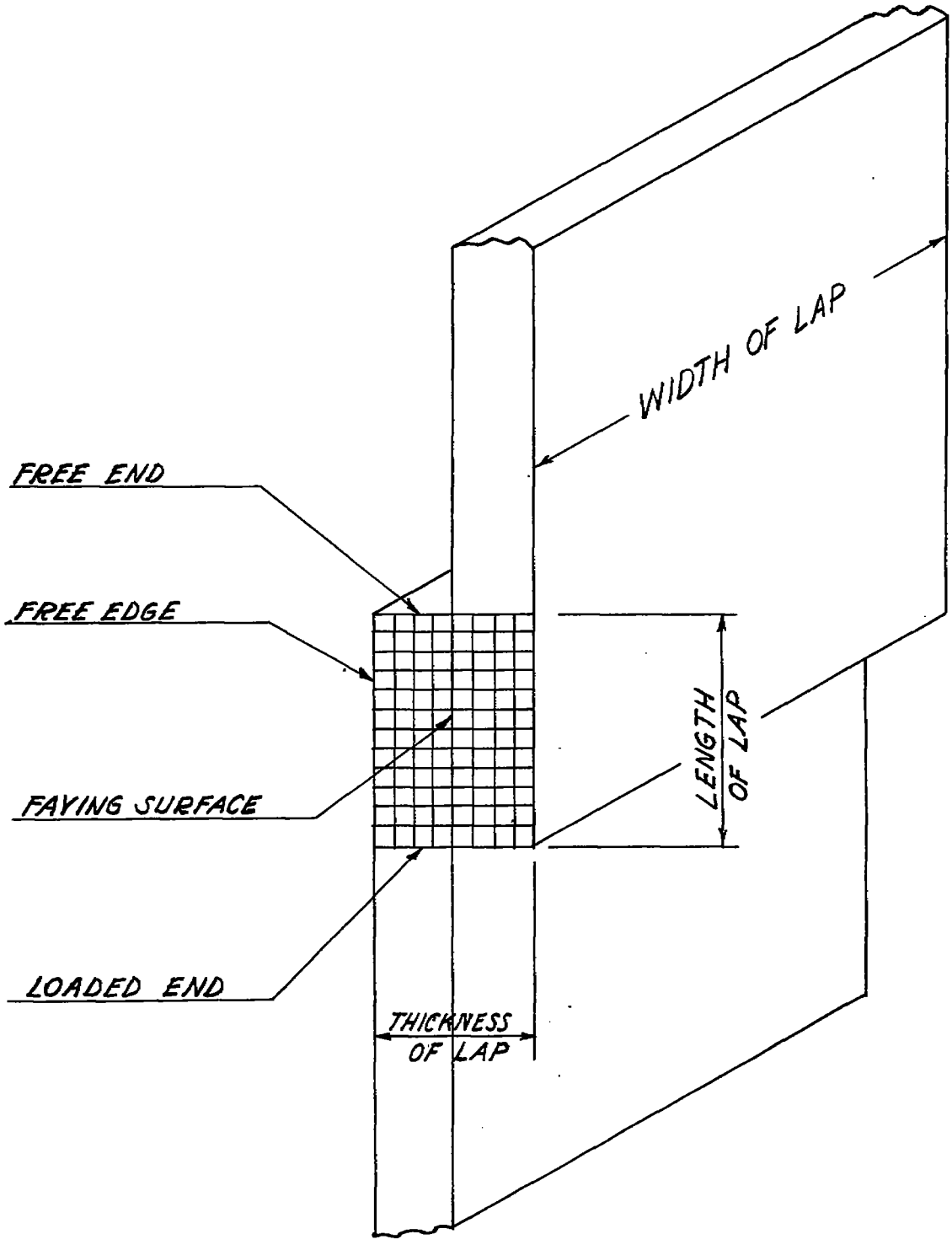

Figure 5.- A simple lap joint.

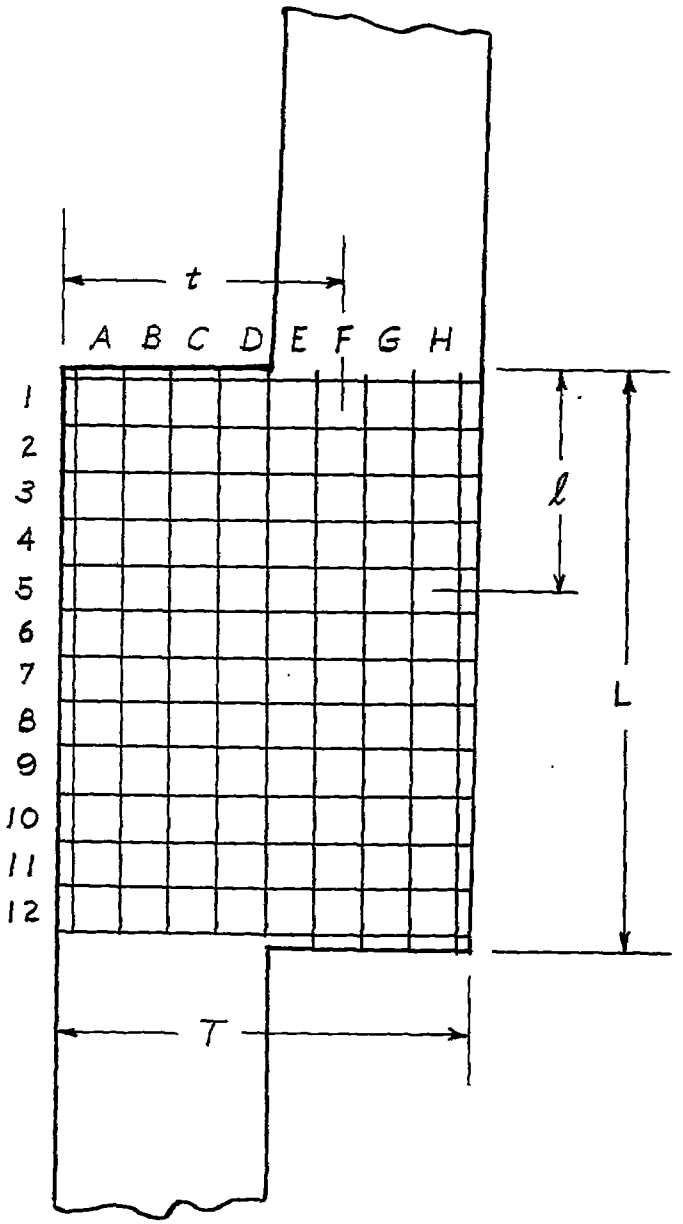

(a) No load.

Figure 6.- Tracing from full-scale print.

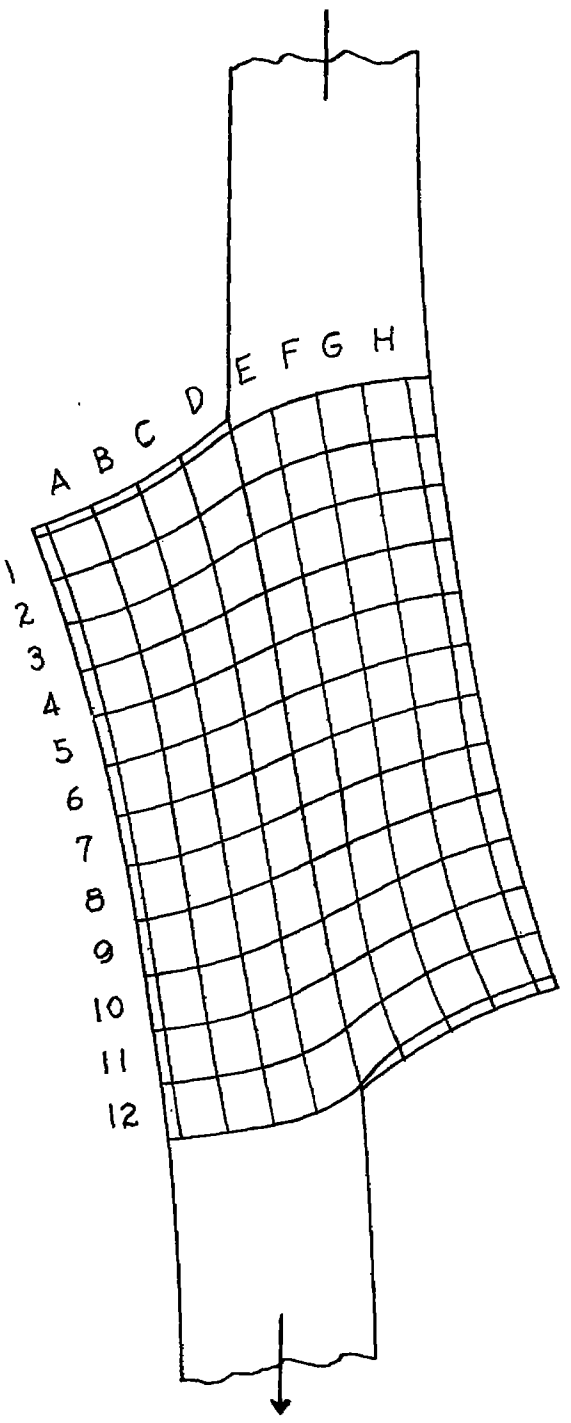

(b) 16-pound load.

Figure 6.- Concluded.

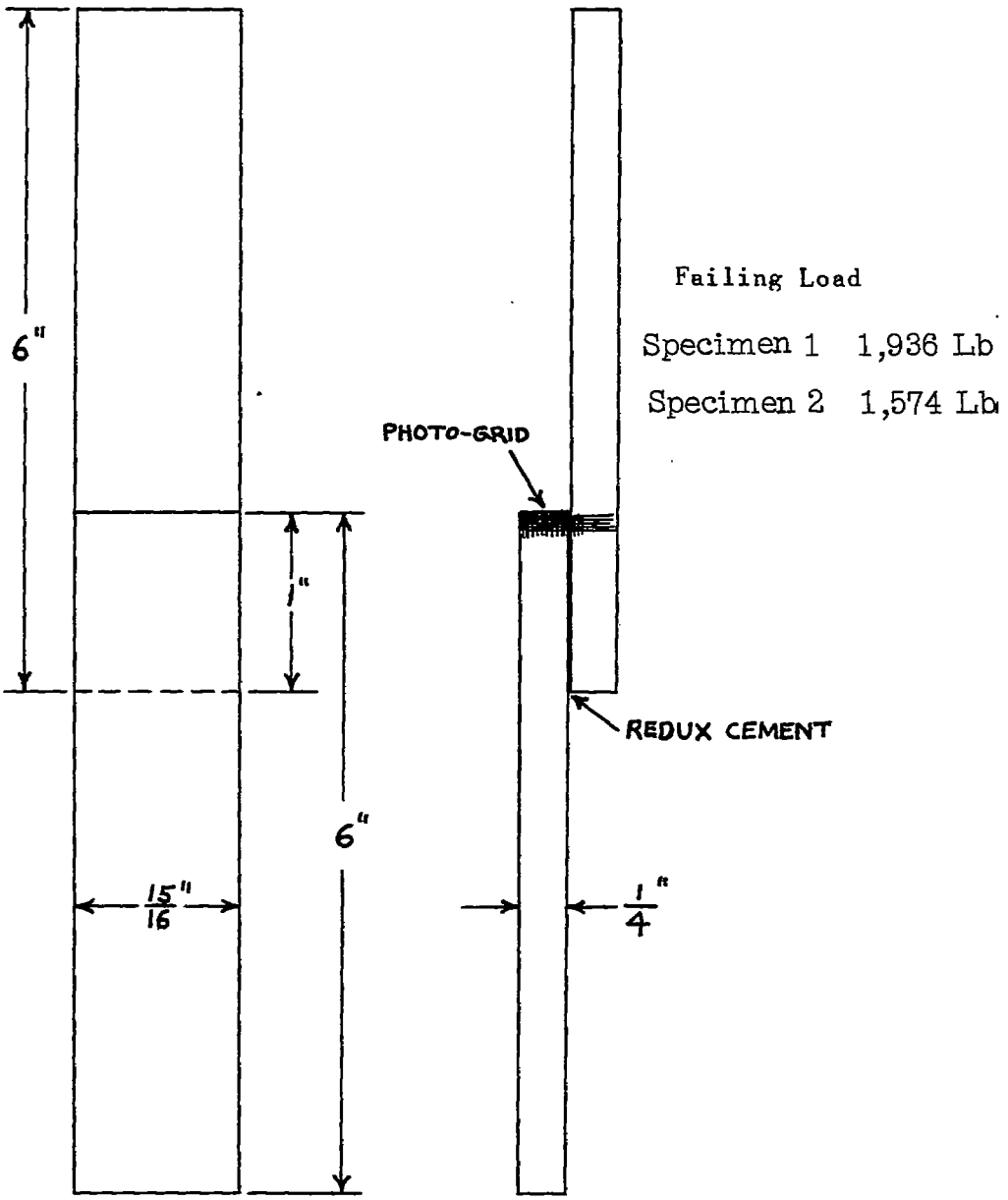

(a) Single lap.

Figure 7.- Cemented magnesium joint.

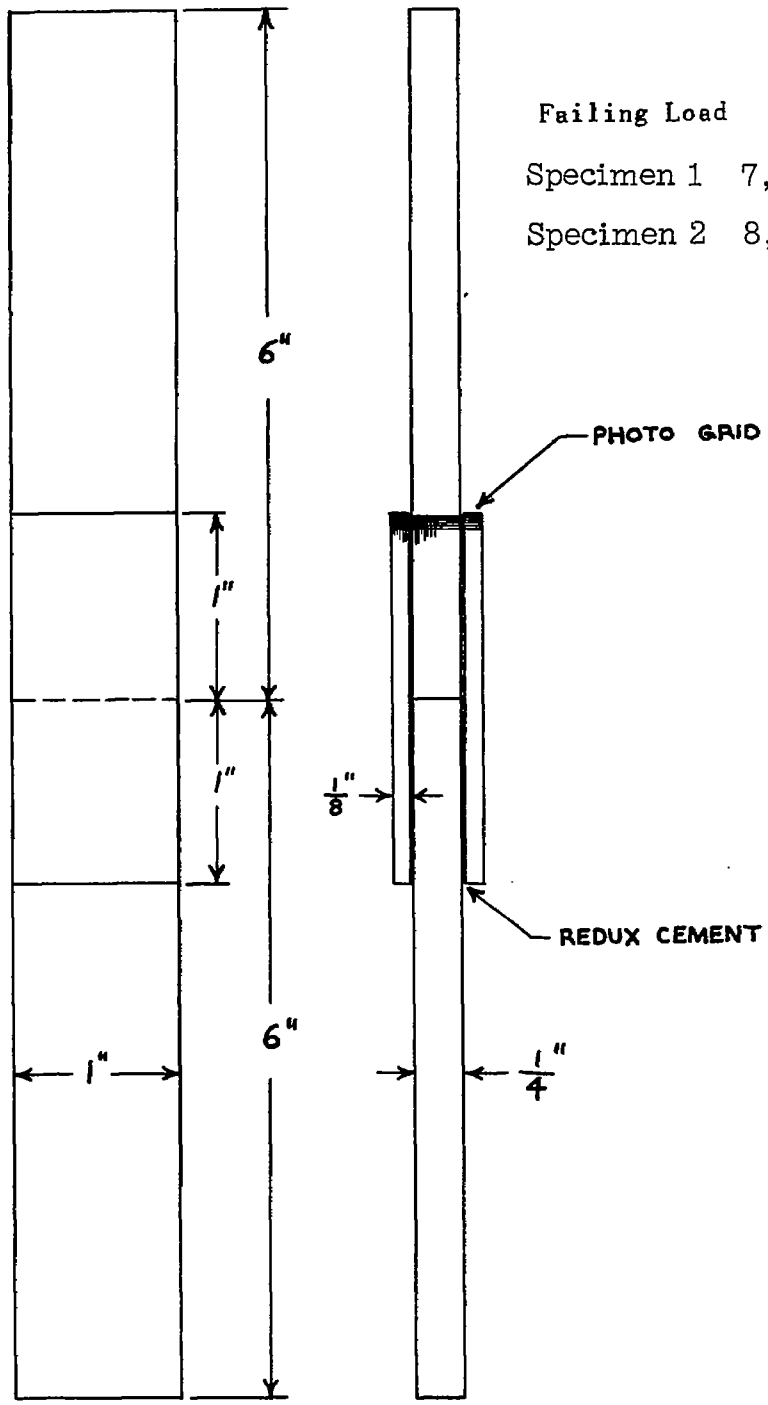

(b) Double lap.

Figure 7.- Concluded.

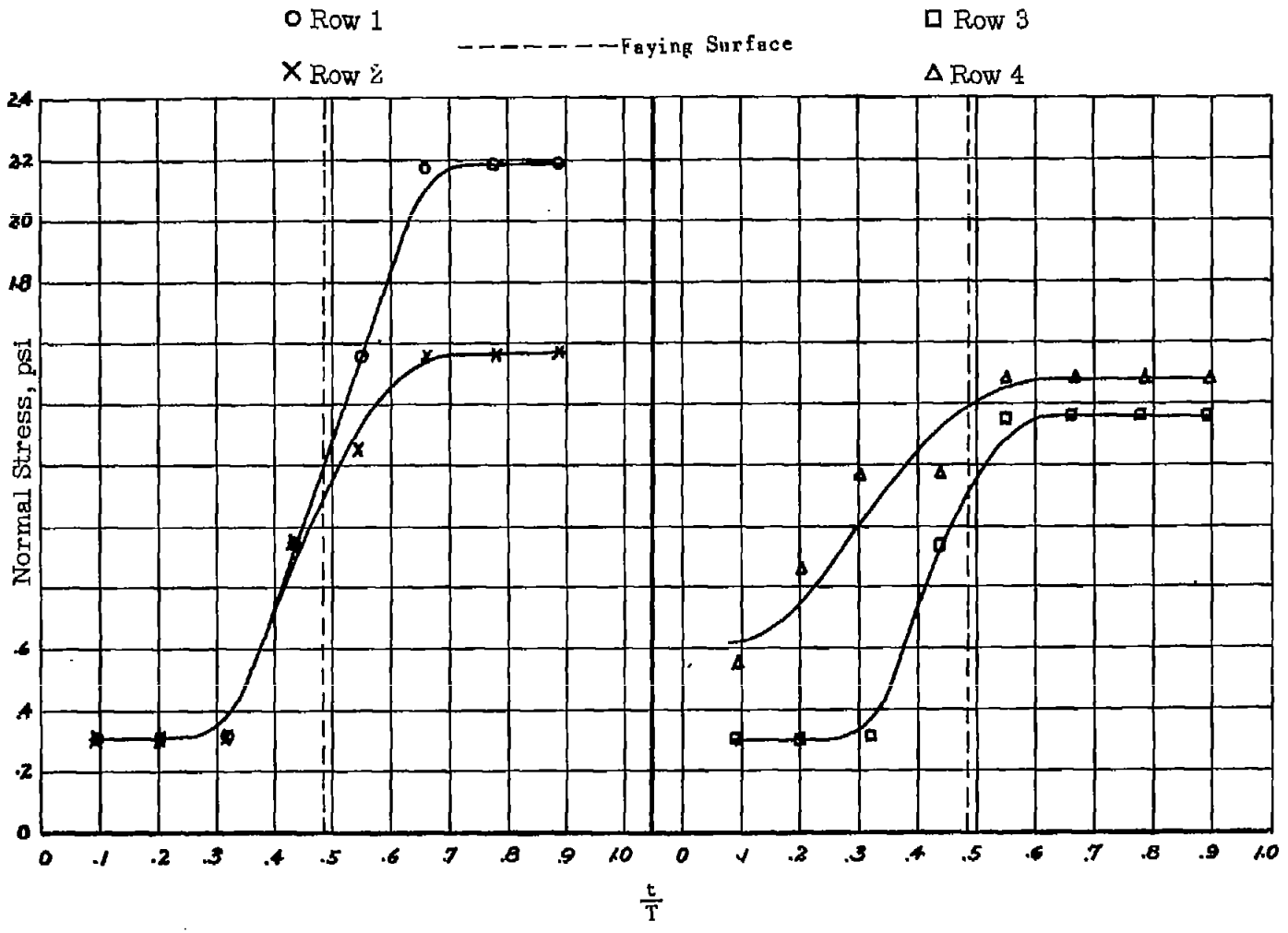

(a) Row 1, row 2.

(b) Row 3, row 4.

Figure 8.- Normal stress distribution across lap.

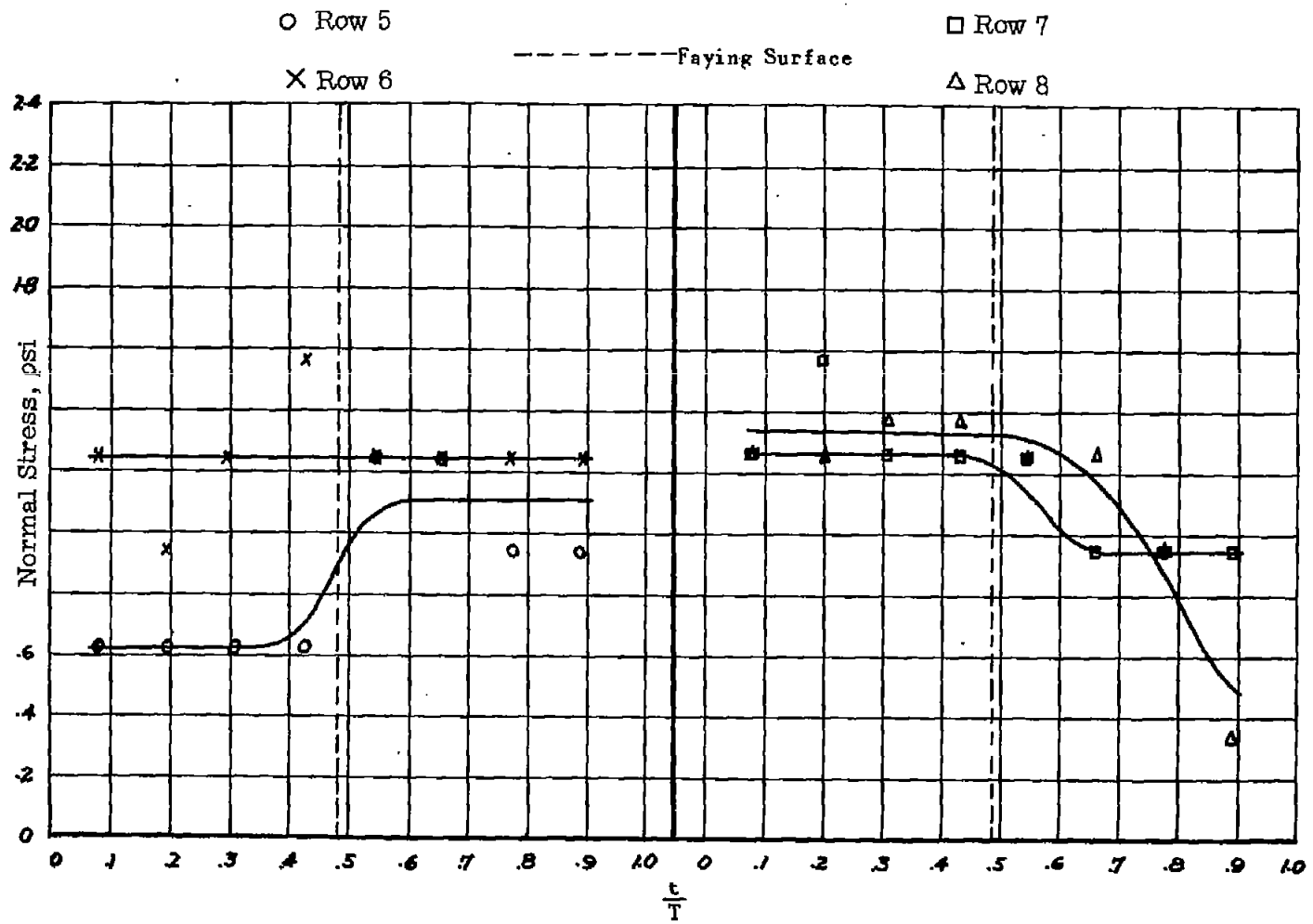

(c) Row 5, row 6.

(d) Row 7, row 8.

Figure 8.- Continued.

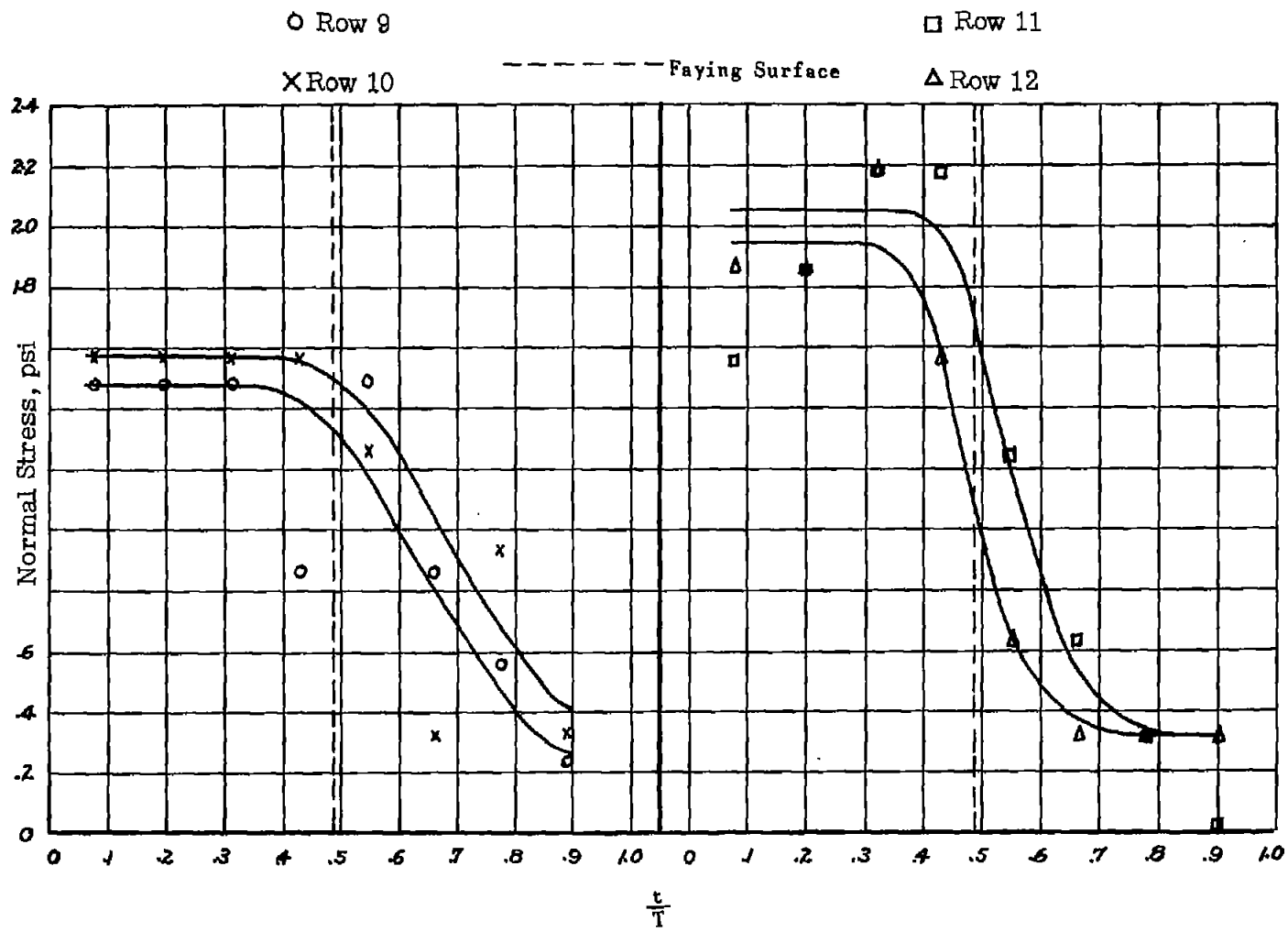

(e) Row 9, row 10.

(f) Row 11, row 12.

Figure 8.- Concluded.

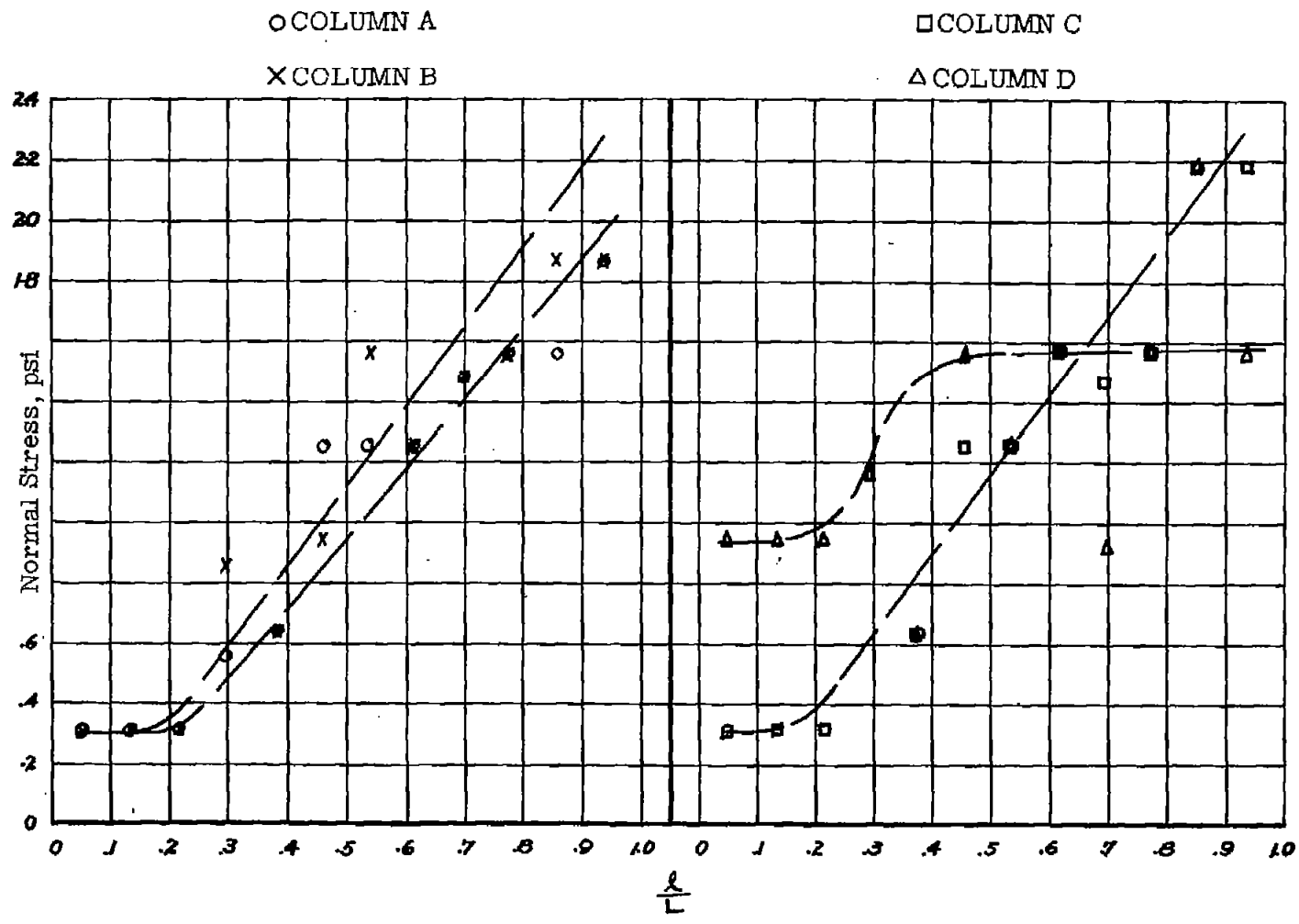

(a) Column A, column B.

(b) Column C, column D.

Figure 9.- Normal stress distribution along the lap.

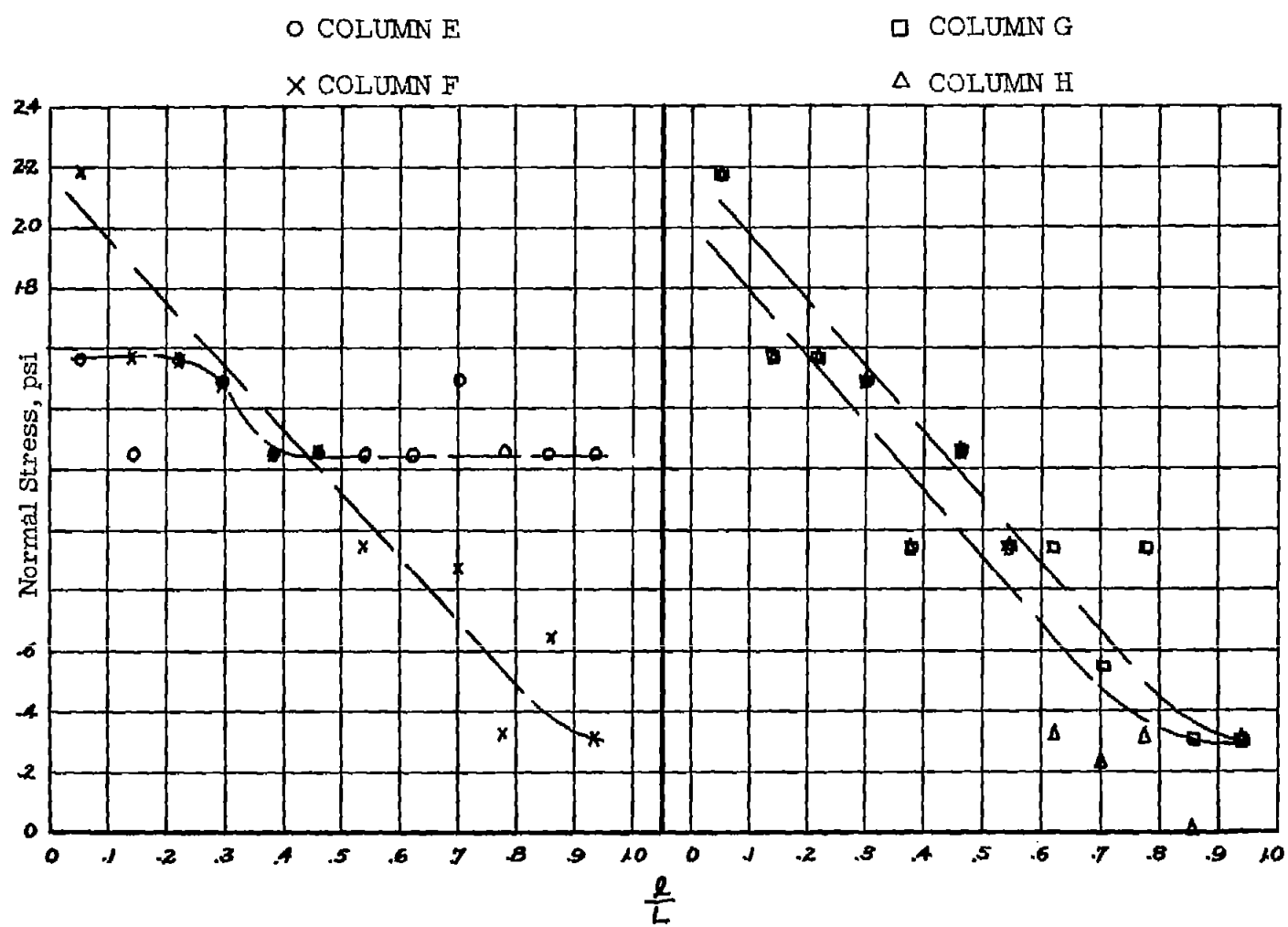

(c) Column E, column F.

(d) Column G, column H.

Figure 9.- Concluded.

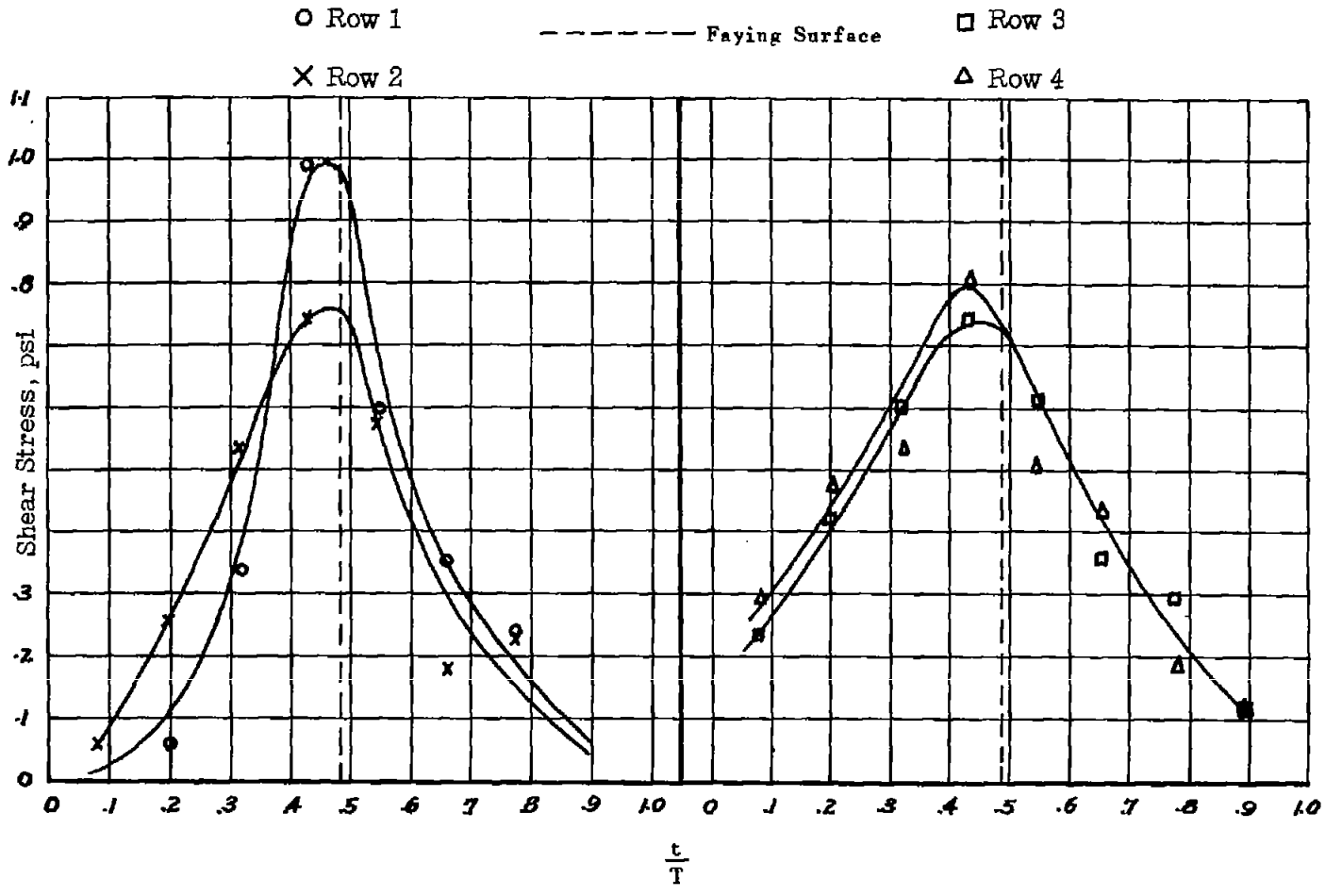

(a) Row 1, row 2.

(b) Row 3, row 4.

Figure 10.- Shear stress distribution across lap.

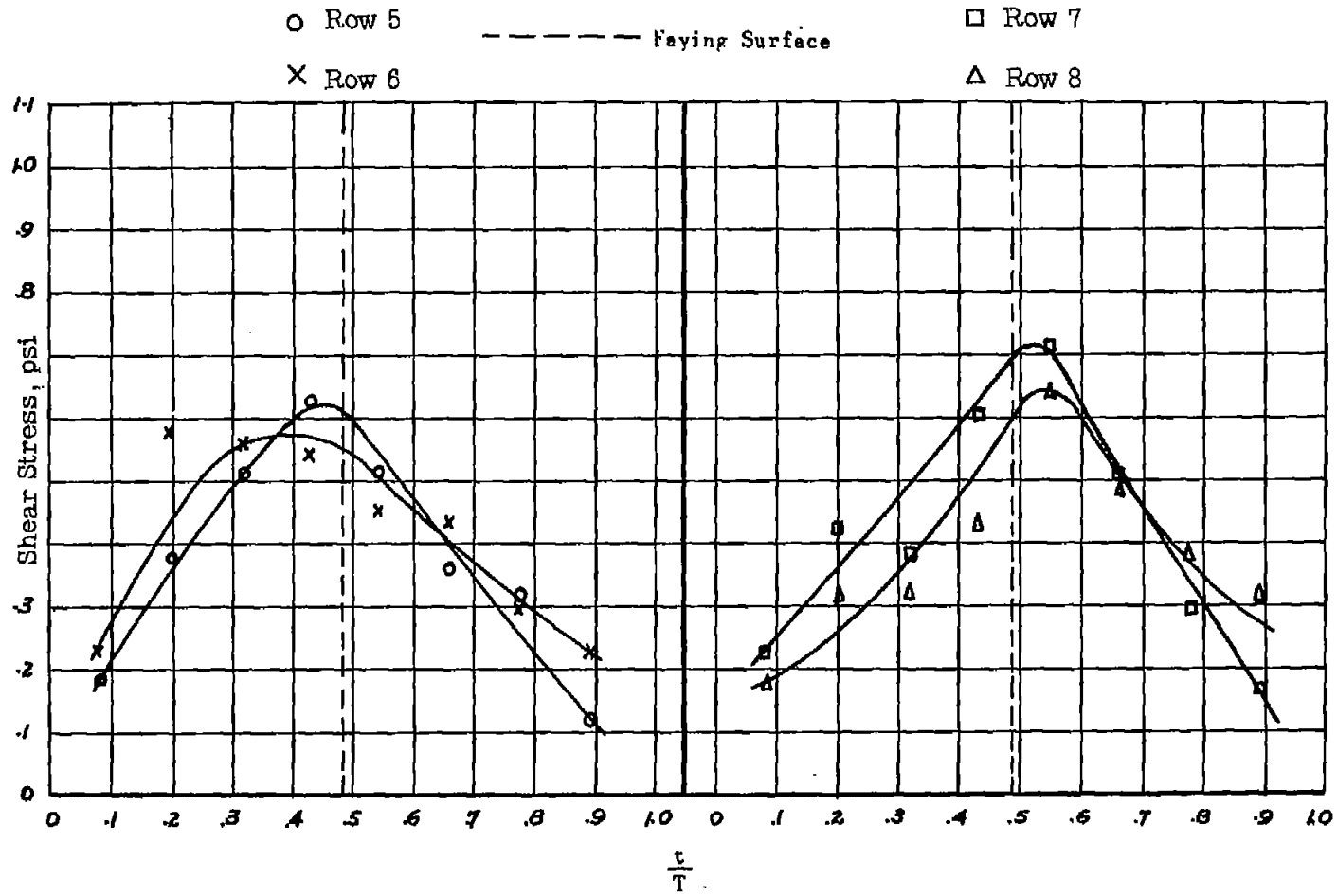

(c) Row 5, row 6.

(d) Row 7, row 8.

Figure 10.- Continued.

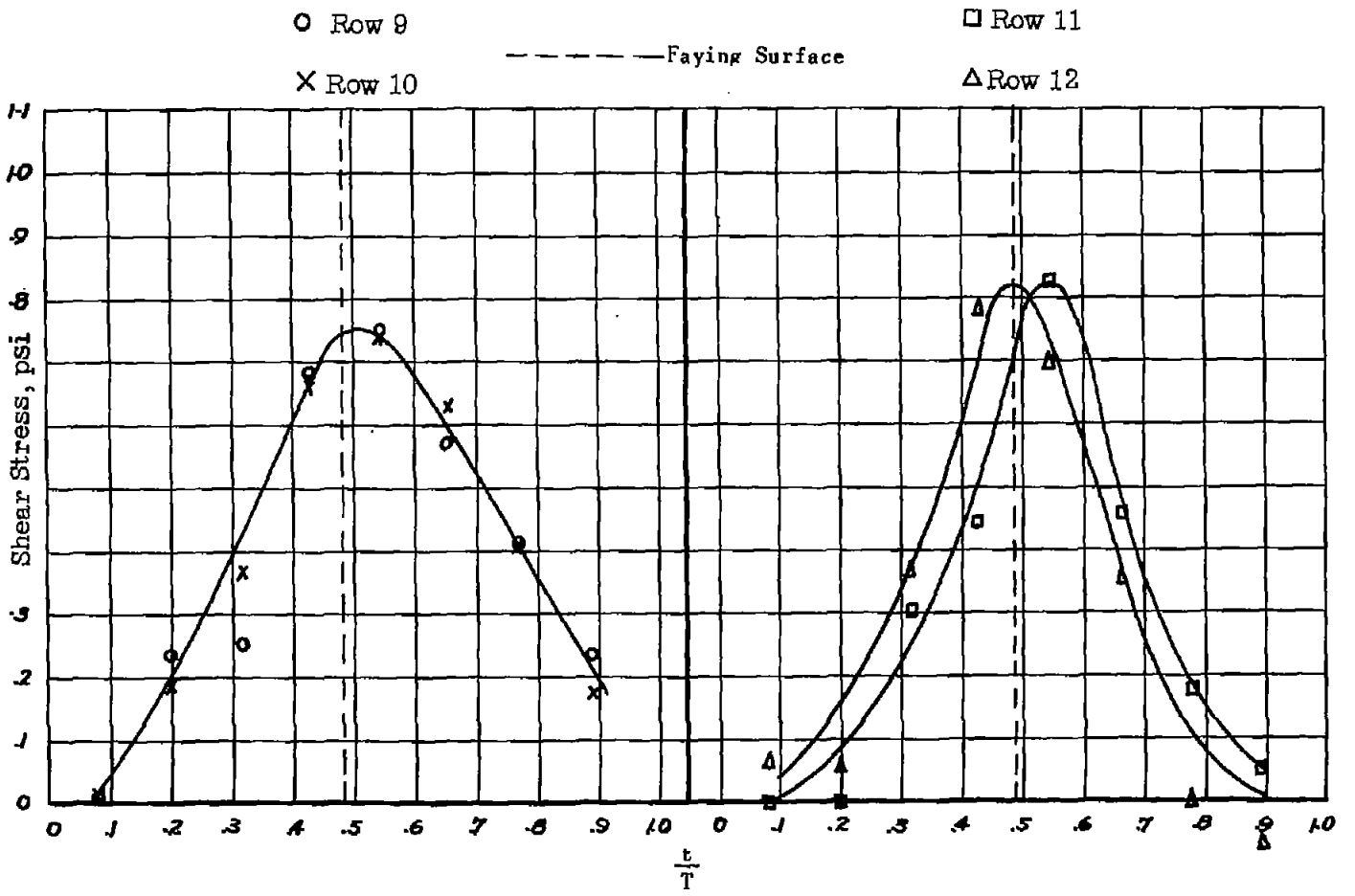

(e) Row 9, row 10.

(f) Row 11, row 12.

Figure 10.- Concluded.

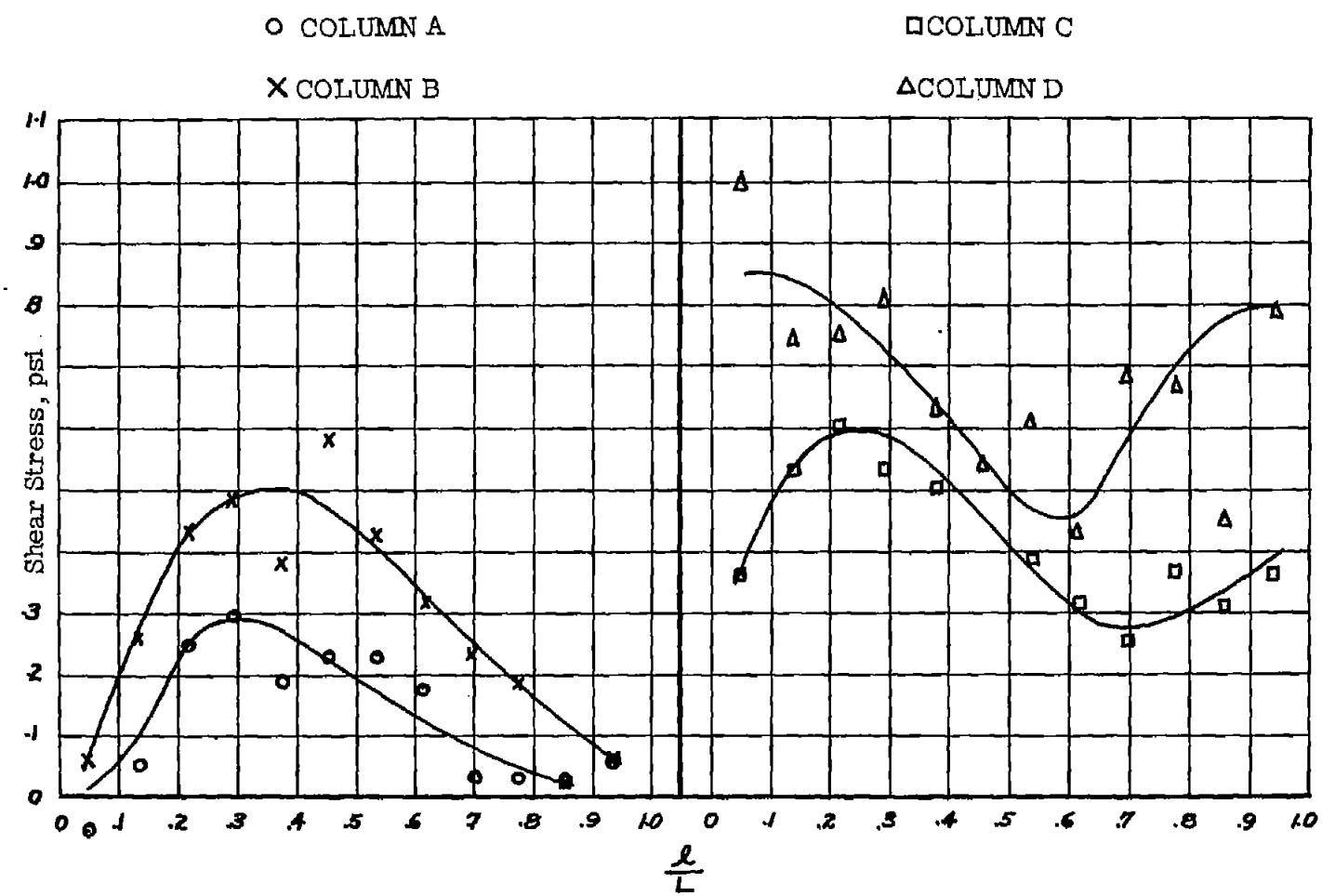

(a) Column A, column B.

(b) Column C, column D.

Figure 11.- Shear stress distribution along the lap.

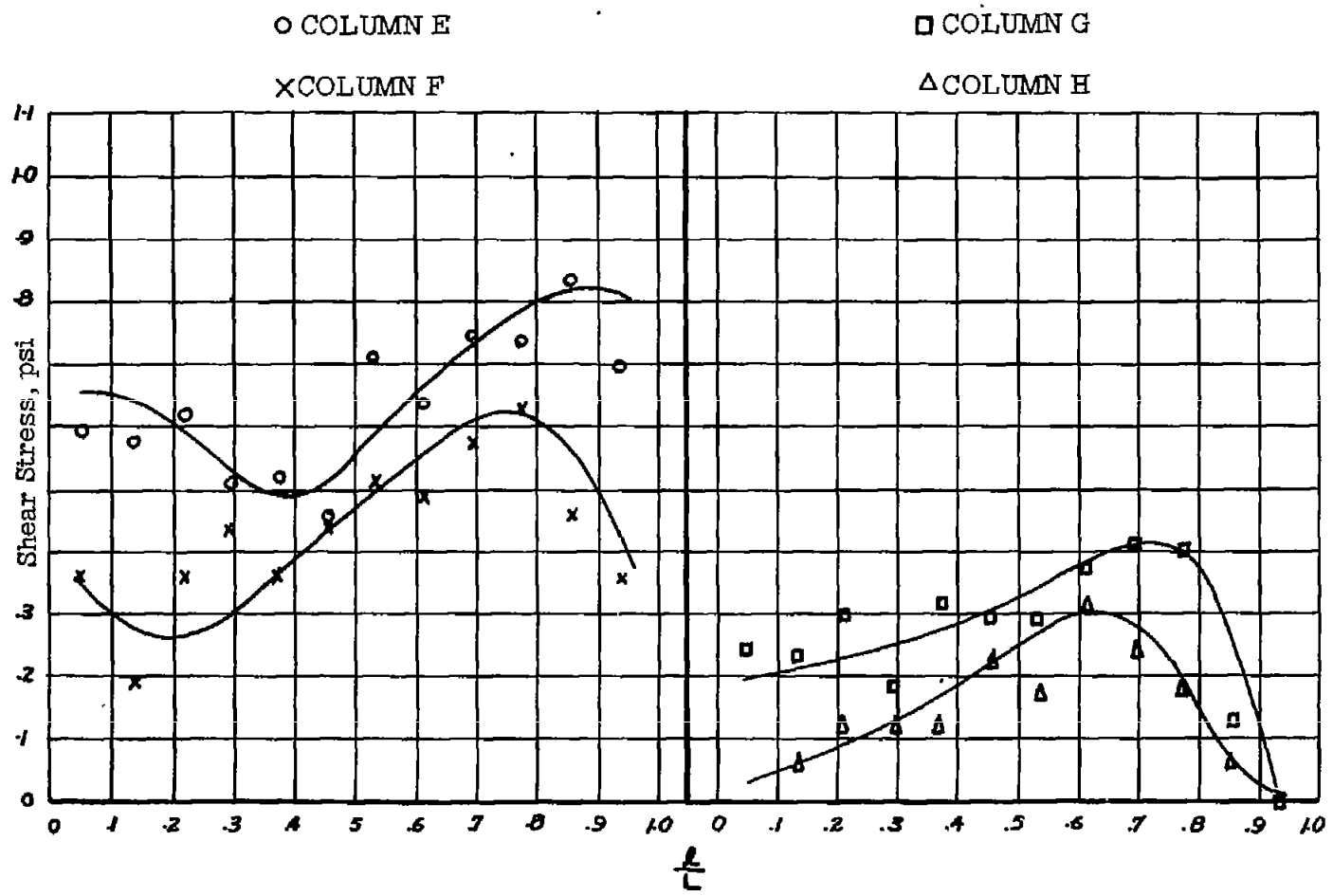

(c) Column E, column F.

(d) Column G, column H.

Figure 11.- Concluded.

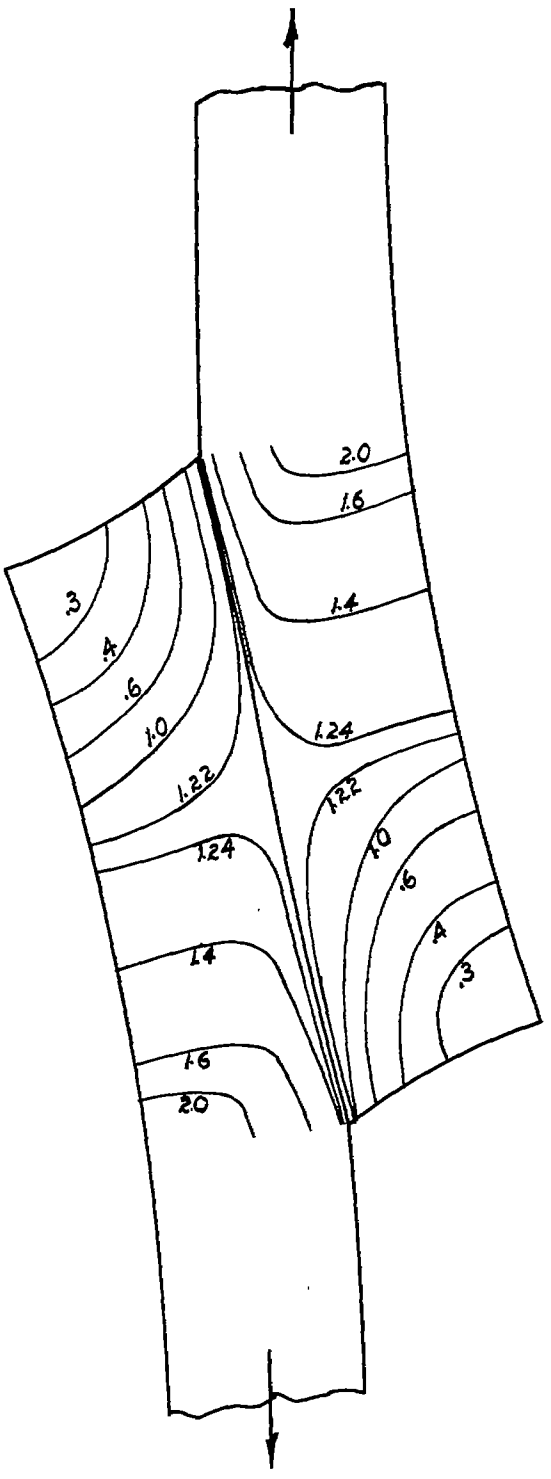

Figure 12.- Normal stress distribution in pounds per square inch. Load approximately 16 pounds.

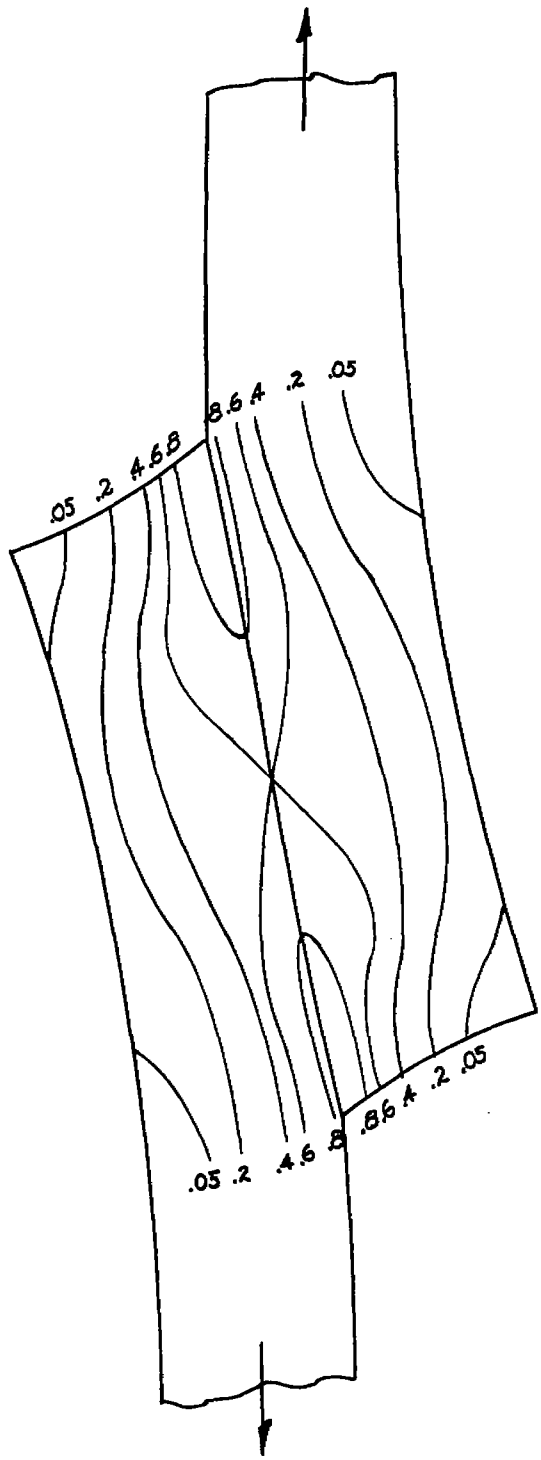

Figure 13.- Shear stress distribution in pounds per square inch. Load approximately 16 pounds.

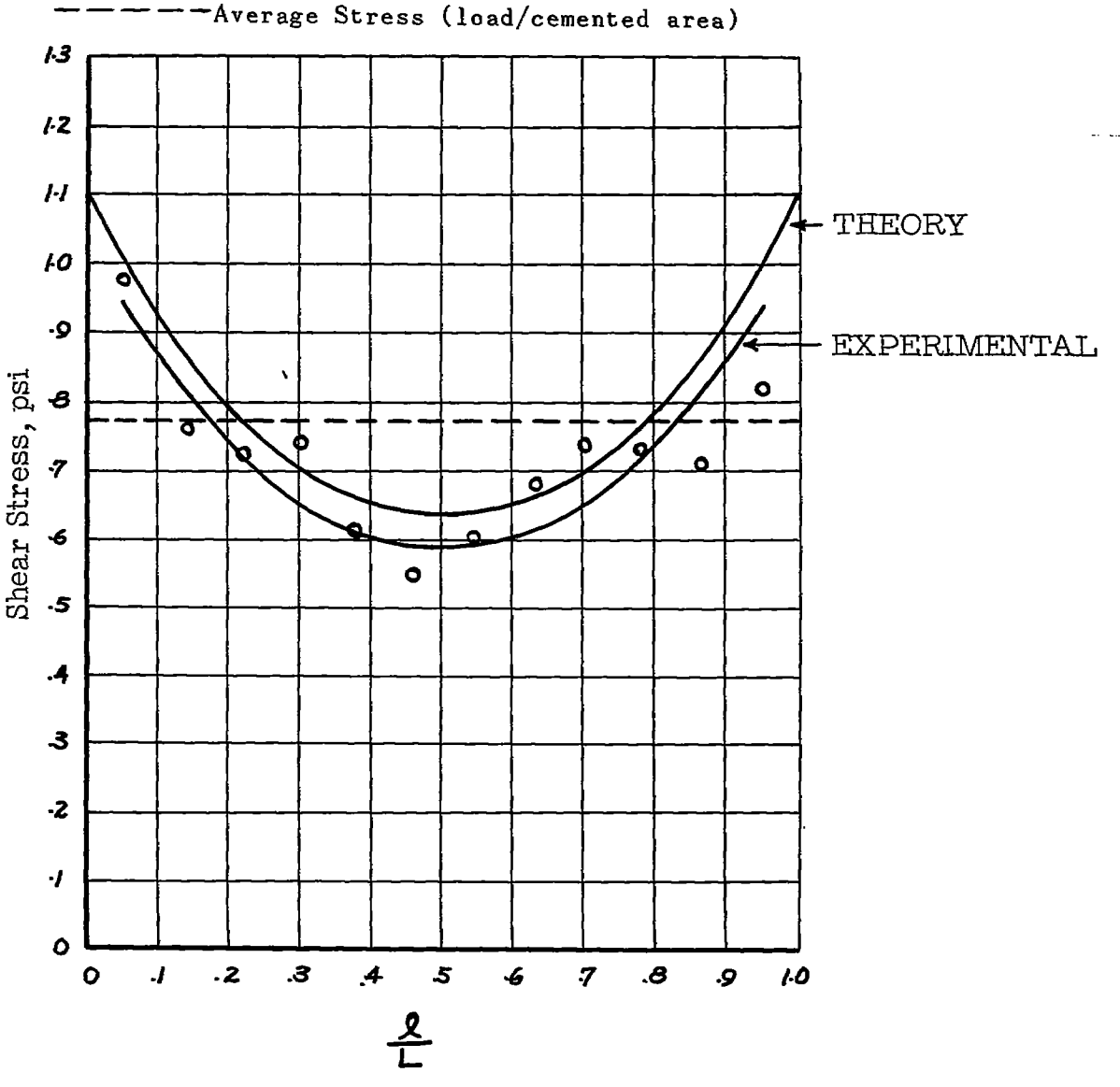

Figure 14.- Comparison of theoretical and experimental shear stress distribution along faying surface.

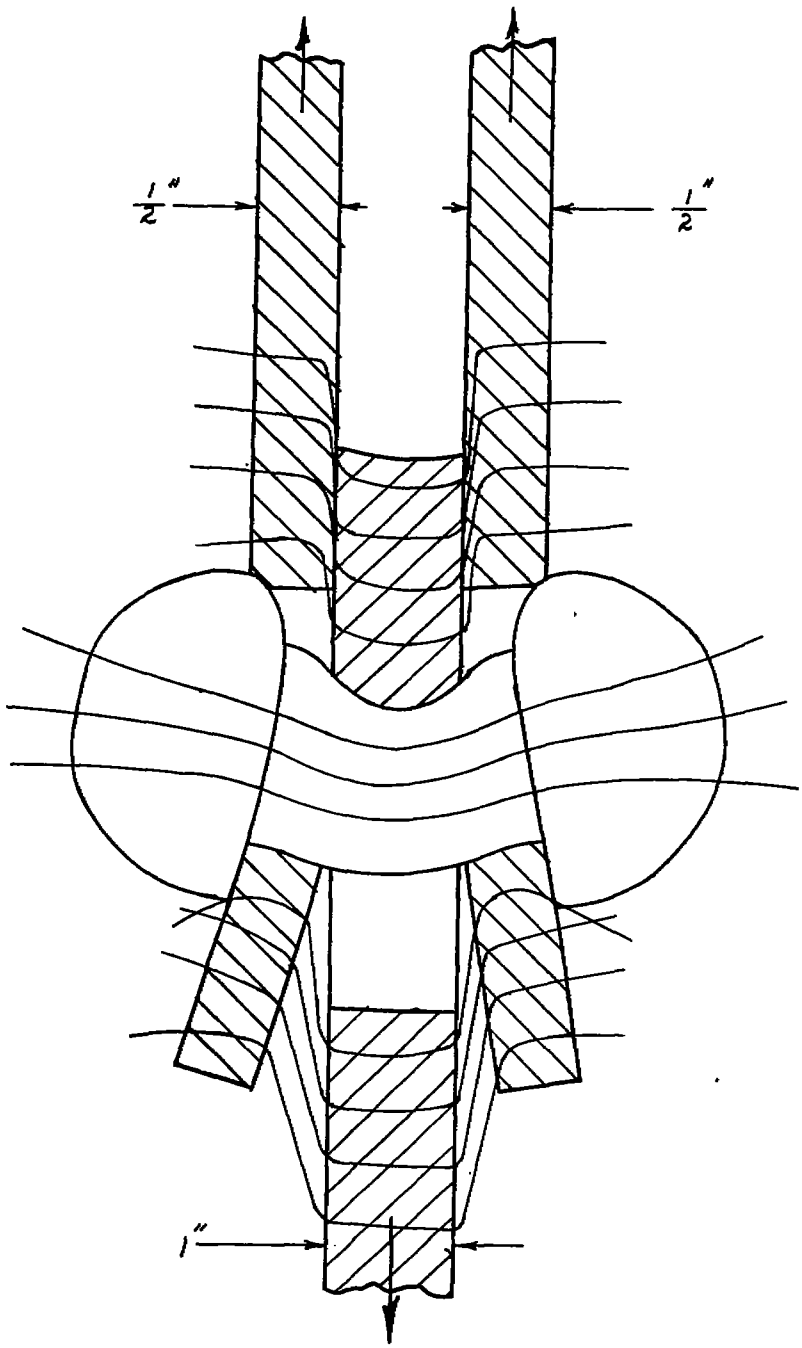

(a) Edge view.

Figure 15.- X-ray tracing of a single-rivet double lap joint under load.

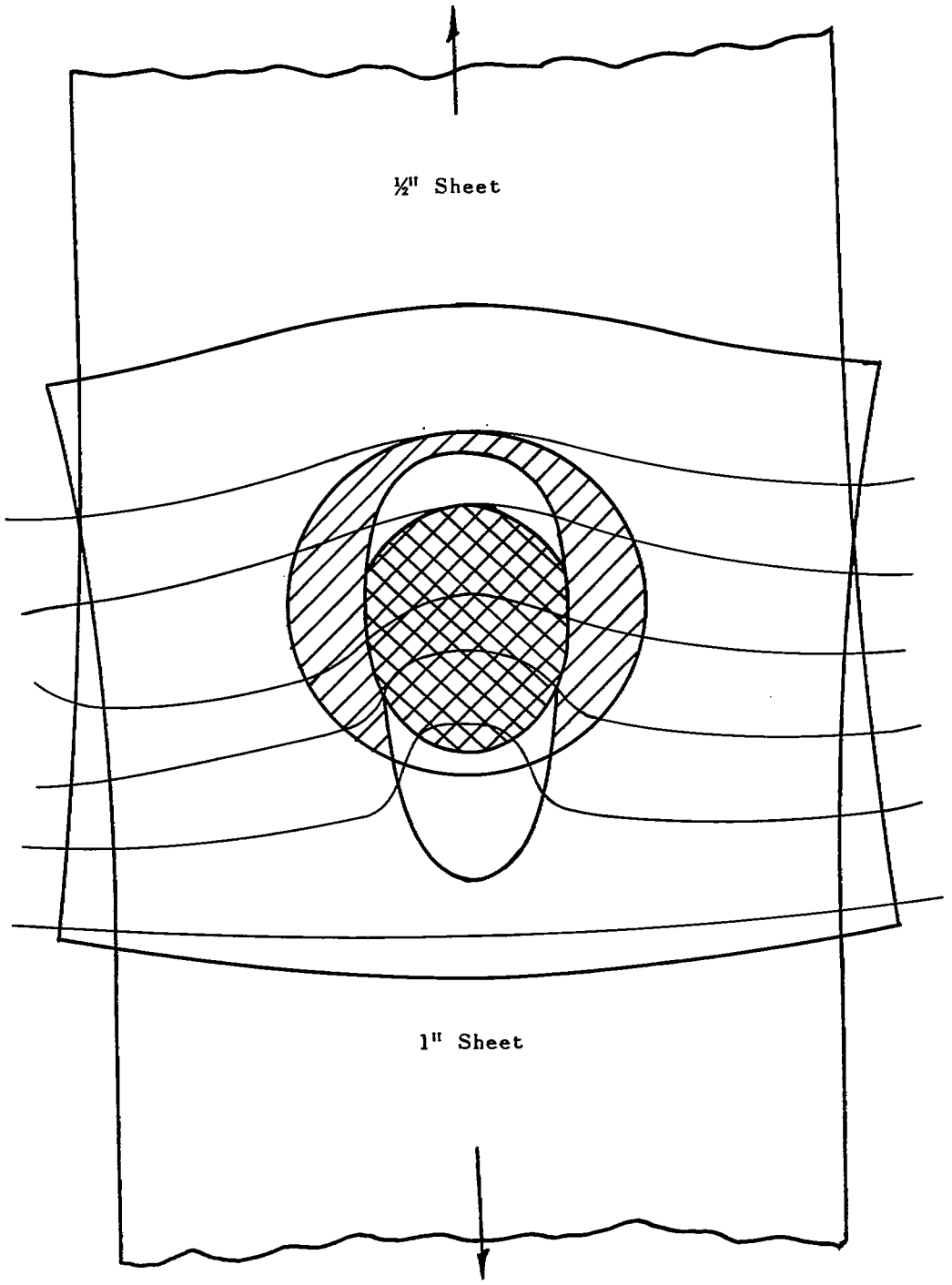

(b) Side view.

Figure 15.- Concluded.

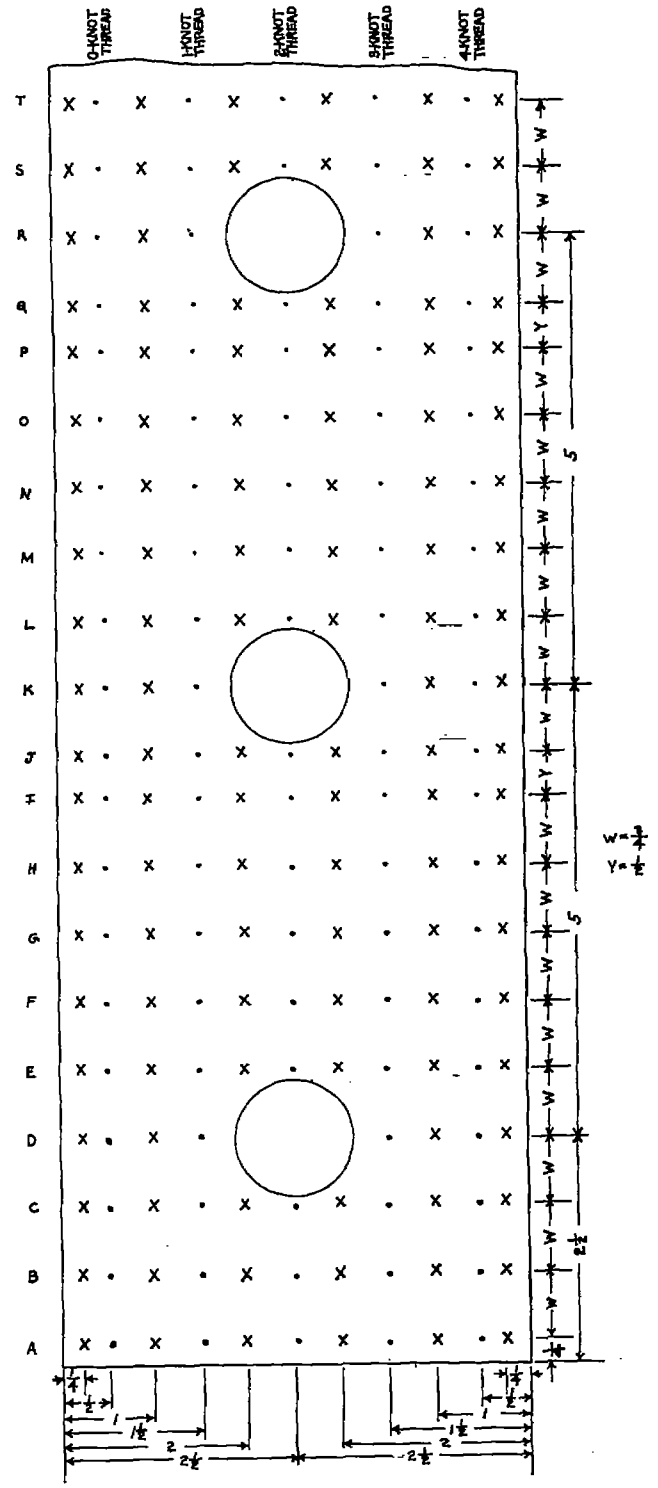

Figure 16.- Location of markers in two- and three-rivet joints.

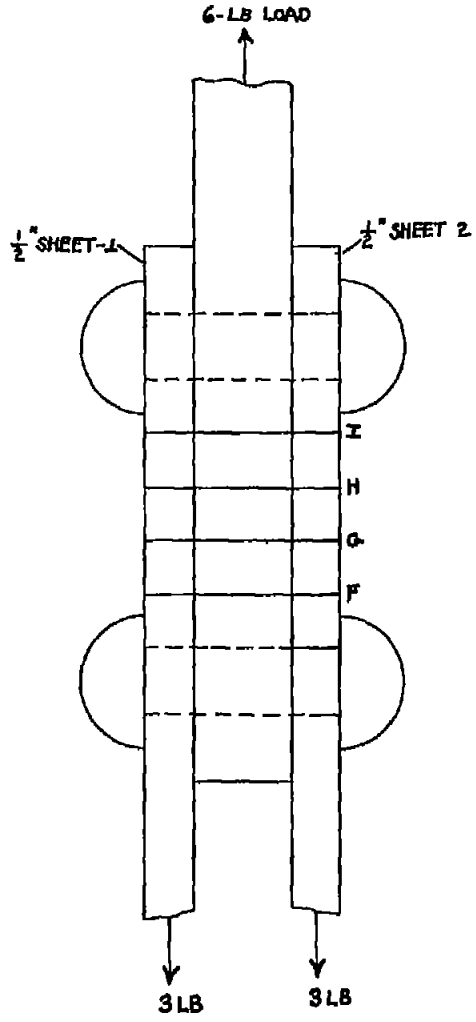

Load Distribution on a Two-Rivet Joint for 6-Lb Load

½" Sheet 1		1" Sheet		½" Sheet 2		Total Load
Sheet	Rivet	Sheet	Rivet	Sheet	Rivet	
	[1.43]		[3.01]		[1.28]	5.72
1.43		2.99		1.28		5.70
	[1.57]		[2.99]		[1.72]	6.28

Percent of Load on Rivets			Average Percent of Total Load on Each Rivet
47.6	50.2	42.7	46.8
52.3	49.8	57.3	53.1

(a) Two-rivet joint.

Figure 17.- Load distribution.

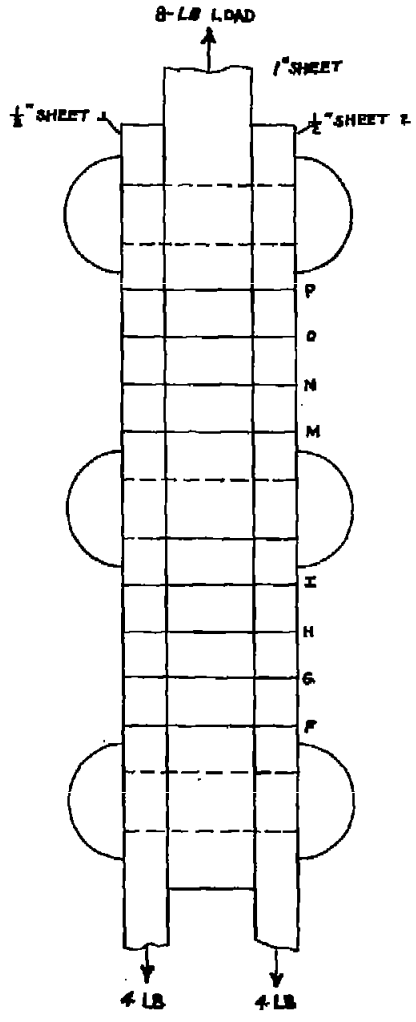

Load Distribution on a Three-Rivet Joint for 8-Lb Load

1/2-in. Sheet-1		1-inch Sheet		1/2-inch Sheet-2		Total Load
Sheet	Rivet	Sheet	Rivet	Sheet	Rivet	
	1.43		3.28		1.20	5.91
1.43		4.72		1.20		7.35
	1.02		2.09		1.16	4.27
2.45		2.63		2.31		7.39
	1.55		2.63		1.69	5.87

Percent of Load on Rivets			Average Percent of Total Load on Each Rivet
35.7	40.9	29.8	35.4
25.5	26.1	37.8	26.4
38.7	32.9	42.2	37.9

(b) Three-rivet joint.

Figure 17.- Concluded.

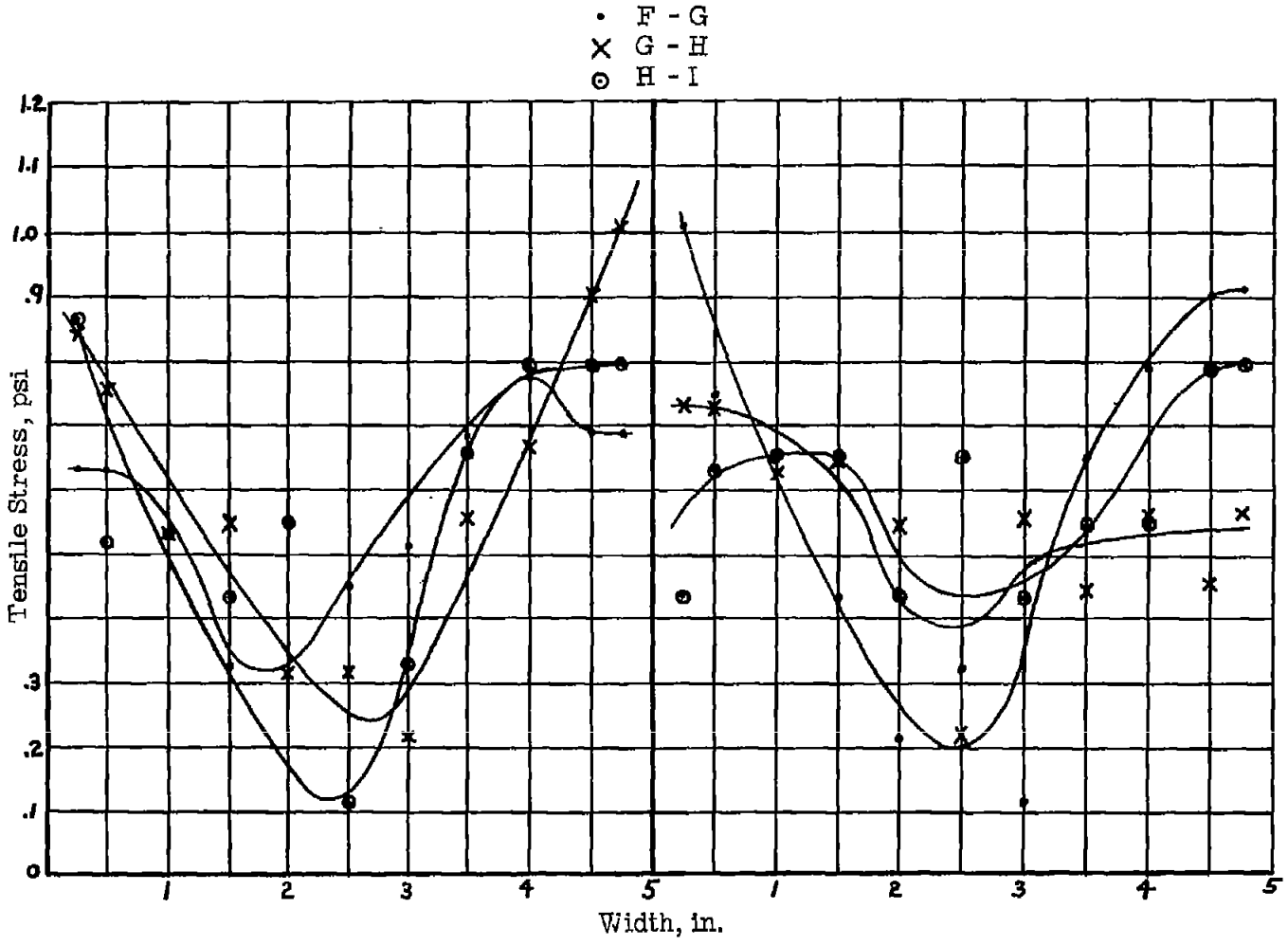

(a) 1-inch sheet.

(b) $\frac{1}{2}$ - inch sheet 1.

Figure 18.- Tensile stress distribution across sheets between rivets in two-rivet joint.

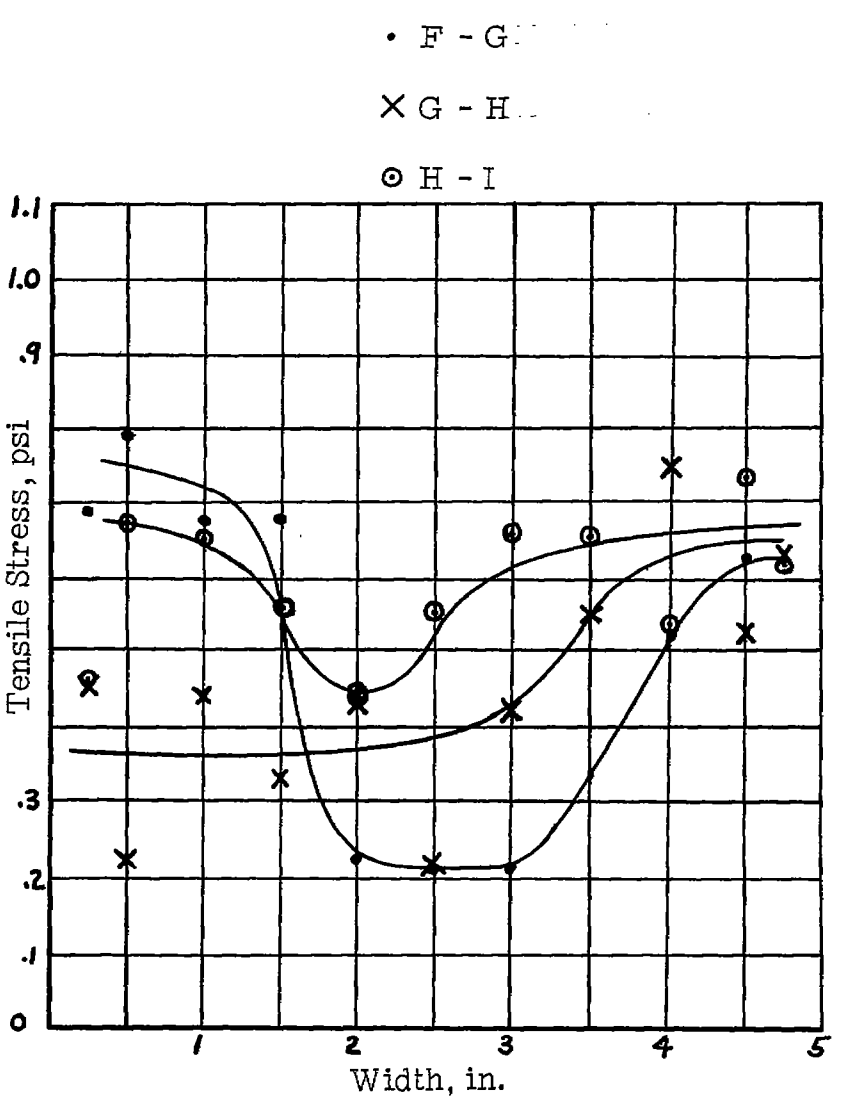

(c) $\frac{1}{2}$- inch sheet 2.

Figure 18.- Concluded.

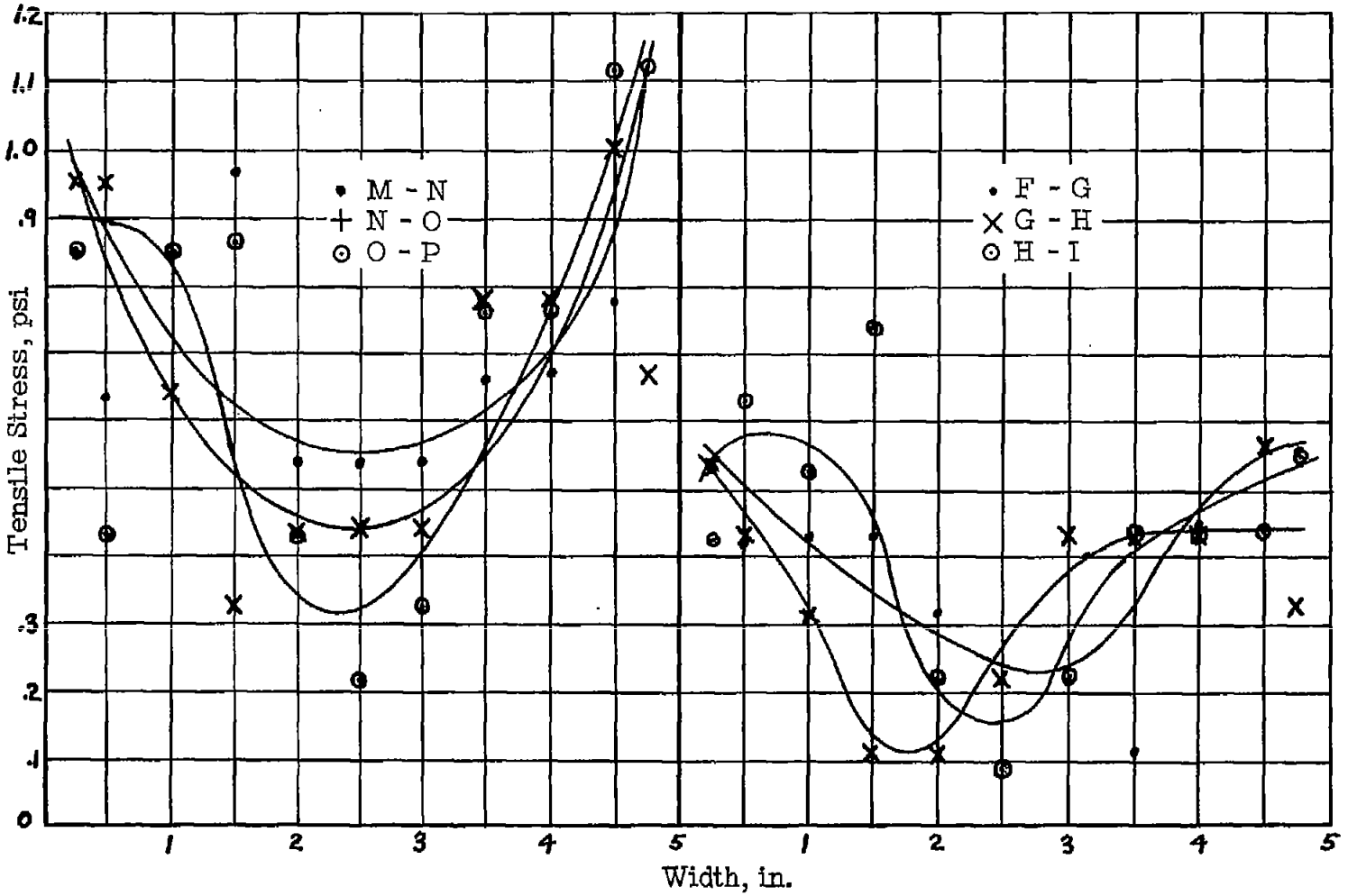

(a) 1-inch sheet, upper rivet. (b) 1-inch sheet, lower rivet.

Figure 19.- Tensile stress distribution across sheets between rivets in three-rivet joint.

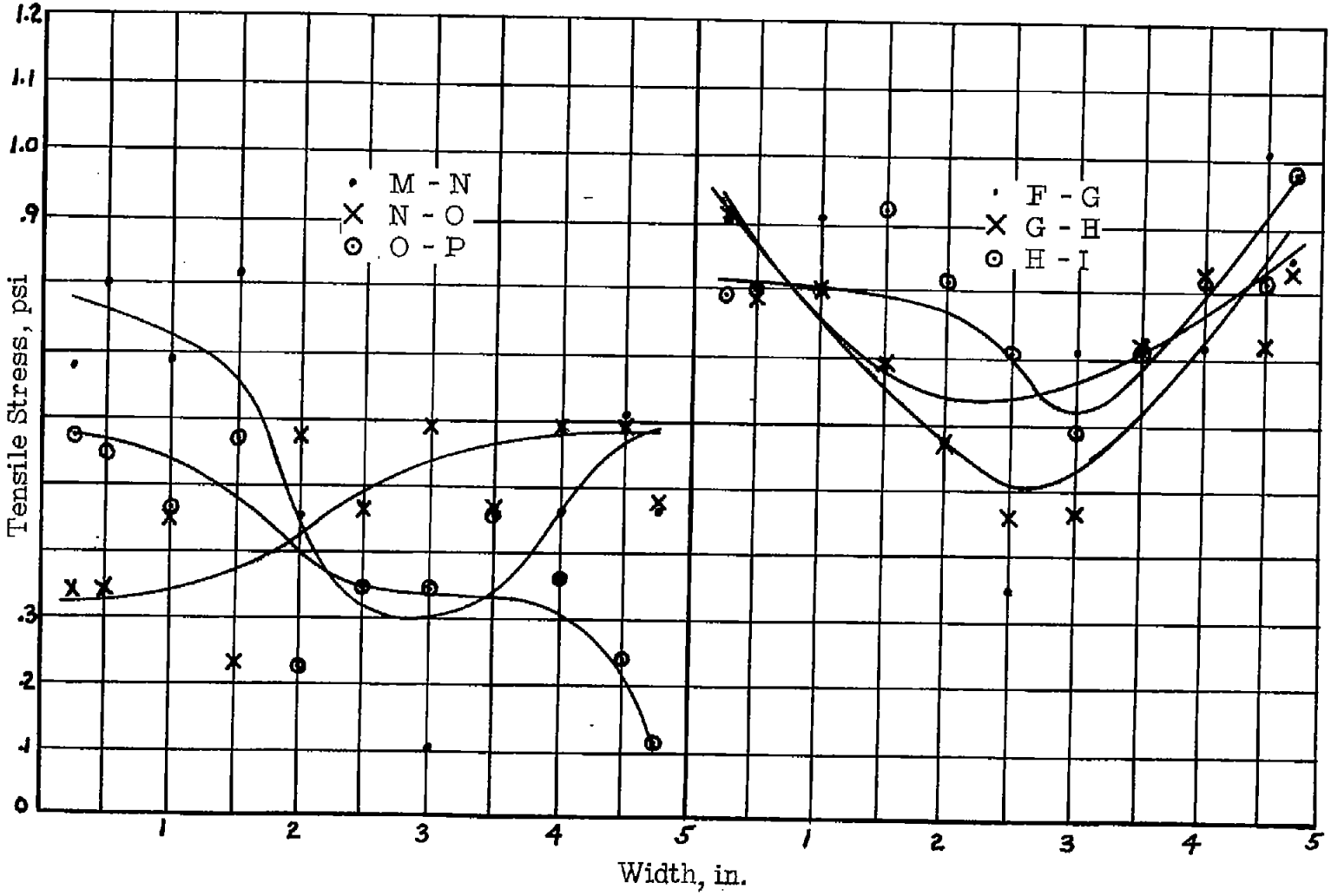

(c) $\frac{1}{2}$-inch sheet 1, upper rivet.

(d) $\frac{1}{2}$-inch sheet, lower rivet.

Figure 19.- Continued.

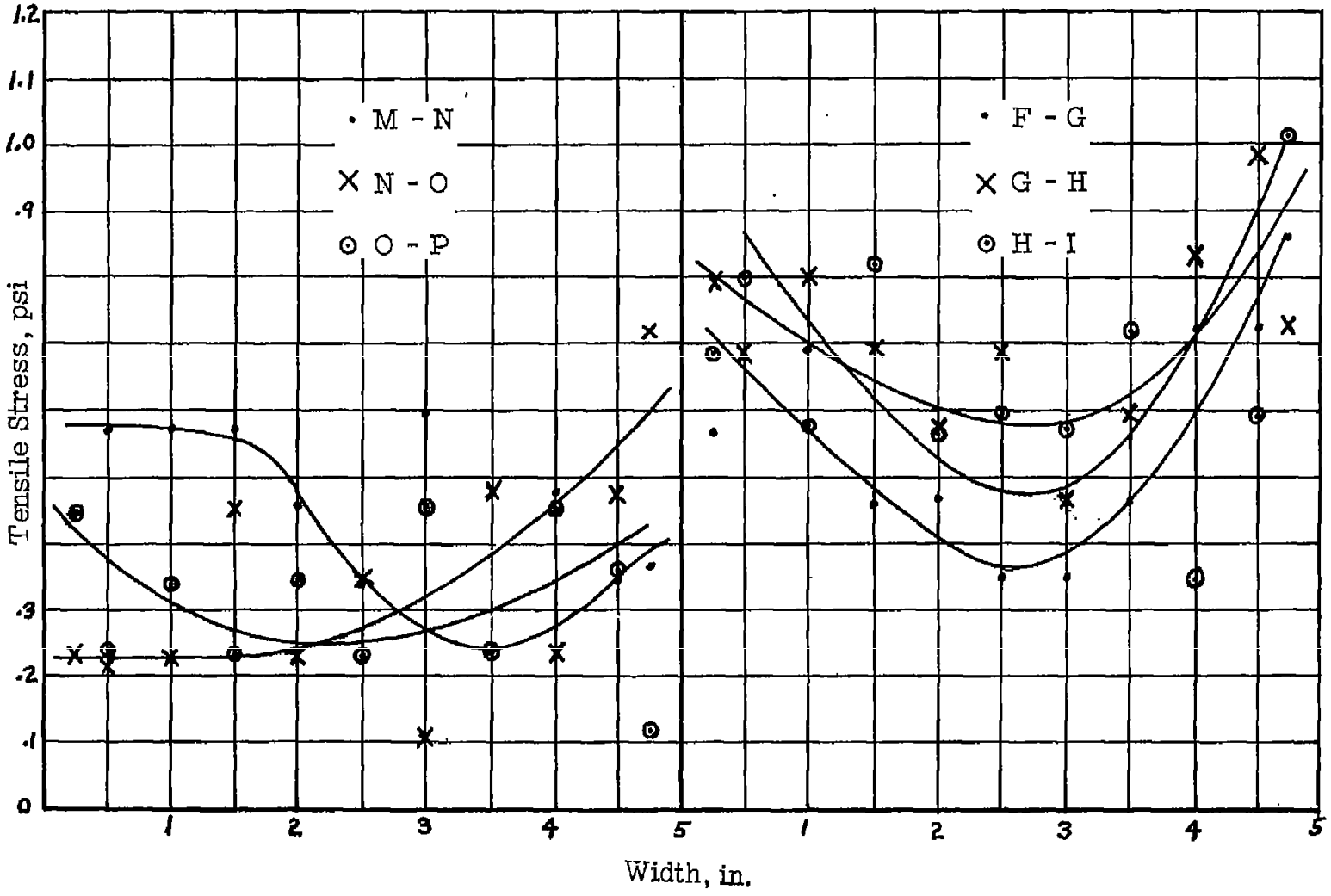

(e) $\frac{1}{2}$-inch sheet 2, upper rivet.

(f) $\frac{1}{2}$-inch sheet 2, lower rivet.

Figure 19.- Concluded.

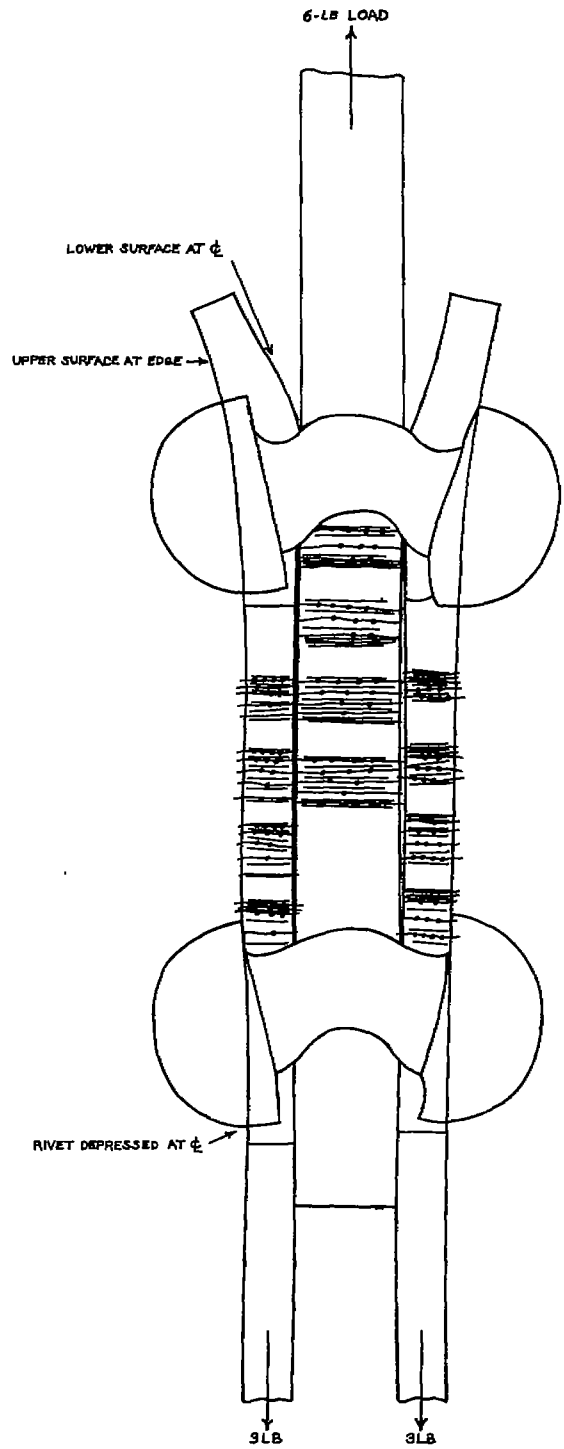

(a) Two-rivet joint.

Figure 20.- X-ray tracing of joints under load.

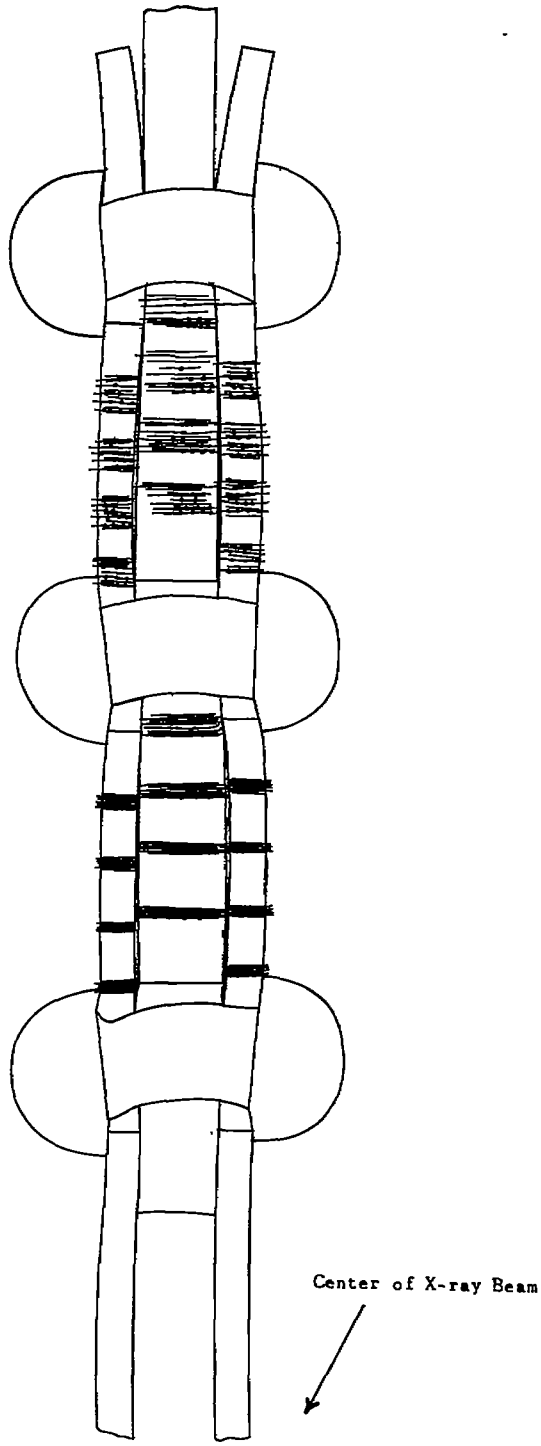

(b) Three-rivet joint.

Figure 20.- Concluded.

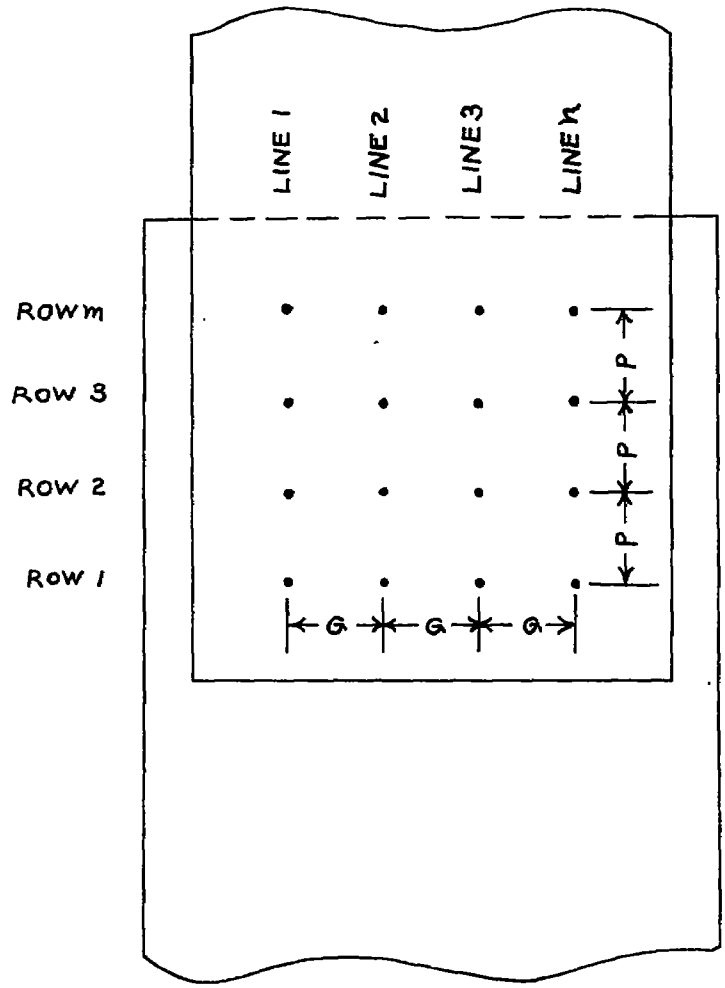

Figure 21.- Definition of pitch and gage. P, rivet pitch in lines; G, rivet gage in rows.

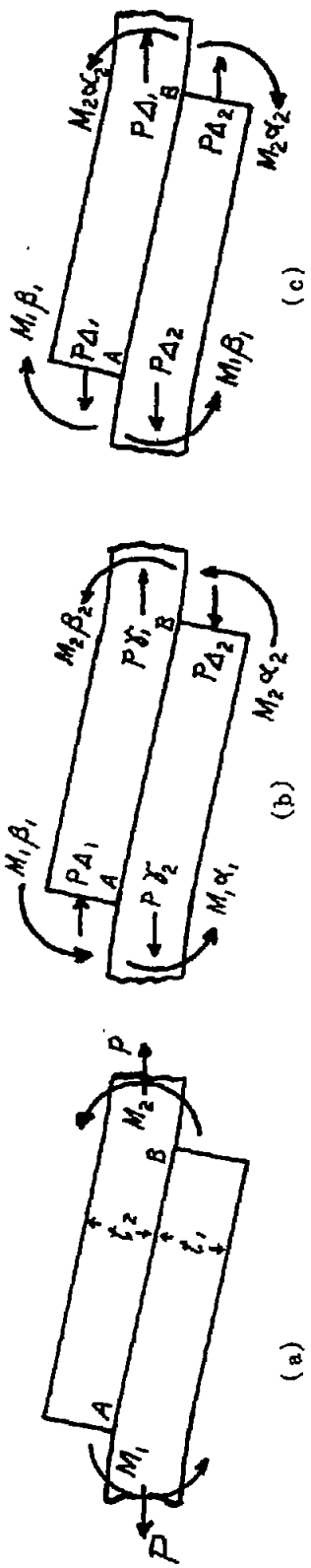

Figure 22.- Resolution of forces and moments in cemented joint.

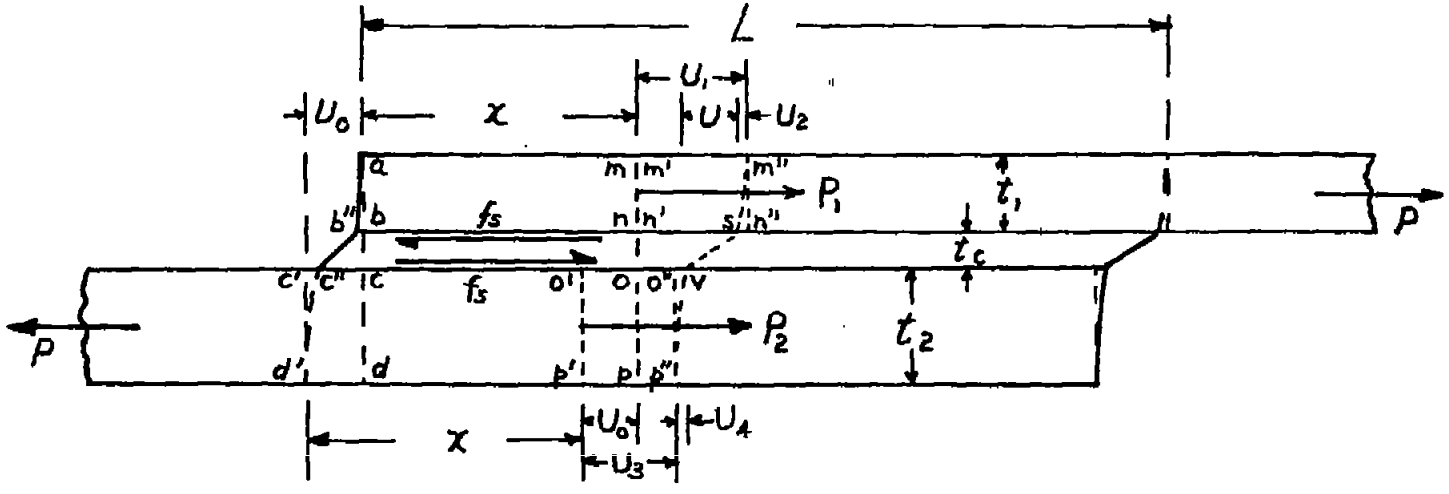

Figure 23.- Single lap joint showing displacement under load.

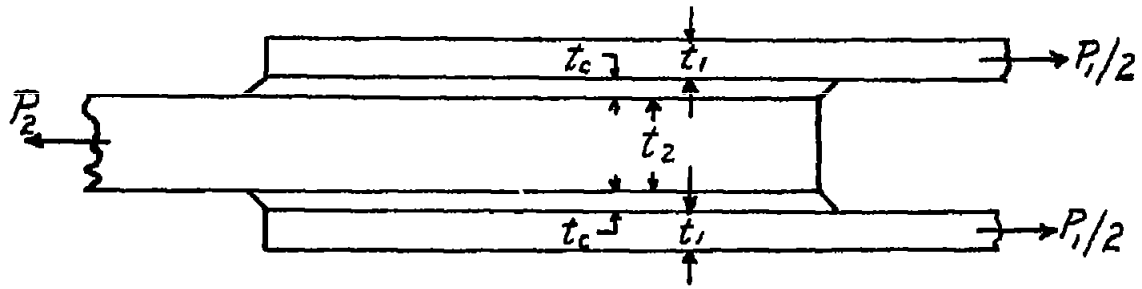

Figure 24.- Symmetrical double lap joint used in cemented-joint analysis.

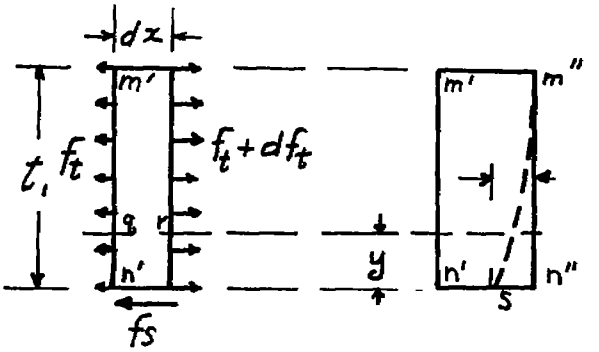

Figure 25.- Stress and displacement in a sheet element.

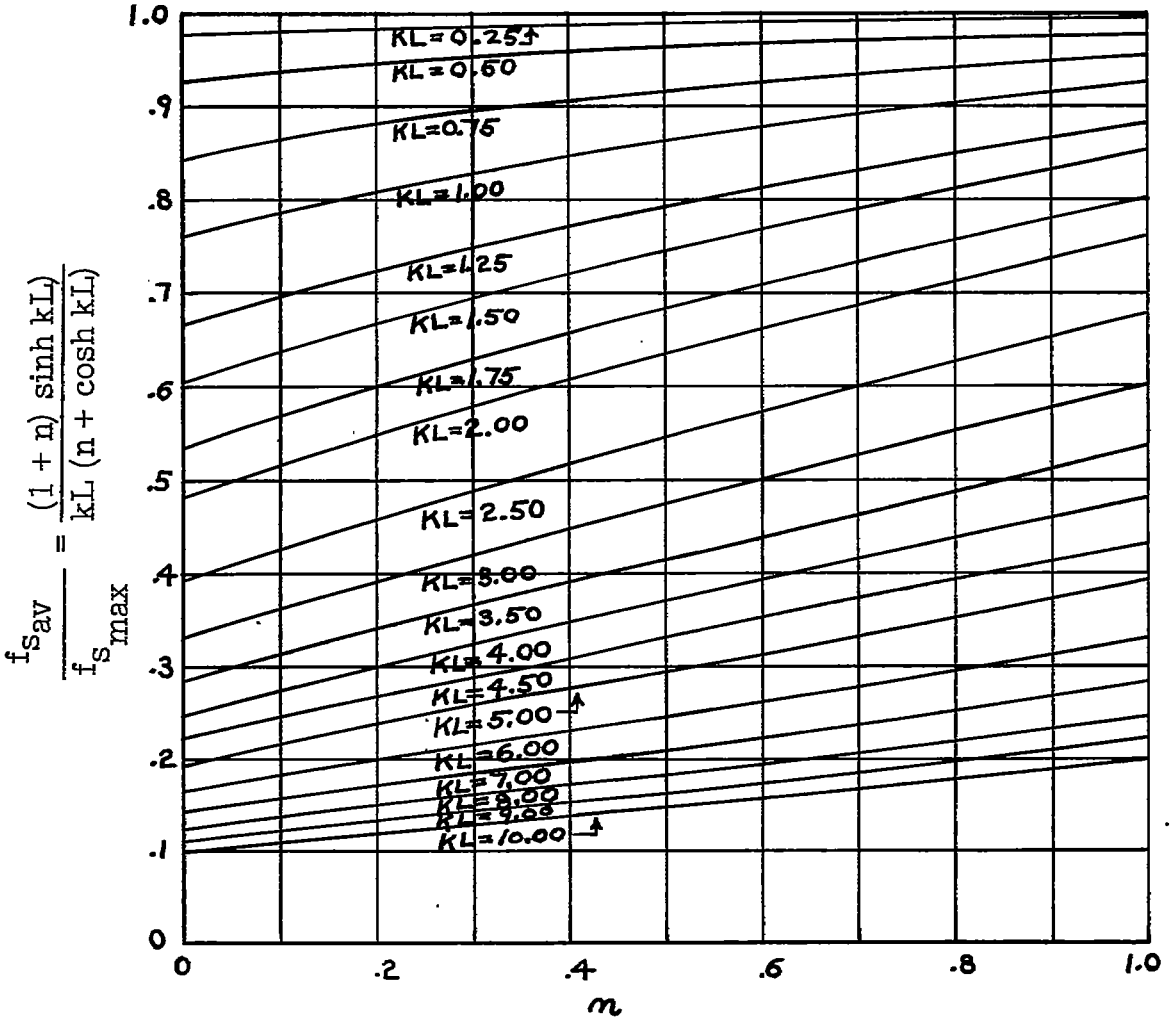

Figure 26.- Ratio of average shear stress to maximum shear stress plotted against n.

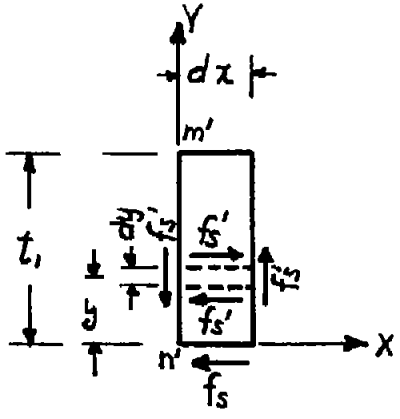

Figure 27.- Shear stress analysis in element of cemented sheet.

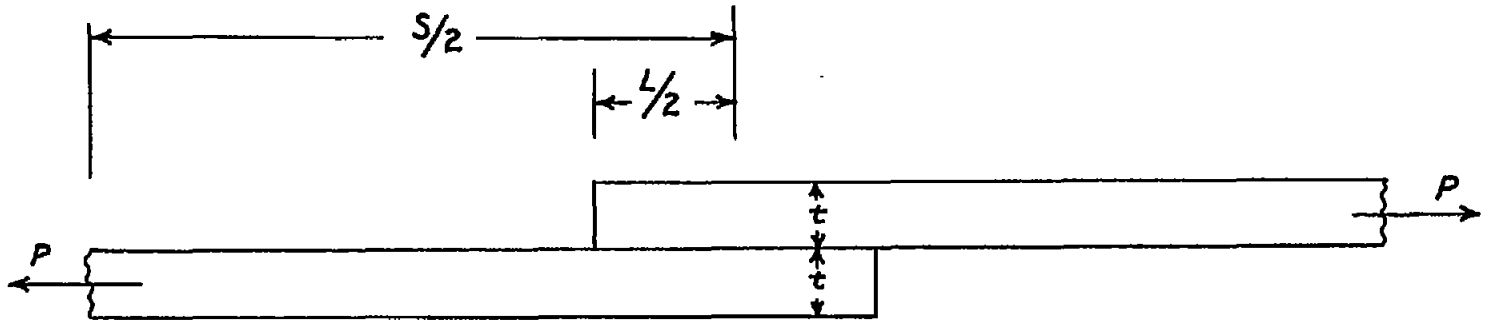

(a) No load.

Figure 28.- Single lap cemented joint.

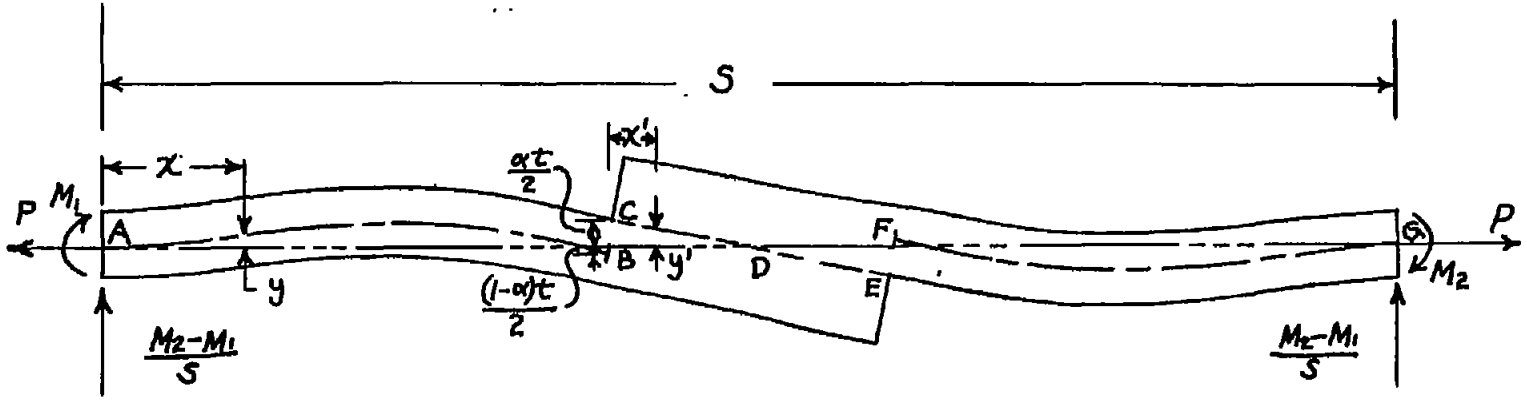

(b) Axial tensile load.

Figure 28.- Concluded.

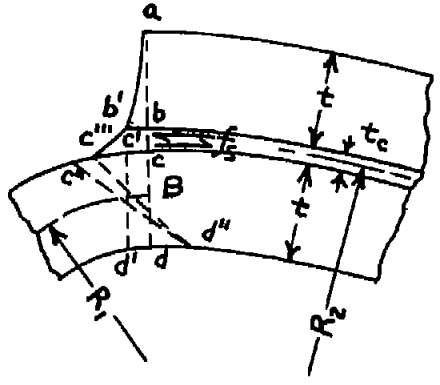

Figure 29.- Displacements in cement at end of top sheet.

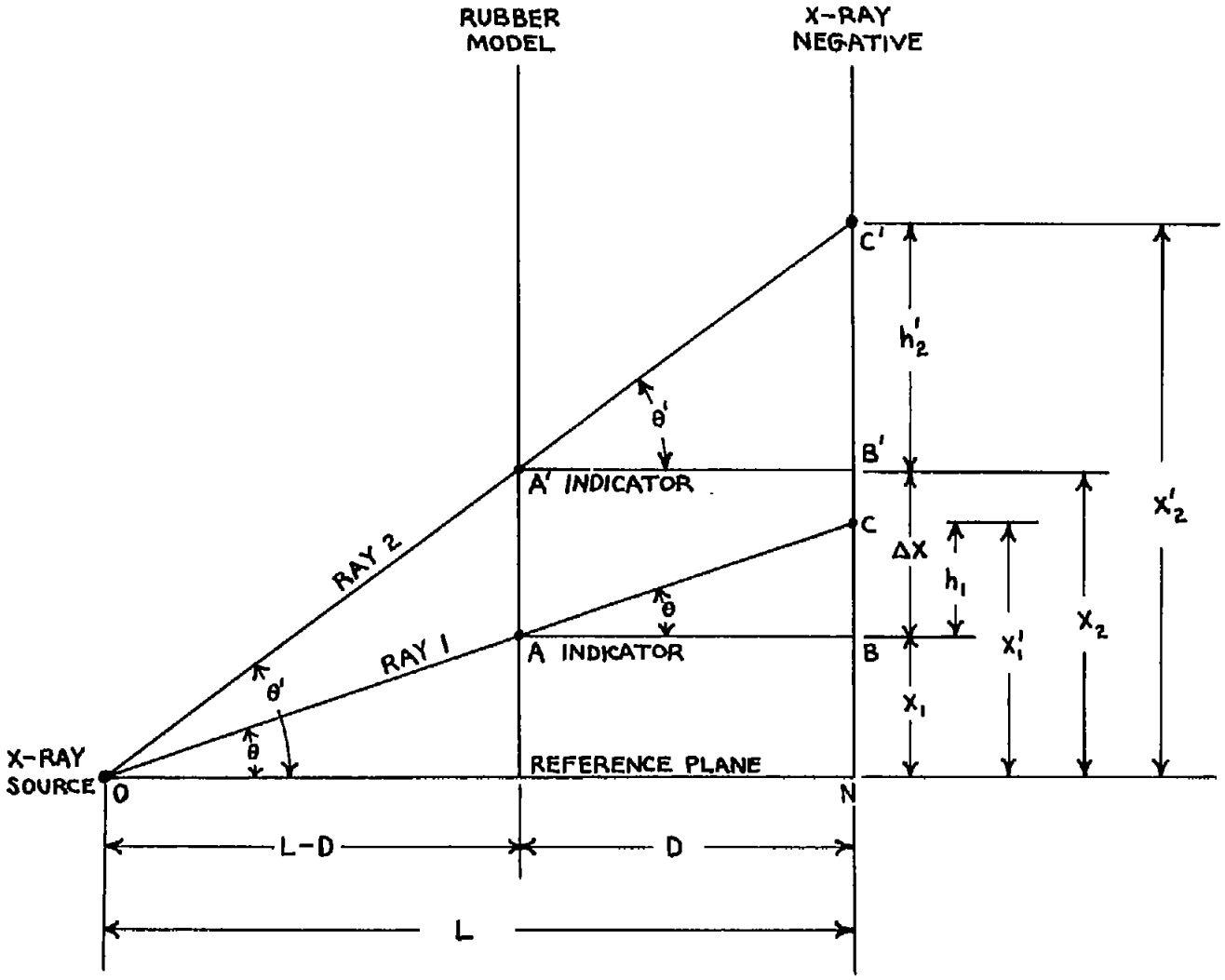

Figure 30.- Geometry of parallax in X-ray photography.